Published in final edited form as:
Prog Nucl Magn Reson Spectrosc. 2010 May ; 56(4): 360–405. doi:10.1016/j.pnmrs.2010.03.002.

Structural Dynamics of Bio-Macromolecules by NMR: The Slowly Relaxing Local Structure Approach

Eva Meirovitch[1,*], **Yury E. Shapiro**[1], **Antonino Polimeno**[2,*], and **Jack H. Freed**[3,*]

[1] The Mina and Everard Goodman Faculty of Life Sciences, Bar–Ilan University, Ramat-Gan 52900 Israel

[2] Department of Physical Chemistry, University of Padua, 35131 Padua, Italy

[3] Baker Laboratory of Chemistry and Chemical Biology, Cornell University, Ithaca, NY 14853-1301, U.S.A

Keywords

NMR spin relaxation; protein dynamics; SRLS; stochastic motional models

1. Introduction

Protein dynamics by NMR has been reviewed extensively in recent years [1–10]. These surveys show decisively that information on structure should be complemented by information on motion both to properly characterize the protein, and to understand its function. The time scale accessible by NMR extends from picoseconds to days, with different methods accessing different parts of this time axis. Here we focus on heteronuclear NMR spin relaxation used to study *ps* to *ns* protein dynamics. The slow limit of this time regime is determined by the global tumbling of the protein, with the rates for internal motion of the probe being typically faster.

Based on experience gained over nearly a decade we came to the conclusion that the traditional method of NMR spin relaxation analysis in proteins and nucleic acids, called "model-free" (MF) [11–13], does not extract adequately and fully the information inherent in the experimental data largely because it is oversimplified. We have developed an approach that overcomes many of the MF deficiencies. This method, called the slowly relaxing local structure (SRLS) [14–20], may be regarded as a generalization of MF. SRLS predates the MF approach, and even provided derivations of the exact equivalents of the MF equations [15,21].

Corresponding authors: eva@nmrsgi5.ls.biu.ac.il, phone: 972-3-5318049, fax: 972-3-7384058; jhf@ccmr.cornell.edu, antonino.polimeno@unipd.it.

[1] In the equivalent of the B.-O. approximation one should replace Γ_Ξ by $[\Gamma_\Xi + E_m(\Xi)]$, leading to eigenfunctions $|\nu_{m,q}(\Xi)>$ in Eq. (11), but we are assuming that the overall slow motion is unaffected by the local probe motion.

[2] The fact that Y_M is the main ordering axis in the C++OPPS fitting scheme for SRLS [90], whereas X_M is the main ordering axis in our previous fitting scheme for SRLS [20], is related to a different definition of the local ordering frame, M. This is inconsequential as far as the physical picture is concerned.

[3] The Euler angles Ω_{MQ} have been defined as $(0°,\beta_{MQ}°,\gamma_{MQ}°)$ in the fitting scheme developed in Ref. [20], and as $(\alpha_{MQ}°,\beta_{MQ}°,0°)$ in the fitting scheme developed in Ref. [90]. The calculations presented in Sections 2 – 5 of Appendix F were carried out with the fitting scheme of Ref. [20].

The primary issue is how to address the great complexity of protein dynamics, including global and restricted local motions. The typical probe for backbone motion in proteins is the $^{15}N–^{1}H$ bond, with ^{15}N relaxation observed [1–10]. The typical probe for side-chain motion is the uniformly ^{13}C-labeled, fractionally deuterated, $^{13}CDH_2$ methyl group, with deuterium relaxation observed [6,22–24]. A given probe might move independently of the protein or be coupled to it dynamically. Any general theoretical approach should account for the relationship between the global and local motions, for the local ordering, and for the relevant magnetic interactions. The respective tensorial properties should be realistically chosen within the scope of the data sensitivity. Thus, the model should include the appropriate parameter combinations. All of these features and capabilities are inherent to SRLS. Correlations along the protein backbone might well be important [3,25–27], but the local factors mentioned above must first be accounted for. That the latter are important was shown in theoretical studies [16,17], and confirmed experimentally [18–20]. Effects from statistical interdependence of the various motions we have referred to as “mode-coupling”.

NMR spin relaxation in liquids pertains to the Redfield limit where only relaxation parameters can be measured [28,29]. The number of experimental data points is limited; one acquires typically three data points (^{15}N T_1, T_2, and $^{15}N–\{^{1}H\}$ *NOE*) for amide ^{15}N and two (^{2}H T_1 and T_2) for methyl ^{2}H at each magnetic field. Hence, it is not practical to treat explicitly the complex local motions coupled to the global motion and to account explicitly for correlations along the protein backbone. However, the latter can affect the analysis implicitly *via* the values of the parameters determined [20].

As currently implemented to treat NMR spin relaxation in proteins and nucleic acid fragments, SRLS is a stochastic two-body coupled-rotator diffusive approach [16–20]. It can be generalized to three (or more) bodies that are coupled, as well as the inclusion of inertial effects in these motions [16], as opposed to the purely diffusive limit currently utilized for convenience. In this limit a Smoluchowski equation is solved to obtain the time correlation functions whose Fourier transforms are the spectral densities that underlie the expressions for the experimentally measured relaxation parameters.

The two rotators represent the protein and the spin-bearing probe, with their rotational degrees of freedom “coupled” by a local potential exerted by the immediate protein surroundings at the site of the motion of the probe. All the tensors that are needed (e.g., ordering tensor, magnetic tensors) are featured, including their general properties. Diffusion within two (or more) wells, with less frequent jumps between the wells, can also be modeled within this approach [17]. When the rate of the global motion is much slower than the rate of the local motion, then “mode-coupling” is represented in a Born-Oppenheimer (B.-O.) type approximation also implicit in the simpler MF approach [15,16]. In this limit one recovers a key part of the (complex) theories of rigid-body motion in the presence of a space-fixed mean-field potential [14,30–33]. That experimental data from probes reorienting in the presence of restricting potentials require this complexity for proper analysis is amply documented in the literature [32,33].

Within the scope of this picture, we consider SRLS to be a realistic general approach that also allows for refinements. The analysis is typically carried out with data fitting [19,20,34,35]. Over-fitting and force-fitting are discernable provided the criteria for result acceptance include appropriate statistics *and* physical viability of the best-fit parameters. It has been found that the parameter combinations that match the data sensitivity for ^{15}N amide and ^{2}H methyl relaxation can be determined with SRLS [20].

The philosophy underlying MF is different. According to it, the experimental data are scarce, and the great complexity of protein dynamics cannot be possibly captured by a tractable

stochastic model. Therefore, only simple approaches are justified, and good statistics suffice for result acceptance.

The simplest approximation to the actual (normalized) time correlation function, $C(t)$, is an initial exponential descent from unity to a plateau value followed by a slower exponential decay, with rate constant $1/\tau_m$, to zero at long times due to the global tumbling; that is, τ_m is the correlation time for overall rotational reorientation. The initial descent is taken to be given by a single decay constant, $1/\tau_e$. This (bi-exponential) form of $C(t)$ assumes implicitly only the simplest geometrical description. It is valid when the protein is "frozen", i.e., $\tau_m = \infty$, and within a good approximation when $\tau_e \ll \tau_m$ and only two correlation times are sufficient [11]. As noted above, a stochastic derivation leading to a very similar expression, but also including the tensorial properties of the magnetic and ordering tensors, was provided earlier [15].

Stochastic approaches have shown that actual time correlation functions associated with restricted motions in liquids are given by sums of weighted exponents [14,30–33]. It is often possible to least-squares fit such functions to the bi-exponential MF function with good statistics. This constitutes parameterization of the measurable time correlation function in terms of τ_e and the plateau value, which by itself is appropriate. However, one wishes to gain insight into the physical nature of the protein dynamics. For that, it is necessary to determine the conditions under which the MF parameters may be viewed as physical parameters.

These conditions cannot be specified within the scope of MF, given its "model-free" characteristic. They can be specified using SRLS, which is general in nature and yields MF in simple limits. The parameter τ_e will represent an effective local motional correlation time, and the plateau value will represent the square of an axial order parameter, $(S_0^2)^2$, under the following conditions. (1) The time scale separation between the reorientation of the probe and the reorientation of the protein is large. (2) The local ordering is either weak or strong. (3) All the second rank tensors are as simple as possible. (4) The eigenfunctions of the local motional diffusion operator take on a simple form, despite the presence of a local potential. Based on previous work on restricted motions in liquids [14,30–33] these conditions are not likely to be fulfilled, as confirmed recently [19,20,34,35]. If a given time correlation function, or the spectral density obtained from it by Fourier transformation, are used outside of their validity range, the best-fit parameters will be physically vague.

The "model-free" point of view has been extended further. The plateau of the MF time correlation function was defined mathematically as the square of a "generalized" order parameter, S^2. As shown below, this is an artificial order parameter. Nevertheless its expression is used to calculate order parameters from molecular dynamics (MD) trajectories [36] using a formula valid in simple limits [37]. Furthermore, S^2 is designated as an amplitude of motion, and conformational entropy has been calculated from it [6].

For methyl dynamics the situation is more challenging because a single local motion – rotation about the C–CH_3 axis within the scope of the tetrahedral carbon geometry featuring the angle 110.5° (which corresponds to taking r_{CH}=1.115 Å in analyzing cross-correlates HC-HH relaxation [24]) – does not lead to good statistics in fitting the experimental data [38]. MF addressed this problem by introducing a second local motion – axial fluctuations of the C–CH_3 axis – though factorization of S^2 into the product $0.1\times S_{axis}^2$, and assuming that one may assign τ_e to both motions [11,12,36]. The factor $P_2(\cos(110.5°))^2 = 0.1$ is taken to represent the squared order parameter associated with the motion about the C–CH_3 axis; S_{axis}^2 is taken to be the squared order parameter for the motion of the C–CH_3 axis. The two local motions are assumed to be decoupled from one another and from the global motion.

The typical probe is the deuterium nucleus in the $^{13}CDH_2$ methyl group [22]. The MF spectral density described above can represent either motion about C–$^{13}CDH_2$ as described above, or axial fluctuations of C–$^{13}CDH_2$. It cannot represent simultaneously both motions if one wishes to sustain a physical scenario.

The issues brought up above will be addressed in detail in the review. It will be shown that analogous, but physically distinct, SRLS and MF analyses often yield substantially different results, indicating that the oversimplifications inherent in MF have unfavorable practical implications. Within a broader perspective, we illustrate the disadvantages of applying parameterization instead of setting forth models, using mathematical instead of physical parameter definitions, and not abiding by the assumptions underlying the various equations used. We offer the concepts that underlie SRLS as an alternative to the model-free point-of-view, and we describe and illustrate how SRLS can be implemented in a practical fashion. We also indicate how improvements to the current SRLS approach can be introduced.

2. Perspectives of protein dynamics by NMR

2.1. The Slowly Relaxing Local Structure (SRLS) approach

Relaxation rates of nuclear spins in biological macromolecules, particularly proteins, are a rich source of information on kinetic, structural, geometric and thermodynamic properties [1–10, 22–24]. The spin-bearing moieties are engaged in both the global tumbling of the protein and at least one local motion. The latter is restricted by the local structure, i.e., the immediate (mobile) protein surroundings. This is a complex two-body (protein and probe) scenario [16–20].

To extract properly the information inherent in the experimental data a reasonable but tractable dynamic model, which matches data sensitivity, is required. The problem will be simplified significantly if it is appropriate to assume that (1) the global and local motions occur on very different time scales, (2) the properties of the second rank tensors involved are very simple, and (3) the local ordering is weak. This scenario was treated in early work by Freed within the scope of an SRLS model wherein the probe reorients (diffusively) rapidly in a “cage” which experiences slow motion [15]. The cage (probe) can be considered to represent the protein (spin-bearing moiety); the cage motion can be associated with the motion of the protein that of course provides spatial restrictions at the site of the motion of the probe.

For weak axial local ordering, probe diffusion approximated as isotropic and cage motion taken isotropic, $C(t)$ comprises three terms [15]. They represent effects of the slow large-body motion, the reorientation of the probe with respect to the mean field (ordering) potential, and a negative cross-term between these two processes, which represents their statistical inter-dependence from the point-of-view of the probe. By analogy with treating, in quantum mechanics, the motion of a low mass particle relative to a heavy particle, this was also called a Born-Oppenheimer (B.-O.) approximation [15] (see also Ref. [39]). The Fourier transform of $C(t)$ (the derivation of which is outlined in Section 3.2.1.) is given by:

$$j(\omega)=(S_0^2)^2\,\tau_m/(1+\omega^2\tau_m^2)-(1-(S_0^2)^2)\,\tau/(1+\omega^2\tau^2), \quad (1)$$

where S_0^2 is the axial order parameter defined in terms of a Legendre polynomial of rank 2, $\tau_m = 1/(6\,R^C)$ is the correlation time for slow cage reorientation, and $\tau = 1/(6\,R^L)$ is the correlation time for fast “probe” reorientation, with $\tau \ll \tau_m$. The parameters R^C and R^L denote the rate constants for global and local diffusion, respectively. For local ordering/local diffusion and magnetic frames taken the same, $j(\omega)$ given by Eq. (1) is the measurable spectral density, $J(\omega)$, in terms of which the experimental relaxation parameters are defined.

Note that the form of $C(t)$, hence of $J(\omega)$, is simple not only because of the large time scale separation aspect, but also because the symmetry-related and geometry-related properties of the second rank tensors involved are likewise simple. Finally, the eigenfunctions of the diffusion operator of the probe in the presence of a local ordering potential are the same as the eigenfunctions of the "bare" diffusion operator describing a freely diffusing axial probe. These eigenfunctions are the generalized spherical harmonics (Wigner functions). In general the local potential alters the basis set of the "bare" diffusion operator [14,30–33]. In the limit of very weak potentials and large time scale separation [15] this basis set may be preserved.

In the limit in which a spherical particle reorients rapidly in the presence of a strong axial potential the eigenfunctions of the diffusion operator become again simple to express [14,31]. Then the correlation time is $\tau_{ren} \sim 2\tau/c_0^2$, with the dimensionless coefficient, c_0^2, denoting the strength of the axial local potential as compared to k_BT; τ_{ren} represents a "renormalized" correlation time [14]. In the limit of large time scale separation and strong axial local potential the full SRLS solution features a dominant local motional correlation time which agrees with τ_{ren} [20,40], and has eigenfunctions given in Ref. [14]. We have shown that in this limit Eq. (1) with τ replaced by τ_{ren} is a good approximation to the SRLS spectral density [20].

The MF time correlation function is the same as $J(\omega)$ given by the B.-O. limit simple SRLS time correlation function in Eq. (1) with S^2 representing $(S_0^2)^2$, and τ_e representing τ for small S^2 and τ_{ren} for large S^2 (on a 0 – 1 scale). As pointed out above, actual applications do not abide by the limiting conditions underlying MF. More general versions of SRLS are required to treat them properly.

The full SRLS theory, where all the restrictions mentioned above have been eliminated, was developed by Polimeno and Freed by solving a two-body coupled-rotator Smoluchowski equation [16]. In this development the effect of the coupling/ordering potential on the eigenfunctions of the uncoupled diffusion operators, and statistical interdependence, or mode-coupling, between the global and local motions, are accounted for rigorously in the diffusive limit. The time scales of the global and local motions may be arbitrary. The global diffusion, the local diffusion, the local ordering and the magnetic tensors are allowed their full asymmetry and they may be oriented arbitrarily. The magnitude of the local potential is not limited. In the limit of large time scale separation and strong potentials, and in the limit where τ is practically the same as τ_m, inertial aspects of the probe motion become important, and a full Fokker-Planck-Kramers treatment is advisable. This was also developed in Ref. [16]; efforts geared toward the application of this approach to NMR spin relaxation in proteins are underway.

One may envision an NMR, ESR, fluorescence-related, etc., probe embedded in surroundings that represent a protein or DNA fragment. SRLS is applicable to all of these scenarios. It thus constitutes a general theoretical/computational tool for analyzing bio-macromolecular dynamics. Clearly, it is not practical to use it in its most general form in a given calculation. The parameter combination appropriate for analyzing given experimental data is determined by requiring both good correspondence between theory and experiment, and physical relevance of the results. In the context of ESR the SRLS approach was applied over the years to various systems (e.g., see Refs. [41,42]), including bio-macromolecules [18,43–45]. The parameter sets required exceed the scope of the MF limit.

We first applied the full SRLS theory to NMR spin relaxation in proteins in 2001 [19]. Further developments, and many applications, are described in Refs. [20,34,35,40,46–50]. In this review article, we present typical results and suggest further developments in modeling.

2.2. Model-Free

The MF spectral density is given by [11]:

$$J(\omega)=S^2\,\tau_m/(1+\tau_m{}^2\,\omega^2)+(1-S^2)\,\tau_e{}^{|}/(1+\tau_e{}^{|2}\,\omega^2), \quad (2)$$

where $1/\tau_e{}^{|}=1/\tau_m+1/\tau_e$, and $1/\tau_e{}^{|}\sim 1/\tau_e$ by virtue of $\tau_m \gg \tau_e$. This spectral density is based on the premise that the global motion of the protein and the local motion of the probe are statistically independent. By virtue of this assumption the total time correlation function, $C(t)$, is factored into the product $C^C(t)\times C^L(t)$, with $C^C(t)$ ($C^L(t)$) denoting the time correlation function for global (local) motion. The derivation of Eq. (2) is outlined in Section 3.2.3. Here we only point out the meaning of the various MF parameters in comparison with their physically precise SRLS counterparts.

Equation (2) is "model-free" since no physical model was used to derive it. For simple motional and ordering properties its form is valid rigorously for a "frozen" protein with $\tau_m=\infty$, and approximately for $\tau_m \gg \tau_e$ [11]. Restricted local motions are in principle multi-exponential [30–33]. In practice there exist limiting conditions under which these motions may be represented by a single decay constant. For wobble-in-a-cone in a square-well potential this approximation is valid for a semi-cone angle smaller than 50° [51]. For wobble-in-a-cone in a cosine squared potential the threshold is 15° [20]. For diffusive local motion in a strong axial potential the dimensionless coefficient c_0^2 must be larger than 10 and the time scale separation larger than 100 for a single correlation time given by $2\tau/c_0^2$ to be valid [20].

The parameter τ_e is defined based on the theory of moments as the area of the exact time correlation function for internal motion divided by $(1-S^2)$. No limits are imposed on the value of this mathematical quantity.

The parameter S^2 represents $C^L(\infty)$. In Ref. [52] it was shown based on a stochastic model that $C^L(\infty)$ is equal to the square of the axial physical order parameter $(S_0^2)^2=\langle P_2(\cos\theta)\rangle^2$. This agrees with $C^L(t)$ defined in Ref. [11] as the (axial) time correlation function of $P_2(\cos\theta)$. The time-dependent variable, θ, is the angle between the axial "interaction" (i.e., magnetic) frame and an axial protein-fixed frame. By using the magnetic frame in defining $C^L(t)$ [11] it is assumed implicitly that the local ordering and magnetic frames are the same. This is certainly not obvious.

In Ref. [11] $C^L(\infty)$ is re-defined as $S^2=\sum_{m=0,\pm1,\pm2}\langle|Y_{2m}(\theta,\varphi)|\rangle^2$, where Y_{2m} are the spherical harmonics of Brink and Satchler [53]. This quantity is denoted as the square of a "generalized" order parameter. The azimuthal angle φ is not defined, nor is it clear how does $C^L(\infty)\equiv S^2$ [11] relate to the original definition of $C^L(\infty)\equiv(S_0^2)^2=\langle P_2(\cos\theta\rangle^2\propto\langle Y_{2,0}(\theta)\rangle^2$ [52].

As mentioned above, when order parameters are derived from molecular dynamics (MD) trajectories one typically calculates S instead of S_0^2 [36]. The expressions for these two types of order parameters are clearly different. Moreover, S is calculated using a simple formula based on the results of Normal Mode Analysis, which is valid for local motions in the extreme motional narrowing limit and for strong axial local ordering [37]. Yet, this formula is being used more generally, e.g., even in the presence of *ns* local motions; in some cases it is considered "exact" [54]. The mathematical expression for S has also been used to calculate order parameters of various models for internal motion in proteins [6,8].

The parameter S^2 is considered as a measure of the amplitude of the local motion. This interpretation, appropriate in the limit of strong axial local ordering and local motion in the extreme motional narrowing limit [18], prompted the utilization of S^2 to calculate conformational entropy [6,8,55–58]. The physical meaning of the latter quantity is thus problematic outside the limit where $S^2 \rightarrow (S_0^2)^2 = <P_2(\cos\theta)>^2$, θ is small, and $\tau_e \rightarrow 0$.

The extended MF (EMF) spectral density was developed for cases where small experimental $^{15}N–\{^1H\}$ *NOE* values were encountered [13]; such data could not be fitted with the MF spectral density. Besides a fast local motional term with correlation time τ_f the EMF spectral density also comprises a slow local motional term with correlation time τ_s, which helps to reproduce the small *NOE* values. In principle, all three dynamic modes, represented by τ_m, τ_f and τ_s, are assumed to be decoupled from one another. In practice, τ_s often occurs on the same time scale as τ_m. The basic MF premise of statistical independence may well be in conflict with τ_s being on the order of τ_m, because this similarity implies mode-coupling in the limit of overdamped diffusive motions [16], as illustrated, e.g., in Ref. [20].

Lin and Freed [21] provided an extension of SRLS in the large time scale separation limit for weak rhombic local ordering and axial local diffusion – see Eq. (B6) of Ref. [21]. For a 90° tilt between the axial magnetic frame and the main local ordering axis the measurable spectral density of this expansion is, within a good approximation, mathematically the same as the EMF spectral density. Note, however, that the spectral densities developed in Ref. [21] include general properties of the magnetic and ordering tensors, rendering them physically different from the EMF spectral density. That is, the effective correlation times, τ_f and τ_s, considered in MF to represent two independent decoupled local motions are in this SRLS spectral density the parallel and perpendicular components of the axial local diffusion tensor. The MF order parameters S_f and S_s, associated in MF with independent local motions, can be expressed as functions of S_0^2 and S_2^2, which define a rhombic local ordering tensor [21]. Since Eq. (B6) of Ref. [21] is a B.-O. limit spectral density, the EMF formula should not be used when τ_s and τ_m occur on the same time scale.

As mentioned above, for methyl dynamics the MF spectral density given by Eq. (2) has been re-interpreted to represent two local motions. One is described by Woessner's model [59] applied to rotation about the C–CH_3 axis, and the other consists of local axial fluctuations of the C–CH_3 axis [11]. $P_2(\cos 110.5°)^2 = 0.1$ is taken to represent [11,12,36) the squared order parameters of Woessner's model [59]. Yet, this model has implicitly an order parameter of 1 [59]; its $P_2(\cos 110.5°)$ is actually a transformation of the axes frame. S_{axis}^2 is associated with restricted fluctuations of the C–CH_3 axis. Yet, in Woessner's model the motion of this axis is given by $\tau_\perp = 1/(6R_\perp^L)$, which represents the isotropic global tumbling. Thus, $\tau_e = \tau_\perp = \tau_m$. The local motion is given in Woessner's model by $\tau_\parallel = 1/(6R_\parallel^L)$. Thus, $\tau_e = \tau_\parallel$. Clearly, this scenario is not physically sound. The model developed in Ref. [60] treats methyl dynamics within the scope of two separate motions (about the C-CH_3 bond and of the C-CH_3 bond), although $P_2(\cos 110.5°)^2 = 0.1$ is also considered to be an order parameter.

With S_{axis}^2 designated as the amplitude of axial C–CH_3 fluctuations one expects correspondence between its value and various structural properties. Such correspondence could in general not be established [61,62] (with a few exceptions [63]). Inconsistencies associated with S_{axis}^2 have been reported in the literature (see, for example, Ref. [64]).

It is indicated in Ref. [11] that S^2 and τ_e may be interpreted within the scope of various models for restricted motions in proteins. There are numerous examples indicating that experimental data from probes engaged in motions restricted by a potential of mean torque require accounting for general tensorial properties (e.g., non-spherical local diffusion tensor, rhombic ordering

tensor, and their respective principal axes frames tilted from the magnetic tensor frames) for proper analysis [14,30–33]. Probes reorienting inside proteins experience such restricted motions. Thus, even in the mode-decoupling limit Eq. (2) is too simple to treat adequately protein dynamics.

There is compelling evidence within the scope of NMR spin relaxation in proteins for motion about the $C^{\alpha}_{i-1} - C^{\alpha}_{i}$ axis, which is tilted from the N–H bond direction [20,46–50,65,66], which thus represents non-trivial geometry, and for asymmetric motions [20,34,35,46,48–50,67–71]. The current MD-based picture visualizes that short-range correlations between dihedral-angles dominate protein dynamics, with information propagating through the protein in a diffusion-like manner via local interaction networks [72]. This picture implies rhombic ordering at N–H sites, in agreement with motion about the $C^{\alpha}_{i-1} - C^{\alpha}_{i}$ axis.

The scenario described above can be handled with SRLS; it is outside the scope of MF, which has no provision for tilted and/or rhombic tensors. Therefore S^2 and τ_e cannot be interpreted in terms of realistic models for restricted motions in proteins.

The overview presented above has been demonstrated quantitatively by comparing formally analogous SRLS and MF parameters. The application of SRLS and MF in parallel to a large number of data sets has shown that MF is frequently a force-fitting to the experimental data [19,20,34,35,46–50]. Namely, the statistical criteria are fulfilled but the best-fit parameters are inappropriate for physical interpretation, having absorbed unaccounted for factors. In most cases the differences between analogous SRLS and MF analyses were found to be quantitative in nature; in some cases substantial qualitative differences were detected [20].

3. Theories

3.1. Local motion without the global motion

3.1.1. General relaxation limit theory—Nordio and Busolin [30], and Freed and co-workers [31], treated diffusive rotational reorientation of an axial probe in a uniaxial liquid crystal. These developments can be viewed as treatments of diffusion-restricted local motion in proteins with the global motion frozen (alternatively, they apply to the overall motion of a biomacromolecule, such as a protein, embedded within a membrane). They are general in allowing for an arbitrary tilt between the local ordering/local diffusion and magnetic frames, and for magnetic tensors of arbitrary symmetry and orientation. Szabo also treated local motion with an axial ordering frame tilted from an axial interaction frame within the scope of fluorescence depolarization [52,73]. Polnaszek and Freed [14] extended the development of Ref. [31] by allowing for rhombic local molecular ordering.

In the theories developed in Refs. [30] and [31] one solves the rotational diffusion equation for the probability density $P(\Omega,t)$ for the orientation of the probe:

$$\partial P(\Omega,t)/\partial t = -\Gamma_{\Omega} P(\Omega,t),$$
$$\text{where } -\Gamma_{\Omega} = R\nabla_{\Omega}^{2} P(\Omega,t) - (R/k_{B}T)(\sin\beta)^{-1}\partial/\partial\beta[\sin\beta\, \mathrm{TP}(\Omega,t)]. \quad (3)$$

Equation (3) is appropriately referred to as a Smoluchowski equation. Here Γ_{Ω} is the diffusion operator, R is the isotropic rotational diffusion coefficient, ∇_{Ω}^{2} is the rotational diffusion operator in the Euler angles $\Omega \rightarrow \alpha, \beta, \gamma$, and T is the restoring torque. The latter is equal to $-\partial U/\partial\beta$ in the case of an axial restoring potential, e.g., $U \cong 3/2\, c_0^2 \cos^2\beta$ (c_0^2 is in units of $k_B T$). One diagonalizes the operator Γ_{Ω}, typically using the normalized forms of the Wigner rotation matrix elements, $D^{L}_{KM}(\Omega)$, as a convenient basis set, to obtain the eigenfunctions and

eigenvalues of Γ_Ω. Then the time correlation functions of these normalized $D^L_{KM}(\Omega)$ (as well as their cross-correlation functions with $D^{L'}_{K'M'}(\Omega)$ where $L' \neq L$, $K' \neq K$, and/or $M' \neq M$) may be expressed in terms of these eigenfunctions and eigenvalues. Their Fourier transforms yield the spectral densities from which the magnetic resonance relaxation parameters, such as T_1, T_2 and heteronuclear *NOE*, are calculated.

These time correlation functions are, in general, found to be a sum of exponential decays, where the decay constants are the respective eigenvalues, and the weighting factor of each decaying exponential gives the relative importance of that eigenfunction in the correlation function. The general expressions for rhombic $\boldsymbol{R}$ tensor and rhombic potential $U(\Omega)$, that replace the respective quantities in the Γ_Ω of Eq. (3), are given in Ref. [14]. Again, the time correlation functions for the $D^L_{KM}(\Omega)$ are found to be sums of exponential decays determined by the eigenfunctions and eigenvalues of the more general diffusion operator, Γ_Ω.

3.1.2. Specific models for internal mobility—Kinosita et al. [51] developed a stochastic model for wobble-in-a-cone in the presence of a square-well potential for a fluorescent probe embedded in a practically static membrane. The absorption (or emission) fluorescence dipole was taken collinear with the axial wobbling probe, the symmetry axis of which represents the local ordering/local diffusion axis. When the latter is collinear with the axial interaction axis, i.e., the "diffusion tilt" is zero, one has $C(t)=C^{\mathrm{L}}_{K=0}(t)$. The equilibrium probability density is given by $P_{\mathrm{eq}}(\theta) = (2\pi\sin\theta)^{-1}\,\delta(\theta - \theta_{\max})$, with $\theta_{\max}$ denoting the cone semi-angle. The function $C^{\mathrm{L}}_{K=0}(t)$ is given by:

$$C^{\mathrm{L}}_{K=0}(t)=\sum_{i=1,\infty} A_i \exp(-D_{\mathrm{w}} t/\sigma_{\mathrm{i}}). \tag{4}$$

The parameters $1/\sigma_{\mathrm{i}}$ are the eigenvalues of the Smoluchowski operator that describes the wobbling motion of an axial probe in a square-well potential. The parameters A_{i} are the corresponding weighting factors, and $D_{\mathrm{w}} = 1/(6\tau_\perp)$ is the wobbling rate constant. $D_{\mathrm{w}}/\sigma_\infty \rightarrow 0$, which implies $\exp(-tD_{\mathrm{w}}/\sigma_\infty) \rightarrow 1$, represents the rate constant associated with the practically static membrane.

It was shown that an effective decay constant, $D_{\mathrm{w}}/\langle\sigma\rangle$, where $\langle\sigma\rangle = \sum_i A_i\sigma_i$, with the summation running over the local motional terms, is valid for $\theta_{\max} \leq 50°$. When this condition is fulfilled, one has:

$$C^{\mathrm{L}}_{K=0}(t)=A_\infty+(1 - A_\infty)\exp(-D_{\mathrm{w}} t/\langle\sigma\rangle), \tag{5}$$

i.e., the function $C^{\mathrm{L}}_{K=0}(t)$ decays with rate constant $D_{\mathrm{w}}/\langle\sigma\rangle$ to a plateau value A_∞. The latter was shown to be given by:

$$A_\infty=[\,1/2\cos\theta_{\max}(1+\cos\theta_{\max})]^2. \tag{6}$$

Wang and Pecora [74] treated wobble-in-a-cone for a rhombic equilibrium probability density of probe orientations. For biaxial (rhombic) local ordering, a solution yielding analytical time correlation functions, $C^{\mathrm{L}}_K(t)$, does not exist, even when the global motion is frozen. However,

a numerical solution, given in terms of associated Legendre polynomials of non-integer degree, was obtained.

London and Avitabile [38] found that experimental ^{13}C relaxation data from methionine methyl groups in dihydrofolate reductase cannot be reproduced with free diffusion or symmetric jumps about the S–$^{13}CH_3$ axis (Woessner's model [59]) combined with axial fluctuations of the S–$^{13}CH_3$ axis. The experimental data could only be reproduced when the motion of the S–$^{13}CH_3$ axis was allowed to be asymmetric. Thus, the sensitivity of the experimental data to rhombic ordering at methyl sites in proteins was detected already in early solution work with a model-based approach. Partially averaged rhombic ^2H powder patterns from polycrystalline samples were also observed in early work [75]. A recent solid-state NMR study has shown with an elaborate analysis that the local ordering at the methyl sites of a given leucine residue of the chicken villin headpiece subdomain protein (HP36) is rhombic [76].

Wittebort and Szabo [77] developed spectral densities for a general jump model and illustrated it for the concerted motions of a lysine side chain.

The 3D Gaussian Axial Fluctuations (3D GAF) model [78] provides an analytical description of anisotropic peptide plane motion in terms of 3D harmonic local reorientational fluctuations that is consistent with molecular dynamics simulations. In its application to ^{15}N and $^{13}C'$ spin relaxation for the relatively rigid protein ubiquitin, 3D GAF reproduced the experimental data of 76% of the peptide planes studied [65]. The local fluctuations were found to be anisotropic, with the largest amplitude associated with motion about the $C^{\alpha}_{i-1} - C^{\alpha}_{i}$ axis. Thus, 3D GAF has proven that appropriate analysis of ^{15}N relaxation data from well-structured parts of the protein requires allowing for a "diffusion tilt" and anisotropic local restrictions. Experimental data from flexible regions of the protein backbone could not be reproduced with 3D GAF [65].

Internal motions in proteins have been treated by Wallach [79], Woessner [59,80], Daragan and Mayo [67], LeMaster [81], Korzhnev et al. [82], Atkinson and Kieffer [83], and others.

3.2. Local motion decoupled from the global motion

3.2.1. The Slowly Relaxing Local Structure: an early version—We provide here a simple version of the derivation first presented in Ref. [15] that led to an expression now commonly referred to as the model-free spectral density. That derivation was based upon straightforward stochastic considerations. It considers the reorientation of a local (spin) probe that is coupled to a slower reorienting object as a joint stationary Markov process. The local motion is restricted in its range of reorientation by the "local structure" around it; these restrictions are represented by a restoring potential. In the case of a spin-bearing entity on a protein, the overall tumbling of the protein is the slowly reorienting object, to which the spin-bearing entity is attached, and engaged in local diffusive motion relative to the slower moving frame of the protein.

We can describe the time-dependent Euler angles representing the orientation of the protein relative to a static lab frame by Ξ, and the Euler angles representing the probe orientation relative to the static lab frame by Ω. Then the joint probability density, $P(\Omega, \Xi, t)$, in the Euler angles Ω and Ξ becomes a composite (or multi-dimensional) Markov process, obeying the diffusion equation:

$$\partial P(\Omega, \Xi, t)/\partial t = -(\Gamma_{\Omega}+\Gamma_{\Xi})\, P(\Omega, \Xi, t), \tag{7}$$

where Γ_{Ω} is the rotational diffusion operator in Ω for the local probe motion. Because of the restoring potential, Γ_{Ω} will depend on the orientation of the protein, i.e., $\Gamma_{\Omega} = \Gamma_{\Omega}(\Xi)$, while

Γ_Ξ is the rotational diffusion operator associated with the protein tumbling. It is not necessary at this stage even to specify its exact form, although we give examples below.

Now we introduce the assumption that Ξ relaxes much more slowly than Ω. This assumption for the diffusion equation (7) above is analogous to the Born-Oppenheimer approximation in quantum mechanics. In fact, since diffusion equations such as (7) are mathematically similar to (but clearly physically very different from) quantum mechanical equations (i.e., the Schrödinger equation), we can employ similar methods of solution [84,85]. This B.-O. approximation can be written as:

$$P(\Omega, \Xi, t) \cong P_\Xi(\Omega, t) f(\Xi, t). \tag{8}$$

Here, $f(\Xi,t)$ is the probability density for the overall (protein) tumbling, which we take as independent of the local probe dynamics, so it obeys the simple rotational diffusion equation:

$$\partial f(\Xi, t)/\partial t = -\Gamma_\Xi f(\Xi, t), \tag{9}$$

(where we usually let $\Gamma_\Xi = -R^C \nabla_\Xi^2$, which is the standard rotational diffusion Laplacian operator acting on the Euler angles Ξ; in Section 3.3. these angles are denoted Ω_{LC}), whereas the much faster motion of the probe obeys the diffusion equation:

$$\partial \mathrm{P}_\Xi(\Omega, t)/\partial t = -\Gamma_\Omega(\Xi)\, \mathrm{P}_\Xi(\Omega, t), \tag{10}$$

where $\mathrm{P}_\Xi(\Omega,t)$ is the probability density function in Ω (denoted $\Omega_{C'M}$ in Section 3.3.) for a fixed value of Ξ. An explicit form for the diffusion operator $\Gamma_\Omega(\Xi)$ (not required in the derivation below) is $-\nabla_\Omega \cdot R^L \cdot \nabla_\Omega\, [1 + U(\Omega,\Xi)/k_B T]$. Here R^L is the rotational diffusion tensor for the local motion, and $U(\Omega,\Xi)$ is the potential for the local motion in Ω relative to the slowly relaxing orientation of the large body specified by Ξ. Note that Eq. (3) is a special case of Eq. (10) for isotropic $\boldsymbol{R}^{\mathbf{L}}$ and an axial potential.

Equations (9) and (10), being diffusion equations, have respective eigenfunctions and eigenvalues, as already noted in Section 3.1.1. The general solution to these equations may then be written as eigenfunction expansions. That is:

$$f(\Xi, t) = \sum_q d_q |\nu_q(\Xi)\rangle \exp(-\varepsilon_q t) \tag{11}$$

and

$$P_\Xi(\Omega, t) = \sum_m c_m |u_m(\Omega, \Xi)\rangle \exp(-E_m t) \tag{12}$$

written in eigen-ket notation, with ε_q and E_m the respective eigenvalues.[1]. Then from Eqs. (8), (11) and (12) we obtain the overall solution:

$$P(\Omega, \Xi, t) \cong \sum_{m,q} a_{m,q} |u_m(\Omega, \Xi)\rangle\, |\nu_q(\Xi)\rangle \exp[-(E_m + \varepsilon_q)t]. \tag{13}$$

The expansion coefficients $a_{m,q}$ are determined by an appropriate set of initial conditions. The conditional probability density, $P(\Omega_0,\Xi_0|\Omega,\Xi,t)$ arises from letting $\Omega = \Omega_0$ and $\Xi = \Xi_0$ at $t = 0$, corresponding to Dirac delta functions:

$$P(\Omega, \Xi, t=0)=\delta(\Omega - \Omega_0)\,\delta(\Xi - \Xi_0). \tag{14}$$

Then by Eq. (8) we have:

$$P(\Omega_0, \Xi_0|\Omega, \Xi, t) \cong P_{\Xi}(\Omega_0|\Omega, t) f(\Xi_0|\Xi, t). \tag{15}$$

Also, we have for stationary Markov processes the general relation:

$$P(\Omega_0, \Xi_0, \Omega, \Xi, t)=P_{eq}(\Omega_0, \Xi_0)P(\Omega_0, \Xi_0|\Omega, \Xi, t) \tag{16}$$

for the joint probability density in Ξ_0, Ξ, Ω_0 and Ω.

For spin relaxation, one is interested in the correlation function of the Wigner rotation matrix elements (cf. Section 3.2.1):

$$C_{-KM,K'M'}(t)= \langle D^{2*}_{KM}(\Omega_0)\, D^{2}_{K'M'}(\Omega)\rangle \tag{17}$$

in isotropic fluids. We will only consider here $K' = K$, $M' = M$ and isotropic fluids, for which $\langle D^2_{KM}(\Omega)\rangle = 0$; the general case is given in Ref. [15], including anisotropic fluids (e.g., membranes, liquid crystals). Also, for convenience of presentation in the following we will drop the 2 superscript and the K and M subscripts. Thus we have:

$$\langle D^*(\Omega_0)\, D(\Omega)\rangle = \int d\,\Xi_0 \int d\Omega_0 D^*(\Omega_0) P_{eq}(\Omega_0, \Xi_0) \int d\Xi \int d\Omega\, D(\Omega)\, P(\Omega_0, \Xi_0|\Omega, \Xi, t) \cong \int d\Xi_0 f(\Xi_0) \int d\Omega_0 P_{eq,\Xi}(\Omega)\, D^*(\Omega_0) \int d\Xi f(\Xi_0|\Xi, t) \int d\Omega\, P_{\Xi}(\Omega_0|\Omega, t)\, D(\Omega), \tag{18}$$

where the approximate equality results from the B.-O. approximation. Equation (17) can now be rearranged into the sum of three terms by straightforward application of the general properties of stationary Markov processes [15] to yield:

$$C(t)=C^{(1)}(t)+C^{(2)}(t)+C^{(3)}(t). \tag{19}$$

Here we have (somewhat simplified for present purposes):

$$C^{(1)}(t)= \int d\Omega_0 D^*(\Omega_0) \int d\Xi_0 f_{eq}(\Xi_0)\, P_{eq,\Xi 0}(\Omega_0) \int d\Omega\, D(\Omega) \int d\Xi f_{eq}(\Xi)\, P_{\Xi}(\Omega_0|\Omega, t) \tag{20a}$$

$$C^{(2)}(t)= \int d\Xi_0 f_{eq}(\Xi_0) \int d\Xi f(\Xi_0|\Xi, t) \int d\Omega\, D^*(\Omega_0)\, P_{eq,\Xi 0}(\Omega_0) \int d\Omega\, D(\Omega)\, P_{eq,\Xi}(\Omega) \tag{20b}$$

$$C^{(3)}(t)=\int d\Xi_0 f_{eq}(\Xi_0)\int d\Xi f(\Xi_0|\Xi,t)\cdot\int\cdot d\Omega_0\, D^*(\Omega_0)\, P_{eq,\Xi 0}(\Omega_0)\int d\Omega\, D(\Omega)\,[\,P_{\Xi}(\Omega_0|\Omega,t)-P_{\Xi eq}(\Omega_0|\Omega,t)]. \quad (20c)$$

Now consider $C^{(1)}(t)$ given by Eq. (20a) in more detail. First note that for isotropic systems $f_{eq}(\Xi) = 1/(8\pi^2)$ independent of Ξ. Then we have:

$$\int d\Xi_0 f_{eq}(\Xi_0)\, P_{eq,\Xi 0}(\Omega_0)=P_{eq}(\Omega_0)=1/(8\pi^2) \quad (21a)$$

and

$$\int d\Xi f_{eq}(\Xi)\, P_{\Xi}(\Omega_0|\Omega,t)=P_{eq}(\Omega_0|\Omega,t). \quad (21b)$$

Then

$$C^{(1)}(t)\cong\int d\Omega_0\, P_{eq}(\Omega_0)\, D^*(\Omega_0)\int d\Omega\, D(\Omega)\, P_{eq}(\Omega_0|\Omega,t). \quad (22)$$

Equation (22) is readily seen to be just the standard correlation function associated with the faster probe motion, independent of the overall tumbling. For a simple exponential decay we get $\langle[D(\Omega)]^2\rangle \exp(-t/\tau)= (1/5)\exp(-t/\tau)$ for a second rank $D^2_{KM}(\Omega)$. Thus, the effect of the overall tumbling must come from $C^{(2)}(t)$ and $C^{(3)}(t)$.

Now consider $C^{(2)}(t)$ for which the integral:

$$\int d\Omega\, D(\Omega)\, P_{eq,\Xi}(\Omega)\equiv S(\Xi) \quad (23)$$

refers to the restricted average of $D(\Omega)$ over Ω for a specific value of protein orientation, Ξ. This is the definition of the order parameter for the probe, S, relative to Ξ. Thus we may write:

$$C^{(2)}(t)=\int d\Xi_0 f_{eq}(\Xi_0)\, S(\Xi_0)\int d\Xi f(\Xi_0|\Xi,t)\, S(\Xi). \quad (24)$$

In the limit of low ordering, $S(\Xi) = S_\ell\, D(\Xi)$ [15], where S_ℓ is the local order parameter of the probe, so Eq. (24) becomes:

$$C^{(2)}(t)\cong S_\ell^2\int d\Xi_0 f_{eq}(\Xi_0)\, D(\Xi_0)\int d\Xi f(\Xi_0|\Xi,t)\, D(\Xi), \quad (25)$$

which is just S_ℓ^2 times the standard correlation function for the slow overall motion, so that for a simple exponential decay we get $S_\ell^2\ (1/5)\exp(-t/\tau_m)$, $\tau_m \gg \tau$.

More generally, with $f_{eq}(\Xi_0) = 1/(8\pi^2)$ for an isotropic medium, and letting $f(\Xi_0|\Xi,t) \propto \delta(\Xi - \Xi_0)\exp(-t/\tau_m)$, we get:

$$C^{(2)}(t)=\langle S^*(\Xi_0)\, S_0(\Xi_0)\rangle\exp(-t/\tau_m). \quad (26)$$

Given the definition of $S(\Xi_0)$ as the value of $S(\Xi)$ at $t = 0$, it is reasonable to identify its average over $f_{eq}(\Xi_0)$ to yield:

$$C^{(2)}(t) \approx (1/5)\, S_\ell{}^2 \exp(-t/\tau_m). \tag{27}$$

We now consider $C^{(3)}(t)$, which involves the combined time dependences on Ξ and Ω, and thus has the property of being a cross-term. It arises because of the statistical dependence of $\Omega(t)$ on Ξ, i.e., the orientation of the probe is coupled to that of the protein. As a result, its evaluation is somewhat more complex than $C^{(1)}(t)$ or $C^{(2)}(t)$. Here we will again let $f(\Xi_0|\Xi,t) \propto \delta(\Xi - \Xi_0)\exp(-t/\tau_m)$, and $[P_\Xi(\Omega_0|\Omega,t) - P_{\Xi eq}(\Omega_0|\Omega,t)] = -P_{eq,\Xi}(\Omega)\exp(-t/\tau)$, which can be shown to follow from letting

$$P_\Xi(\Omega_0|\Omega,t) = P_{eq,\Xi}(\Omega) + [\delta(\Omega - \Omega_0) - P_{eq,\Xi}(\Omega)]\exp(-t/\tau). \tag{28}$$

Then:

$$C^{(3)}(t) \approx -\int d\Xi_0 f_{eq}(\Xi_0) \int d\Xi \exp(-t/\tau_m) \int d\Omega_0 D^*(\Omega_0)\, P_{eq,\Xi 0}(\Omega_0) \int d\Omega\, D(\Omega) P_{eq,\Xi}(\Omega) \exp(-t/\tau). \tag{29}$$

This expression is seen to be very similar to that of Eq. (25) and may now be evaluated in an equivalent manner to yield

$$C^{(3)}(t) \approx -(1/5)\, S_\ell{}^2 \exp(-t/\tau_m)\exp(-t/\tau). \tag{30}$$

Collecting terms we now have:

$$C(t) \approx (1/5)\,[\exp(-t/\tau) + S_\ell{}^2 \exp(-t/\tau_m) - S_\ell{}^2 \exp(-t/\tau_m)\exp(-t/\tau)], \tag{31}$$

which when Fourier transformed yields the spectral density:

$$j(\omega) = (1/5)\,\{\tau/(1+\omega^2\tau^2) + S_\ell{}^2[(\tau_m/(1+\omega^2\tau_m{}^2) - \tau^{|}/(1+\omega^2(\tau^{|})^2)]\}, \tag{32}$$

where $(\tau^{|})^{-1} \equiv (\tau)^{-1} + \tau_m{}^{-1} \cong (\tau)^{-1}$, since $\tau_m{}^{-1} \ll (\tau)^{-1}$ by hypothesis. This expression is identical to that of Eq. (5.5) in Ref. [15] for the case of an isotropic medium. That expression also includes the effect of the large body (e.g., protein) in an ordered medium (e.g., a membrane bilayer). Disregarding the coefficients 1/5, which is often included in the definition of the squared magnetic interaction, Eq. (32) is equivalent to Eq (1): $S_\ell{}^2$ in Eq. (32) is the same as $(S_0^2)^2$ in Eq. (1); one obtains a local motional term multiplied by $(1 - S_\ell{}^2)$, by analogy with a local motional term multiplied by $(1 - (S_0^2)^2)$ in Eq. (1).

We have also introduced a number of simplifications in this derivation to provide simpler insight. The more detailed derivation with its subtleties is given in Ref. [15]. Note that the essence of the derivation is simply based on a fast process coupled to a slow process following Markov statistics. This is sufficient to yield Eq. (32) provided we simplify the tensorial properties of the spin Hamiltonian and the "double tensor" properties of the $D^L_{KM}(\Omega)$ [86], as

well as use only the simplest form of the diffusive motions and local probe ordering by neglecting their full tensorial properties. Reference [15] explicitly considers these tensorial properties, but keeps them simple.

This approach has been generalized in Ref. [21] to include a rhombic potential term. Then along with the full tensorial properties of the $D^{L}_{KM}(\Omega)$ it yields the more general time correlation functions, $C_{-K,-K',M}$, and by Fourier-Laplace transformation the more general spectral densities, $j_{-K,-K',M}(\omega)$:

$$C_{-K,-K',M}(t) = \langle D^{2*}_{K',M}(\Omega_0)\, D^{2}_{KM}(\Omega)\rangle \tag{33}$$

$$j_{-K,-K',M}(\omega) \equiv \Re\int_0^\infty dt\, C_{-K,-K',M}(t)\exp(-i\omega t) = (1/5)\{\tau_K/(1+\omega^2\tau_K{}^2) + [\tau_m/(1+\omega^2\tau_m{}^2) - \tau^{|}_K/(1+\omega^2(\tau^{|}_K)^2)]\langle S^*_{\ell,K}, S_{\ell,K}\rangle\}, \tag{33a}$$

where $S_{\ell,K}$ are the spherical tensorial order parameters (K, K' = 2, 1, 0, −1, −2).

The other limit of SRLS that leads within a good approximation to an equation formally analogous to Eq. (1) was described in Section 2.1. It involves the same simplifications of the tensorial properties in the limit of large time scale separation, but it requires the prevalence of strong axial, instead of weak axial, local potentials [14,31]. In this limit one has a dominant "renormalized" local motional correlation time given by $2\tau/c_0^2$, which may replace τ in Eq. (1).

3.2.2. Specific models for decoupled internal motions—Halle and Wennerström [87] developed Eq. (1) in the context of ^{2}H relaxation of water in heterogeneous systems A two-step model featuring slow isotropic overall motion, fast isotropic local motion, and small axial local ordering collinear with an axial magnetic tensor, was set forth. Rhombic (biaxial) magnetic tensors are also allowed for. However, the equation that justifies this generalization (Eq. (137), Ch. VIII, Ref. [28]) applies in the extreme motional narrowing limit for the local motion. The various steps pursued in developing the two-step model involve casting the local motion in the form of equilibrium averages, and expressing the spin Hamiltonian as a sum of a quasi-single-crystal slow motional term, and a fast motional term that represents the departure from this equilibrium value. These features also rely on the assumption of extreme motional narrowing for the local motion.

Brainard and Szabo [60] developed a model featuring the global motion, τ_m, a local motion on the surface of a cone with semi-cone angle β and correlation time $\tau_{\|}$, and axial fluctuations of the cone axis with order parameter called SD and correlation time $\tau_\perp$. The various dynamic modes are assumed statistically independent of one another. The factor $P_2(\cos\beta)$ is taken as the order parameter for the parallel motion. An analytical local motional time correlation function is developed as a Padé approximant. With β set equal to 110.5°, this time correlation function yields the MF formula for methyl dynamics, with τ_e replacing both $\tau_{\|}$ and $\tau_\perp$. It is indicated in Ref. [60] that the overall order parameter, S, may be set equal to $P_2(\cos\beta)\times SD$ when $\tau_{\|} \to 0$ and $\tau_\perp \to 0$. As pointed out in Ref. [38], this model could not reproduce experimental ^{13}C relaxation data from the methionine methyl groups of dihydrofolate reductase (DHFR). Note that in Woessner's model [59], which is the same as the model for the parallel motion in the present development, $\tau_\perp$ represents τ_m.

Lipari and Szabo [88] applied the function $C^{L}_{K=0}(t)$ developed by Kinosita et al. [51] to NMR spin relaxation in proteins in the form of $C(t)=\exp(-t/\tau_m) \times C^{L}_{K=0}(t)$. An analytical expression for τ_e as a function of $\cos\theta_{max}$ and D_w, valid for $\theta_{max} < 50°$, was developed. In Ref. [52] Szabo solved a Smoluchwski equation for axial local ordering and zero "diffusion tilt" to obtain (in agreement with previous developments [14,30–33]) $S^2_0 = <P_2(\cos\theta)>$ for the value of $C^{L}_{K=0}(\infty)$.

In a subsequent paper Lipari and Szabo [89] considered all three components $C_K(t)$, $K = 0$, 1 and 2, of wobble-in-a-cone for non-axial ordering in the presence of a square well potential [89]. Padé approximants were developed for $C_K(t)$. For $0 < \theta_{max} < 90°$, $K = 0, \pm 2$, and $0 < \theta_{max} < 75°$, $K = \pm 1$, the decay constants, $1/\tau_K$, and the $j_K(0)$ values, are given analytically as functions of $\cos\theta_{max}$ and D_w. The availability of all three $C_K(t)$ functions allows for the possibility of local ordering/local diffusion axes tilted from the magnetic frame. To our knowledge, this capability has not been utilized.

The next papers in the series of Lipari and Szabo papers are Refs. [11] and [12]. Here Eq. (2) is set forth in a "model-free" manner. The assumptions and implications associated with this concept are outlined in the next section.

3.2.3. Model-free—The MF spectral density is given by Eq. (2) [11,12]. The following considerations lead to this formula. The total time correlation function, $C(t) = C^C(t) \times C^L(t)$, is defined as $<P_2(\cos\theta_{LD}(t))P_2(\cos\theta_{LD}(t+\tau))>$, where L and D denote the axial laboratory and magnetic (dipolar) frames. The time correlation function for isotropic global motion is given by $C^C(t) = \exp(-t/\tau_m)$. The following form is suggested for the time correlation function for the local motion:

$$C^L(t)=S^2+(1-S^2)\exp(-t/\tau_e), \tag{34}$$

where S^2 is the squared generalized order parameter, and τ_e is the effective correlation time for the local motion. The Fourier transform of the time correlation function obtained by multiplying Eq. (34) by $C^C(t) = \exp(-t/\tau_m)$ yields Eq. (2).

The squared generalized order parameter, S^2: The parameter S^2 represents $C(\infty)$. The latter quantity is set equal to $\sum_{m=0,\pm1,\pm2} <|Y_{2m}(\theta,\varphi)|>^2$, based on the addition theorem of spherical harmonics, and S^2 is designated as the square of a "generalized" order parameter. As outlined in Section 2.2., the angle φ is undefined, and the relation of S to $S^2_0 \propto <Y_{20}>$ is unclear.

Within the scope of spin relaxation, order parameters are principal values of ordering tensors, defined in terms of local potentials [14,30–33]. They represent ensemble averages. In irreducible tensor notation only two order parameters, S^2_0 and S^2_2, persist for $L = 2$ if there is at least 2-fold symmetry around the main ordering axis and 3-fold symmetry around the local director. In Cartesian tensor notation there are in this case three order parameters, S_{xx}, S_{yy} and S_{zz}, with $S_{xx} + S_{yy} + S_{zz} = 0$, with $S^2_0 = S_{zz}$ and $S^2_2 = \sqrt{2/3}(S_{xx} - S_{yy})$.

Thus, as defined in MF S^2 is conceptually an artificial quantity. Since the actual local ordering is rhombic [20,48,50], in practice the experimental data are force-fitted when Eq. (2), which comprises only a single order parameter, is used.

The effective local motional correlation time, τ_e: The parameter τ_e is defined as [11]:

$$\tau_e \equiv \{\int [\sum_{i=1}^{\infty} a_i \exp(-t/\tau_i)]\, dt\}/(1-S^2) = \sum_{i=1}^{\infty} a_i\, \tau_i/(1-S^2). \quad (35)$$

The integrand represents the exact time correlation function for local motion; this assumes that $\tau_0 \equiv \tau_m = \infty$. Although this scenario is clearly unrealistic there might be conditions under which Eq. (35) is valid within a good approximation. The mathematical definition of τ_e prevents identifying these conditions. As pointed out above, S^2 must be either close to zero or close to 1 for the single decay approximation for the local motion to be valid. The parameter τ_e is undefined by Eq. (35) in the limit in which $S^2 \to 1$.

Statistical independence between the global and local motions is contingent upon large time scale separation: The general expression for a time correlation function describing fast restricted Markovian internal motions with correlation times, τ_i, in practically static surroundings reorienting (formally) with correlation time, τ_0, is given by [11]:

$$C^L(t) = \sum_{i=0}^{\infty} a_i \exp(-t/\tau_i), \quad (36)$$

with $\tau_0 = \infty \gg \tau_1, \tau_2, \ldots$ and $a_0 = C(\infty)$. One may write:

$$C^L(t) = a_0 \sum_{i=1}^{\infty} a_i \exp(-t/\tau_i). \quad (37)$$

Let us denote a_0 as S^2. Since $\exp(-t/\tau_0) = 1$ by virtue of $\tau_0 = \infty$, and since in the context of protein dynamics τ_0 represents τ_m, one may write:

$$C(t) = \exp(-t/\tau_m) \times C^L(t) = (C^C(t) = 1) \times C^L(t) = S^2 + \sum_{i=1}^{\infty} a_i \exp(-t/\tau_i). \quad (38)$$

Thus, $C(t)$ is given rigorously by $C^C(t) \times C^L(t)$ when $\tau_m = \infty$. Since the protein is reorienting in solution τ_m is obviously not infinity. However, in the large time scale separation limit where $\tau_m \gg \tau_1, \tau_2, \ldots$, one may assume that within a good approximation $C(t) \sim [C^C(t) = \exp(-t/\tau_m)] \times C^L(t)$. One may restate this to say that the local motion may be treated for "frozen" global motion. This is the meaning of statistical independence, or "mode-decoupling", in MF. Clearly large time scale separation is a contingency, and the factorization of $C(t)$ into $C^C(t) \times C^L(t)$ is an approximation. This is shown rigorously in Section 3.2.1.

Theoretical validation of the MF formula: One has to show that Eq. (34) is a good approximation to Eq. (37). This cannot be accomplished at the level of the time correlation function. The following is done instead. Based on the assumption that statistical independence remains valid when $C^C(t) = 1$ is replaced by $C^C(t) = \exp(-t/\tau_m)$, where $\tau_m \neq \infty$, by virtue of $\tau_m \gg \tau_1, \tau_2, \ldots$, one obtains the expression:

$$C(t) = C^C(t) \times C^L(t) = \exp(-t/\tau_m)\,[S^2 + \sum_{i=1}^{\infty} a_i \exp(-t/\tau_i)]. \quad (39)$$

Fourier transformation of Eq. (39), and the assumption that the local motions are in the extreme motional narrowing limits, lead to:

$$J(\omega)=S^2\,\tau_m/(1+\omega^2\tau_m{}^2)+\sum_{i=1}^{\infty}a_i\,\tau_i. \tag{40}$$

Multiplying Eq. (34) by $C^C(t) = \exp(-t/\tau_m)$, applying Fourier transformation and assuming that $\tau_e \ll \tau_m$, yields Eq. (2). In the extreme motional narrowing limit, Eq. (2) yields:

$$J(\omega)=S^2\,\tau_m/(1+\omega^2\tau_m{}^2)+(1-S^2)\,\tau_e. \tag{41}$$

This is the same as Eq. (40) provided τ_e is defined by Eq. (35). Thus, Eq. (34) is validated in the form of a limiting case of the Fourier transform of its product with $\exp(-t/\tau_m)$, assuming that large time scale separation is in place.

The requirement for large time scale separation is invoked explicitly in the derivation of Eqs. (35) and (41) of Ref. [11], and in the context of Eqs. (57) and (58) of Ref. [11].

The symmetry of the local motion: There is confusion in the literature (e.g., Ref. [54]) with respect to the physical quantity that addresses the symmetry of a restricted local motion. The symmetry of a restricted motion is determined by the manner in which the spatial orientations are sampled. The form of the respective conformational space is given by the equilibrium probability density function, $P_{eq}(\theta,\varphi)\sin\theta\,d\theta\,d\varphi$ (in general, $P_{eq}(\Omega)$, $\Omega \rightarrow (\alpha, \theta, \varphi)$). The function $P_{eq}(\theta,\varphi)$, determined by the form of the local potential, is used to calculate order parameters [32,33]. Thus, the symmetry of a restricted motion is determined by the symmetry of the local ordering tensor, or the symmetry of the local potential in terms of which the order parameters are defined. The highest symmetry of the local potential, and of the local ordering tensor, is axial symmetry.

The local rotational diffusion tensor is determined mainly by the shape of the probe. It is independent of P_{eq}. In principle, the highest symmetry of the local diffusion tensor is axial symmetry, otherwise the orientational restrictions are not “sensed” by the probe. In practice, one may approximate the local diffusion tensor as isotropic in the large time scale separation limit. Clearly, a scalar quantity cannot address the symmetry of the local motion, as suggested in some cases [54].

The local geometry: In general, the local ordering frame (determined by liquid dynamics considerations) and the magnetic frame (determined by quantum mechanical considerations) are not the same. The MF formula does not allow for accommodating the difference between these frames. They are intrinsically identical and axially symmetric in MF.

The effect of the local potential on the eigenfunctions of the uncoupled local motional diffusion operator: The fact that in the presence of a local potential the Wigner functions are no longer eigenfunctions of the (axial) diffusion operator was established in early work [14, 30–33] and outlined in Section 3.1.1. Single exponent representation of the local motional term in MF constitutes simple Wigner function representation of the (uncoupled) local motional diffusion operator. As shown below, the effect of the local potential on the simple (Wigner function) basis set of the uncoupled diffusion operator (Section 3.1.1.) is very large even for weak potentials. This important aspect is completely ignored in MF.

Post-fitting interpretation of the MF parameters: Any model used to interpret S^2 and τ_e obtained with "model-free" fitting should pertain to the large time scale separation limit, have simple functions as eigenfunctions of the uncoupled local motional diffusion operator, and have τ_e limited according to the particular model considered. It should feature isotropic global and local motions, axial local ordering, and collinear local ordering, local diffusion and magnetic frames. Few motions comply with all of these requirements. In general, they are not realistic [20,40].

The extended model-free (EMF) spectral density: The EMF spectral density is given by [13]:

$$J(\omega)=S_f^2[S_s^2\tau_m/(1+\omega^2\tau_m^2)+(1-S_s^2)\,\tau_s^{|}/(1+\omega^2\tau_s^{|2})]+(1-S_f^2)\,\tau_f^{|}/(1+\omega^2\tau_f^{|2}). \quad (42)$$

The parameter τ_f is the effective correlation time for fast local motion, $\tau_s > \tau_f$ is the effective correlation time for slow local motion, and S_s^2 and S_f^2 are squared generalized order parameters associated with these motions. $1/\tau_f^{|} = 1/\tau_f + 1/\tau_m \sim 1/\tau_f$ and $1/\tau_s^{|} = 1/\tau_s + 1/\tau_m$. The large time scale separation assumption requires that $\tau_f \ll \tau_m$ and $\tau_s \ll \tau_m$. As pointed out above, it is inappropriate to use Eq. (42) when τ_s and τ_m occur on the same time scale, because mode-coupling, which dominates the actual spectral density in this parameter range, is ignored. It is also inappropriate to omit the third term of Eq. (42), as is often done, because the coefficients of the various terms in a physical spectral density sum to unity. Hence omitting terms entails force-fitting. Simplifications should be made at the stage where the time correlation functions are set forth; this is clearly not possible with a "model-free" approach. Besides, we found that the SRLS analogue of τ_f, the correlation time $\tau_{\|}=1/(6\,R_{\|}^{L})$, does affect the analysis [90]. Setting $\tau_{\|} \rightarrow 0$ leads to inappropriate results [90].

The MF spectral density adapted to methyl dynamics: As already indicated, in this context S^2 and τ_e are taken to represent both rotation around the C–CH_3 bond, and fluctuations of the C–CH_3 bond. The typical probe is the uniformly ^{13}C-labeled, fractionally deuterium-labeled methyl group $^{13}CDH_2$, with the deuterium nucleus observed [22]. The relevant magnetic interaction for the spin I = 1 ^{2}H nucleus is the quadrupolar interaction, Q. As pointed out above, in the context of HC-HH cross-correlation, a bond length of $r_{CD} = r_{CH} = 1.115$ Å is consistent with a tetrahedral angle of 110.5° [24]. The generalized order parameter, S, is expressed as $S = [P_2(\cos 110.5°)]\times S_{axis} = 0.316\times S_{axis}$, where 0.316 ($S_{axis}$) is the order parameter for motion about (of) C–CH_3. The correlation time, τ_e, is common to both local motions [11,12,36]. This yields the spectral density for quadrupolar spin relaxation in $^{13}CDH_2$:

$$J^{QQ}(\omega)=0.1\times S_{axis}^2\,\tau_m/(1+\omega^2\,\tau_m^2)+(1-0.1\times S_{axis}^2)\,\tau_e^{|}/(1+\omega^2\,\tau_e^{|2}), \quad (43)$$

where $1/\tau_e^{|} = 1/\tau_e + 1/\tau_m \sim 1/\tau_e$.

Extended versions of Eq. (43) for treating methyl dynamics have been also suggested [24].

Equation (43) represents three motional modes: reorientation about the C–CH_3 axis according to Woessner's model [59], axial fluctuations of the C–CH_3 axis, and global tumbling. Let us examine the case wherein $S_{axis}^2 = 1$; in this limit Eq. (43) should reproduce Woessner's model for methyl rotation.

Woessner's model: Diffusive (or jump-type) motion about an axis tilted at a fixed angle, β (110.5° for methyl rotation) from an axial magnetic frame is treated. The decay constants are $(\tau^{|}_1)^{-1} = 1/\tau_m + 1/\tau$ and $(\tau^{|}_2)^{-1} = 1/\tau_m + 4/\tau$, where τ represents the axial correlation time for

local motion about the z-axis of the local diffusion tensor (for symmetric jumps one has $(\tau^{|}_1)^{-1} = (\tau^{|}_2)^{-1} = 1/\tau_m + 1/\tau$, where $1/\tau$ is the jump rate constant). The internal diffusion axis tumbles isotropically with correlation time τ_m, and $\tau_m \gg \tau$. The measurable spectral density (applied here to quadrupolar relaxation of $^{13}CDH_2$) is given by [59]:

$$J^{QQ}(\omega)=0.1\tau_m/(1+\omega^2\tau_m{}^2)+0.323\tau^{|}_1/(1+\omega^2(\tau^{|}_1)^2)+0.577\tau^{|}_2/(1+\omega^2(\tau^{|}_2)^2) \quad (44)$$

$(d^2_{00}(110.5^o))^2=0.1$, $2(d^2_{01}(110.5^o))^2=0.323$ and $2(d^2_{02}(110.5^o))^2=0.577$, where $d^2_{0\kappa}$ denotes the reduced Wigner matrix element and $K = 0$, 1 and 2, transform the local diffusion frame into the magnetic frame. The isotropic tumbling limit, $J^{QQ}(\omega) = \tau_m/(1 + \omega^2\tau_m{}^2)$, is obtained for $\tau \to \infty$, $\beta_{MQ} \to 0$, or both.

The following emerges. (1) Eq. (44) requires that $\tau_m \gg \tau$. Therefore, Eq. (43) should not be used when τ_e is on the order of τ_m. This is actually implicit in MF but often not appreciated (see, for example, Ref. [91]). (2) Eq. (43) does not converge to the isotropic tumbling limit. It yields $J^{QQ}(\omega) = 0.1\tau_m/(1 + \omega^2\tau_m{}^2)$ for $S_{axis}{}^2 = 1$ and $\tau_e \to 0$; this differs from the Woessner model limit (see above). (3) In Woessner's model the diffusion axis tumbles isotropically; Eq. (43) features a diffusion axis fluctuating with axial order parameter, S_{axis}. Therefore S_{axis} is physically vague. (4) The parameter τ_e in Eq. (43) is taken to represent at the same time an effective correlation time for local motion, the axial component of the internal probe diffusion (τ in Woessner's model), and axial fluctuations of the C–CH_3 axis; the latter tumbles isotropically in Woessner's model. Therefore τ_e is physically vague. (5) As already noted, 0.1 in Eq. (43) is a coefficient associated with a frame transformation, not an order parameter. Therefore $S_{axis}{}^2 = S^2/0.1$ is also physically vague, especially since S^2 is taken as a generalized order parameter.

The Very Anisotropic Reorientation (VAR) model [18,92] describes the same physical scenario as Woessner's model in terms of an effective diffusion operator of the form:

$$\widehat{\Gamma}=R^L_{\|}(\widehat{\mathbf{J}}^L_z)^2+R^C(\widehat{\mathbf{J}}^L)^2. \quad (45)$$

$\hat{\mathbf{J}}^L$ is the infinitesimal rotation operator for internal probe diffusion equivalent to ∇_Ω in Eq. (3), $\widehat{\mathbf{J}}^L_z$ refers to its z component (z is the axis about which the internal rotation occurs), and $R^L_{\|} \gg R^C$. The parameters R^C and $R^L_{\|}$ represent the global and internal diffusion coefficients, respectively, with the tilt angle β_{MQ} between the internal diffusion z-axis and the principal z-axis of the magnetic tensor to be specified.

VAR is a limiting case of SRLS wherein the axial coupling potential is very large, i.e., $c^2_0 \to \infty$ equivalent to $S^2 \to 1$. We found that the parameter set comprising $c^2_0=20$, $\beta_{MQ} = 110.5°$ and $R^C = 0.001$ (in units of $R^L_{\|}$) yields, within a good approximation, single-exponential time correlation functions $C_{00}(t)$, $C_{11}(t)$ and $C_{22}(t)$ with eigenvalues of $1/\tau_m$, 1 and 4, respectively. Given that $\tau/\tau_m = 0.001$, these eigenvalues are the same as $1/\tau_m$, $(\tau^{|}_1)^{-1} = 1/\tau_m + 1/\tau \sim 1/\tau$ and $(\tau^{|}_2)^{-1} = 1/\tau_m + 4/\tau \sim 4/\tau$ in Eq. (44); in units of $1/\tau$ one obtains $1/\tau_m$, 1 and 4, respectively.

The physical meaning of Eq. (43): This formula may be taken as a B.-O. limit of SRLS. It represents a diffusive local motion time scale separated from isotropic global motion, taking place in the presence of a weak axial local potential. The corresponding (axial) local ordering tensor has its principal axis tilted at 110.5° from the (axial) magnetic frame.

Let us consider Eq. (33a) for the quantum number M set equal to zero and axial local ordering with $(S_0^2)^2 \equiv <S^*_{\ell,0}S_{\ell,0}>$ (we ignore the coefficient 1/5). The functions $j_{KK}(\omega)$, with $KK = (0,0)$, (1,1) and (2,2), are given by:

$$j_{00}(\omega)=(S_0^2)^2\,\tau_m/(1+\omega^2\tau_m{}^2)+(1-(S_0^2)^2\,\tau_0/(1+\omega^2\tau_0{}^2), \tag{46a}$$

$$j_{11}(\omega)=\tau_1/(1+\omega^2\tau_1{}^2), \tag{46b}$$

and

$$j_{22}(\omega)=\tau_2/(1+\omega^2\tau_2{}^2). \tag{46c}$$

The measurable spectral density, $J^{QQ}(\omega)$, is given by:

$$J^{QQ}(\omega)=(d^2_{00}(110.5^o))^2\,j_{00}(\omega)+2(d^2_{01}(110.5^o))^2\,j_{11}(\omega)+2(d^2_{02}(110.5^o))^2\,j_{22}(\omega)=0.1\,j_{00}(\omega)+0.323\,j_{11}(\omega)+0.577\,j_{22}(\omega). \tag{47}$$

Assuming that $\tau_0 = \tau_1 = \tau_2 = \tau$ (by virtue of $\tau_m \gg \tau_K$), one obtains:

$$J^{QQ}(\omega)=0.1\times(S_0^2)^2\,\tau_m/(1+\omega^2\tau_m{}^2)+(1-0.1\times(S_0^2)^2)\,\tau/(1+\omega^2\tau^2). \tag{48}$$

This is the same as Eq. (43) wherein $S_{axis}{}^2$ is replaced by $(S_0^2)^2$ and τ_e is replaced by τ. The factor 0.1 is $(d^2_{00}(110.5^o))^2$.

The local potential is given by $u(\Omega_{CM})$, where M is the local ordering frame fixed in the probe and C = C′ is the local director fixed in the protein (for isotropic global diffusion C and C′ are the same). The potential in Eq. (48) is axially symmetric and weak. This implies broad axially symmetric distribution of the instantaneous orientation of the C-CH_3 bond (i.e., the Z_M axis) about the equilibrium distribution of the C-CH_3 bond (i.e., the C′ ≡ C axis). This is difficult to rationalize for tightly packed protein cores.

On the other hand, weak but rhombic local potentials imply non-axial distribution of the instantaneous orientation of the bond vector C-C around the local director. Tightly packed protein cores can accommodate such excursions. For example, one may conceive of diffusion in two (or more) rotamer wells with less frequent jumps between them [17], or asymmetric torsional oscillations within a given rotamer well. As shown below, these are the potentials forms determined from the SRLS analysis.

Comments on the MF point of view: Equation (2) represents an approximation to a probe reorienting inside a “frozen” protein. The spatial restrictions at the site of the motion of the probe, i.e., on the M frame, are exerted by the immediate protein surroundings, represented by the C′ frame. This is formally analogous to the spatial restrictions at the site of the motion of a rigid (non-spherical) particle exerted by a liquid crystalline director. Numerous studies of

restricted motions in liquid crystals have shown that general tensorial properties, and the effect of the restricting potential on the eigenfunctions of the diffusion operator, have to be accounted for [14,30–33]. This leads to intricate numerical solutions. Hence, realistic spectral densities for treating protein dynamics cannot be simple (analytical) functions, even when mode-coupling is not important.

When the time scale separation is not large, “mode-coupling” was shown theoretically to be important in the overdamped diffusion limit [16]. This prediction, which involves intricate time correlation functions, was borne out by numerous SRLS applications to ESR spin labeled lipids, gramicidin, proteins and nucleic acid fragments [41–45]. It was further confirmed by SRLS applications to NMR spin relaxation in proteins [19,20,34,35,46–50].

In spite of this evidence, the limitations of the simple MF method are still not generally appreciated. Thus, it is stated in Ref. [54] that (1) the time scale separation is a “merely sufficient but not necessary condition”, (2) “the internal motion can be approximated by a single exponential”, and (3) “the robustness of MF to asymmetric motion is warranted” by recovering similar S^2 values with the MF spectral density and the formula of Ref. [37]. The latter is an analytical expression valid for ultrafast vibrations, librations and stretching motions, based on the results of normal mode analysis. It has been overlooked in Ref. [54] that both expressions used are only valid for simple fast axial local motions.

3.3. Local motions coupled to the global motion: the Slowly Relaxing Local Structure approach

The fundamentals of the stochastic coupled rotator slowly relaxing local structure theory, as applied to NMR spin relaxation in proteins [19,20], are summarized below.

3.3.1. Geometry—The various reference frames that define the SRLS model are shown in Fig. 1a. They are related to the N–H bond as the probe. The laboratory L frame is space-fixed with its Z-axis aligned along the external magnetic field, B_0. The global diffusion frame, C, and the (uniaxial) local director frame, C′, are both fixed in the protein. The Z-axis of the C′ frame lies along the equilibrium orientation of the $^{15}N–^{1}H$ bond (note that the time-independent Euler angles, $\Omega_{CC'}$, are used in Residual Dipolar Coupling (RDC)-based structure-determination protocols). M is the coordinate frame in which the local ordering tensor is diagonal. In previous work we assumed for simplicity that the local diffusion tensor is diagonal in the same frame [19,20]. In our most recent fitting scheme for SRLS [90] the local ordering and local diffusion frame may be distinguished.

The magnetic $^{15}N–^{1}H$ dipolar tensor frame, D, and the magnetic ^{15}N CSA tensor frame CSA, are both fixed in the probe. The Euler angles for rotation from M to D are given by Ω_{MD}, and the Euler angles for rotation from D to CSA by Ω_{CSA}. The Euler angles Ω_{MD} and Ω_{D-CSA} are time independent. The D frame is taken as axially symmetric. If the M frame is also axially symmetric, then $\Omega_{MD} = (0,\beta_{MD},0)$, where β_{MD} is known as ‘diffusion tilt’. The angle β_{MD} is determined with data fitting. Its value identifies the main local ordering axis.

The L frame, with Z_L along the magnetic field, B_0, is an inertial frame with respect to which all the moving frames are defined. The time-dependent Euler angles Ω_{LM} are associated with the local motion; both the local and global motions modulate them. The time-dependent Euler angles Ω_{LC} are associated with the global tumbling; only this motion modulates them.

We consider relative (probe versus protein) coordinates, expressing Ω_{LM} as $\Omega_{LM} = \Omega_{LC} + \Omega_{CC'} + \Omega_{C'M}$. A shorthand notation for indicating sequences of rotations will be employed. Namely, for a generic rotation $\Omega_{12} = \Omega_2 + \Omega_1$, resulting from first applying the rotation involving angles Ω_1, and then applying the rotation involving the angles Ω_2, the explicit relation

among Wigner rotation matrices is $D^L_{MK}(\Omega_{12})=\sum_{M'} D^L_{MM'}(\Omega_1)\, D^L_{M'K}(\Omega_2)$. The time-dependent Euler angles $\Omega_{C'M}$ represent the (typically faster) reorientation of the probe with respect to the protein.

A segment of the protein backbone comprising the atoms C^{α}_i, Ni, HNi, CO_{i-1}, O_{i-1} and C^{α}_{i-1}, the equilibrium positions of which lie within the peptide plane defined by N_i, HN_i, CO_{i-1} and O_{i-1}, is illustrated in Fig. 1b. The axis Z_D, which lies along the N–H bond, and the axis X_M, which for N-H bond dynamics turned out by data fitting to be the main local ordering/local diffusion axis lying along $C^{\alpha}_{i-1} - C^{\alpha}_i$, are shown.

The local motional diffusion tensor, R^L, is diagonal in the M frame. The global motional diffusion tensor, R^C, is diagonal in the C frame. We start by assuming Smoluchowski dynamics for the coupled set of orientational coordinates Ω_{LM} and Ω_{LC}, according to the SRLS approach. Namely, the system consists of two Brownian rotators (or 'bodies'), the N–H bond (probe) and the protein (cage), coupled by an interaction potential which depends on their relative orientation. Each 3D uncoupled rotator (assumed axial, i.e., $R_x = R_y = R_\perp$ and $R_z = R_\parallel$) is associated with three decay rates $\tau_K^{-1}=6R_\perp+K^2(R_\parallel - R_\perp)$, $K = 0, 1, 2$, where R stands for either R^C or R^L. The diffusion equation for the coupled system is given by:

$$\frac{\partial}{\partial t}P(X,t)= -\widehat{\Gamma}P(X,t) \tag{49}$$

where X is a set of coordinates completely describing the system. One has [19]:

$$X=(\Omega_{LM},\Omega_{LC})$$
$$\widehat{\Gamma}=\widehat{J}(\Omega_{LM})\mathbf{R}^L P_{eq}\widehat{J}(\Omega_{LM})\, P_{eq}^{-1}+\widehat{J}(\Omega_{LC})\mathbf{R}^C P_{eq}\widehat{J}(\Omega_{LC})\, P_{eq}^{-1} \tag{50}$$

where $\hat{J}(\Omega_{LM})$ and $\hat{J}(\Omega_{LC})$ are the infinitesimal rotation operators for the probe and the protein, respectively.

Changing to different coordinates is straightforward [20]. It is physically of interest to select the set defined by $\Omega_{C'M}$ and $\Omega_{LC'}$, where the probe motion is described as relative to the overall protein motion. One has [20]:

$$X=(\Omega_{C'M},\Omega_{LC'})$$
$$\widehat{\Gamma}=\widehat{J}(\Omega_{C'M})\mathbf{R}^L P_{eq}\widehat{J}(\Omega_{C'M})\, P_{eq}^{-1}+[\widehat{J}(\Omega_{C'M}) - \widehat{J}(\Omega_{LC'})]\mathbf{R}^C P_{eq}[\widehat{J}(\Omega_{C'M}) - \widehat{J}(\Omega_{LC}')]\, P_{eq}^{-1} \tag{51}$$

The Boltzmann distribution is $P_{eq} = \exp[-U(\Omega_{C'M})/k_BT]/\langle\exp[-U(\Omega_{C'M})/k_BT]\rangle$, where $\Omega_{C'M}(t) = \Omega_{LM}(t) - \Omega_{LC'}(t)$. The Euler angles $\Omega_{C'M}(t)$ represent the motion of the probe relative to the protein, the Euler angles $\Omega_{LM}(t)$ represent the motion of the probe realative to the lab frame, and the Euler angles $\Omega_{LC'}(t)$ represent the motion of the protein relative to the lab frame.

The potential $U(\Omega_{C'M})$ is expanded in the full basis set of the Wigner rotation matrix elements, i.e. $U(\Omega_{C'M})= -\sum_{L,K,M} c^L_M D^L_{KM}(\Omega_{C'M})$. For D_2 point group molecular symmetry, and axial locally ordered media, the terms with $L = 2$ and 4, and $K = 0$, 2 and 4 are preserved. It might be oversimplified to regard the local ordering potential of the probe with respect to the protein as necessarily obeying the macroscopic symmetry constraints of typical ordered phases. One

might expect biaxial character of the local director, C′. Similarly, one might expect that the summation need not be restricted to even L terms. We first note that the anisotropic magnetic interactions in the spin Hamiltonian have $L = 2$. Then we note that second rank correlation functions are qualitatively very similar whether a first-rank or second-rank SRLS potential is used [16].

Thus, for economy in fitting parameters, and for convenience, we restrict L to just even values. In the same spirit, we will ignore any biaxiality in the local ordering potential, so $M = 0$ in the expansion of $u(\Omega_{C'M})$. . The typical SRLS potential used so far has been:

$$u(\Omega_{C'M})=\frac{U(\Omega_{C'M})}{k_B T} \approx -c_0^2 D^2_{0,0}(\Omega_{C'M}) - c_2^2[D^2_{0,2}(\Omega_{C'M})+D^2_{0,-2}(\Omega_{C'M})]. \quad (52)$$

The coefficient c_0^2 is related to the orientational ordering of the N–H bond with respect to the local director, whereas the coefficient c_2^2 is related to the asymmetry of the ordering around the director. Terms corresponding to $L = 4$, $K = 0, 2, 4$, (c_0^4, c_2^4 and c_4^4) (mentioned above) are included in our latest software [90]. This allows for modeling diffusion within two wells with less frequent jumps between them [17,39]. More general jump models may be included by adding appropriate terms in the expansion of $u(\Omega_{C'M})$.

Eq. 51 can be solved in terms of the time dependent probability density function $P(\Omega_{C'M},\Omega_{LC},t)$, which describes the evolution of the system in time and orientational space. Alternatively, it is convenient to directly calculate the time correlation functions $C^J_{M,KK'}(t)=\langle D^{J*}_{M,K}(\Omega_{LM})|\exp(-\widehat{\Gamma}t)|D^J_{M,K'}(\Omega_{LM})P_{eq}\rangle$ (where the brackets $\langle\ldots\rangle$ mean integration over the full space of orientational coordinates), which for appropriate values of the coefficients J,M,K,K' determine the experimental NMR relaxation rates. Actually, the Fourier-Laplace transforms of $C^J_{M,KK'}(t)$ are needed. They are obtained as the spectral densities given by:

$$j^J_{M,KK'}(\omega)=\langle D^{J*}_{M,K}(\Omega_{C'M})|(i\omega+\widehat{\Gamma})^{-1}|D^J_{M,K'}(\Omega_{C'M})P_{eq}\rangle \quad (53)$$

As stated here the model features a large number of parameters including the potential coefficients $C_0^2, C_2^2, C_0^4, C_2^4$ and C_4^4, the principal values of the local diffusion tensor, R_i^L, i= 1, 2, 3, and the principal values of the global diffusion tensor, R_i^C, with i = 1, 2, 3. The geometric parameters featured include the Euler angles α_{MD} and β_{MD} for the relative orientation of the (axial) dipolar and local ordering frames, and the Euler angles $\Omega_{CC'}$ for the relative orientation of the global diffusion and local director frames. The Euler angles for the relative orientation of the local ordering and local diffusion frames (not shown in Fig. 1) can also be varied. Clearly only a small number of parameters are varied in a given calculation. We found that for N–H bond dynamics studied with ^{15}N spin relaxation it is appropriate (i.e., no overfitting is encountered) to vary at most five parameters using data sets that comprise six data points (^{15}N T_1, T_2 and ^{15}N–{^{1}H} *NOE* acquired at two magnetic fields). For methyl dynamics studied with ^{2}H spin relaxation of $^{13}CDH_2$, it is appropriate to vary at most three parameters using data sets that comprise four data points (^{2}H T_1 and T_2 acquired at two magnetic fields). In Appendix A we show examples in which the parameters $c_0^2, c_2^2, R_{\|}^L$ and $R_{\perp}^L$ (c_0^2, c_2^2 and R^L) were varied in analyzing N–H bond dynamics.

The generality of the fitting scheme makes it possible to select various parameter combinations. Also, it is possible to carry out predictive or exploratory simulations.

The global diffusion tensor, $\boldsymbol{R}^{\mathbf{C}}$, takes the following form in the C′ frame:

$$\begin{pmatrix} R_{\perp}^{C}\cos^2\beta_{CC'}+R_{\parallel}^{C}\sin^2\beta_{CC'} & 0 & 1/2(R_{\perp}^{C}-R_{\parallel}^{C})\sin 2\beta_{CC'} \\ 0 & R_{\perp}^{C} & 0 \\ 1/2(R_{\perp}^{C}-R_{\parallel}^{C})\sin\beta_{CC'} & 0 & R_{\perp}^{C}\sin^2\beta_{CC'}+R_{\parallel}^{C}\cos^2\beta_{CC'} \end{pmatrix} \tag{54}$$

Note that for $\beta_{CC'} = 0$ or $R_{\perp}^{C}=R_{\parallel}^{C}$, the global diffusion tensor is diagonal and invariant in both the C and C′ frames.

3.3.2. Numerically exact treatment—We address here the problem of devising an efficient procedure for evaluating numerically accurate spectral densities. We adopt a variational scheme based on a matrix vector-representation of Eq. (53) followed by an application of the Lanczos algorithm in its standard form, developed for Hermitian matrices. It is convenient to express the generic time correlation functions as linear combinations of the normalized auto-correlation functions. By defining $2A^{J}_{M,KK'}=D^{J}_{M,K}+D^{J}_{M,K'}$, the spectral densities of the normalized auto-correlation functions of interest are:

$$j^{S}_{M,KK'}(\omega)=\langle A^{J*}_{M,KK'}(\Omega_{C'M})P_{eq}^{1/2}|(i\omega+\tilde{\Gamma})^{-1}|A^{J}_{M,KK'}(\Omega_{C'M})P_{eq}^{1/2}\rangle/\langle|A^{J}_{M,KK'}(\Omega_{C'M})|^2P_{eq}\rangle \tag{55}$$

and the generic spectral densities are:

$$j_{M,KK'}(\omega)=[2(1+\delta_{K,K'})j^{S}_{M,KK'}(\omega)-j^{S}_{M,KK}(\omega)-j^{S}_{M,K'K'}(\omega)]/2[J], \tag{55a}$$

where $J = 2$ and the symmetrized form of the time evolution operator is $\tilde{\Gamma}=P_{eq}^{-1/2}\hat{\Gamma}P_{eq}^{1/2}$. The value of the quantum number M depends on the interaction(s) involved in the relaxation parameter examined. Thus, $M \neq 0$ for terms including $\hat{I}_{\pm}$, where $\hat{I}$ denotes the spin operator of a nuclear spin of 1/2 or 1. We use the shorthand notation $[J] = 2J + 1$. A numerical calculation is then performed by choosing a basis set of functions, representing in matrix form the symmetrized operator, $\tilde{\Gamma}$, and evaluating Eq. (55) directly by employing a standard Lanczos approach. The latter is reviewed here for completeness in accordance with the standard technique of Moro and Freed [93,94]. Let us suppose that we are interested in calculating the Fourier-Laplace transform of the normalized autocorrelation function of an observable $f(q)$ or a diffusive symmetrized (i.e. Hermitian) operator, $\tilde{\Gamma}$, acting on the coordinate q, in the form of $j(\omega)=\langle\delta f^{*}P_{eq}^{1/2}|(\iota\omega+\tilde{\Gamma})^{-1}|\delta f P_{eq}^{1/2}\rangle/\langle|f|^2P_{eq}\rangle$, where $\delta f = f - \langle f P_{eq}\rangle$ is the observable redefined to yield an average value of zero. In the present case we consider only rotational motion in isotropic fluids, so that $\langle f P_{eq}\rangle = 0$.

The Lanczos algorithm is a recursive procedure for generating orthonormal functions that allow a tridiagonal matrix representation, $\mathbf{T}$, of $\tilde{\Gamma}$. The spectral density can be written in the form of a continued fraction [93,94]. The calculation of the tridiagonal matrix elements can be carried out in finite precision by working in the vector space obtained by projecting all the functions and operators onto a suitable set of orthonormal functions $|\lambda\rangle$. One only needs to define the

matrix **Γ**, and the starting vector elements, $\mathbf{v_1}$, which are given by $\Gamma_{\lambda,\lambda'} = \langle \lambda|\tilde{\Gamma}|\lambda' \rangle$ and $v_\lambda = \langle \lambda|1 \rangle$ respectively.

In the case under consideration, the SRLS diffusion operator is given by Eq. (51) and the starting vector is given by:

$$|1\rangle = A^J_{M,KK'}(\Omega_{C,M})\, P_{eq}^{1/2} / \langle |A^J_{M,KK'}|^2 P_{eq} \rangle = \sqrt{\frac{2[J]}{1+\delta_{K,K'}}} A^J_{M,KK'}(\Omega_{C,M})\, P_{eq}^{1/2}$$

. A natural choice for a set of orthonormal functions is the direct product of normalized Wigner matrices. What is left is the calculation of the matrix elements $\Gamma_{\lambda,\lambda'}$ and the vector elements $<\lambda|1>$. The algebraic intermediate steps are relatively straightforward and based on properties of the Wigner rotation matrices, infinitesimal rotation operators and spherical tensors. We skip the technical details and list the resulting expressions.

3.3.3. Observables—In order to interpret ^{15}N–^{1}H dipolar and ^{15}N CSA auto-correlated relaxation in the presence of axial potentials, only diagonal time correlation components, *KK*, are required. In the presence of rhombic potentials cross-terms, *KK′*, are also required. This scenario is discussed in detail in the following section.

According to standard analysis in the motional narrowing regime (Chapter 12 of Ref. [33]), one may define the observable spectral densities for two magnetic interactions, μ and *ν*, as the real part of the Fourier-Laplace transform of the time correlation function of the second rank Wigner functions. The latter are given in terms of the orientation of the magnetic tensors in the laboratory frame (here μ,ν = D or CSA, $\Omega^D = \Omega_{MD}$, and $\Omega^{CSA} = \Omega_{MD} + \Omega$, cf. Fig. 1a):

$$J^{\mu\nu}_M(\omega) = \int_0^\infty e^{-i\omega t} \langle D^{2*}_{M,0}[\Omega^\mu + \Omega_{C,M}(t)]\, D^{2*}_{M,0}[\Omega^\nu + \Omega_{C,M}(0)] \rangle. \tag{56}$$

Based on standard properties of the Wigner functions one has:

$$J^{\mu\mu}_M(\omega) = \int_0^\infty e^{-i\omega t} \sum_{KK'} D^{2*}_{K,0}(\Omega^\mu) D^2_{K',0}(\Omega^\mu) \langle D^{2*}_{M,K}[\Omega_{C,M}(t)] D^{2*}_{M,K'}[\Omega_{C,M}(0)] \rangle. \tag{56a}$$

$$J^{\mu\mu}_M(\omega) = \int_0^\infty e^{-i\omega t} \sum_{KK'} D^{2*}_{K,0}(\Omega^\mu) D^2_{K',0}(\Omega^\mu) \langle D^{2*}_{M,K}[\Omega_{LM}(t)] D^{2*}_{M,K'}[\Omega_{LM}(0)] \rangle \tag{56b}$$

Based on the symmetry relation $j^J_{M,KK'} = j^J_{M,K'K}$ (cf. Eq. (56a)) we obtain:

$$\Re[J^{\mu\mu}_M(\omega)] = \sum_K |D^2_{K,0}(\Omega^\mu)|^2 \Re[j_{M,KK}(\omega)] + 2 \sum_{K<K'} \Re[D^{2*}_{K,0}(\Omega^\mu) D^2_{K',0}(\Omega^\mu)] \Re[j_{M,KK'}(\omega)] \tag{57}$$

where ℜ stands for the real part. Note that for axial potentials (c_2^2=0) the second term goes to zero. The coefficients $D^2_{K,0}(\Omega^D)$ are readily evaluated, while $D^2_{K,0}(\Omega^{CSA})$ can be calculated in terms of Ω_{MD} and Ω, according to the expression $D^2_{K,0}(\Omega^{CSA}) = \sum_L D^2_{K,L}(\Omega_{MD})\, D^2_{L,0}(\Omega)$.

The spectral densities for ^{15}N–^{1}H dipolar and ^{15}N CSA auto-correlation are thus obtained as $J^{DD}(\omega)=\Re[J_0^{DD}(\omega)]$ and $J^{CC}(\omega)=\Re[J^{CSACSA}(\omega)]$, respectively. The measurable ^{15}N relaxation parameters T_1, T_2 and ^{15}N–{^{1}H} *NOE* are calculated as functions of $J^{DD}(0)$, $J^{DD}(\omega_H)$, $J^{DD}(\omega_N)$, $J^{DD}(\omega_H-\omega_N)$ and $J^{DD}(\omega_H+\omega_N)$ and $J^{CC}(0)$ and $J^{CC}(\omega_N)$, using standard expressions for NMR spin relaxation [28,29]. Note that due to the additional symmetry $j_{M,K,K'}=j_{M,-K,-K'}$, only the nine distinct couples $K,K'=(-2,2)$, $(-1,1)$, $(-1,2)$, $(0,0)$, $(0,1)$, $(0,2)$, $(1,1)$, $(1,2)$, $(2,2)$ need to be considered for rhombic local ordering and magnetic frames. For rhombic local ordering and axial magnetic frames, one has the explicit expression (denoting $j_{KK'}=\Re[j^2_{0,KK'}(\omega)]$ for brevity):

$$\begin{aligned}J^{DD}(\omega)=&(d^2_{00}(\beta_{MD}))^2 j_{00}(\omega)\\&+2(d^2_{10}(\beta_{MD}))^2 j_{11}(\omega)\\&+2(d^2_{20}(\beta_{MD}))^2 j_{22}(\omega)\\&+4d^2_{00}(\beta_{MD})\,d^2_{20}(\beta_{MD})\,j_{02}(\omega)\\&+2d^2_{-10}(\beta_{MD})\,d^2_{10}(\beta_{MD})\,j_{-11}(\omega)\\&+2d^2_{-20}(\beta_{MD})\,d^2_{20}(\beta_{MD})\,j_{-22}(\omega),\end{aligned}\tag{58}$$

with only six couples $K,K'=(0,0)$, $(1,1)$, $(2,2)$, $(0,2)$, $(-1,1)$ and $(-2,2)$ involved. The function $J^{CC}(\omega)$ is obtained using Eq. (56a) with μ representing the ^{15}N CSA interaction.

A convenient measure of the local ordering of the N–H bond is provided by the order parameters $S_0^2=\langle D^2_{00}(\Omega_{C'M})\rangle$ and $S_2^2=\langle D^2_{02}(\Omega_{C'M})+D^2_{0-2}(\Omega_{C'M})\rangle$. They are related to the orienting potential (Eq. (52)), and hence to c_0^2 and c_2^2, via the ensemble averages:

$$\langle D^2_{0n}(\Omega_{C'M})\rangle=\int d\Omega_{C'M}\,D^2_{0n}(\Omega_{C'M})\exp[-u(\Omega_{C'M})]/\int d\Omega_{C'M}\exp[-u(\Omega_{C'M})]\tag{59}$$

One can convert to Cartesian ordering tensor components according to $S_{zz}=S_0^2, S_{xx}=(\sqrt{3/2}\,S_2^2-S_0^2)/2, S_{yy}=-(\sqrt{3/2}\,S_2^2+S_0^2)/2$, with $S_{xx}+S_{yy}+S_{zz}=0$.

In the case of zero potential, $c_0^2=c_2^2=0$, and axial diffusion, the solution of the diffusion equation associated with the time evolution operator features three distinct eigenvalues:

$$1/\tau_K=6R^L_\perp+K^2(R^L_\parallel-R^L_\perp)\text{ for }K=0,1,2,\tag{60}$$

where $R^L_\parallel=1/(6\tau_\parallel)$ and $R^L_\perp=1/(6\tau_\perp)=1/(6\tau_0)$. Only diagonal $j_K(\omega)\equiv j_{K,K}(\omega)$ terms are non-zero, and they can be calculated analytically as Lorentzian spectral densities, each defined by width of $1/\tau_K$. When the ordering potential is axially symmetric, $c_0^2\neq 0$, $c_2^2=0$, again only diagonal $j_K(\omega)$ survive, but they are given as infinite sums of Lorenzian spectral densities, which are defined in terms of the eigenvalues, $1/\tau_i$, of the SRLS operator (Eq. (51)), and the weighing factors, $c_{K,i}$, so that:

$$j_K(\omega)=\sum_i\frac{c_{K,i}\tau_i}{1+\omega^2\tau_i^2}.\tag{61}$$

The eigenvalues $1/\tau_i$ represent normal modes of motion of the system. The weighting factors (eigenmodes) depend on the parameters that define the tenors $\boldsymbol{R}^{\mathbf{L}}$ and $\boldsymbol{R}^{\mathbf{C}}$, and the coefficients of the coupling potential. Although in principle the number of terms in Eq. (61) is infinite, in practice a finite number of terms is sufficient for numerical convergence of the solution. A user-determined quantum number, $L_{\max}$, must be large enough to ensure the convergence of the solution. Note that the eigenmodes depend on a small number of physical parameters.

Finally, when the local ordering potential is rhombic, $c_0^2 \neq 0$, $c_2^2 \neq 0$, both diagonal, $j_K(\omega)$, and non-diagonal, $j_{KK'}(\omega)$, terms are different from zero. The functions $j_{KK'}(\omega)$ are evaluated explicitly according to expressions analogous to Eq. (61).

The spectral densities $j_K(\omega)$ (in general, $j_{KK'}(\omega)$) are the building blocks of a given dynamic model, and the spectral densities $J^{XX}(\omega)$ for auto-correlated relaxation and $J^{XY}(\omega)$ for cross-correlated relaxation are the building blocks for a specific geometric implementation of this model. Together with the magnetic interactions, the appropriate values of the spectral densities $J^{XX}(\omega)$ and $J^{XY}(\omega)$ determine the experimentally measured relaxation parameters [28,29].

To further clarify the relationship between $j_{KK'}(\omega)$ and $J^{XX}(\omega)$ or $J^{XY}(\omega)$, let us consider an internally mobile peptide plane (e.g., as in 3D GAF [65,78]). Several probes, with their equilibrium orientations lying within this plane, are conceivable: ^{15}N–^{1}H, $^{13}C'$–$^{13}C^{\alpha}$, ^{15}N–$^{13}C^{\alpha}$, $^{13}C^{\alpha}$–^{2}H, etc. They all sense the same motion, associated with the local ordering/local diffusion frame, M, which is attached rigidly to the peptide plane. Therefore the same $j_{KK'}(\omega)$ functions may be used to calculate all the auto-correlated and cross-correlated relaxation parameters associated with all of these probes. The various probes differ in (1) their local geometry, i.e., the orientation of the relevant magnetic frame(s) with respect to the M frame, and (2) the relevant magnetic interactions. These properties are not part of the dynamic models. They enter the calculation when $J^{XX}(\omega)$ and $J^{XY}(\omega)$ are assembled out of the $j_{KK'}(\omega)$ functions, and when the relaxation parameters are assembled out of the appropriate values of $J^{XX}(\omega)$ or $J^{XY}(\omega)$.

If the peptide plane is engaged in several different motions, e.g., crank-shaft-type torsions, anti-correlated movements between the dihedral angles Φ_{i-1} and Φ_i, etc., then all the probes with their equilibrium orientations lying within the peptide plane will experience all of these motions. This has not always been appreciated [95].

For practical reasons our first fitting scheme for SRLS was based on pre-calculated 2D grids of spectral densities, $j_{KK}(\omega)$, calculated for axial potentials [19]. The coordinates of these grids are c_0^2 and R^{C} (in units of R^{L}). The parameter combinations used are formally (but not necessarily physically) analogous to models 1–5 of Refs. [96] and [97], and models 6–8 of Ref. [97]. We also made the approximation that $R_{\|}^{L} \gg R_{\perp}^{L}$, in analogy with $\tau_s > \tau_f$ in MF. This fitting scheme for SRLS differs from MF in accounting for mode-coupling and allowing for a "diffusion tilt". The global diffusion tensor, $\boldsymbol{R}^{\mathbf{C}}$, is taken to be isotropic.

Pre-calculated grids of spectral densities are only practical for two coordinates; this limits the number of parameters that can be varied. Imposing axial potentials and taking $R_{\|}^{L} \gg R_{\perp}^{L}$ turned out to be oversimplifications. To improve the analysis we developed a newer fitting scheme for SRLS [20] where the spectral densities are calculated at each iteration step in the minimization process. This fitting scheme allows for rhombic potentials and for arbitrary $R_{\|}^{L}/R_{\perp}^{L}$ ratios. The global diffusion is still taken as isotropic. Enhancing it to axial global diffusion is relatively easy. However, this extension has not been carried out because this fitting scheme is inefficient when the time scale separation is large and the local potential is rhombic, which is the common scenario for "rigid" N–H bonds.

In our most recent fitting scheme [90] the global diffusion tensor, $\boldsymbol{R}^{\mathbf{C}}$, is allowed to be rhombic. Also, the local ordering and local diffusion frame can be distinct. In addition, the local diffusion tensor is allowed to be rhombic. The local potential includes terms with $L = 2$ and $L = 4$, which (as already mentioned) makes possible modeling diffusion within rotamer wells with (less frequent) jumps between the wells [17]. The programming language used is C++ (previously we used the FORTRAN programming language). The computer-intensive parts of the code have been parallelized, and object-oriented programming has been enacted. These features brought about an increase in efficiency of approximately one order of magnitude relative to the earlier fitting scheme developed in Ref. [20]. Importantly, the SRLS program has been integrated with a hydrodynamics-based approach for calculating anisotropic global diffusion tensors [98].

We call this software package C++OPPS (COupled Protein Probe Smoluchowski) [90]. C++OPPS is distributed under the GNU Public License (GPL) v2.0. The software is available at the website http://www.chimica/unipd.it/licc/software.html.

The illustrative calculations presented in Appendix A were carried out using this fitting scheme. We also compare in that Appendix SRLS and MF, using the same number of formally analogous free variables. For MF analysis, we used in our work the programs Modelfree 4.0 [96] or Dynamics [97].

Application to $^{13}CDH_2$ deuterium spin relaxation: The SRLS frames shown in Fig. 2a for methyl dynamics are the same as the frames shown in Fig. 1a, except that the magnetic tensor is in this case the ^{2}H quadrupolar tensor (Q frame). The experimentally determined rhombic local ordering/local diffusion frame, M, and the Q frame, are depicted in Fig. 2b. The axis X_M is the main local ordering axis, aligned parallel to the C–CH_3 axis (the angle β_{MQ} is close to 110.5°).

For an axial quadrupolar tensor, Q, one has:

$$\begin{aligned} J^{QQ}(\omega) = & (d^2_{00}(\beta_{MQ}))^2 j_{00}(\omega) \\ & + 2(d^2_{10}(\beta_{MQ}))^2 j_{11}(\omega) \\ & + 2(d^2_{20}(\beta_{MQ}))^2 j_{22}(\omega) \\ & + 4 d^2_{00}(\beta_{MQ})\, d^2_{20}(\beta_{MQ})\, j_{02}(\omega) \\ & + 2 d^2_{-10}(\beta_{MQ})\, d^2_{10}(\beta_{MQ})\, j_{-11}(\omega) \\ & + 2 d^2_{-20}(\beta_{MQ})\, d^2_{20}(\beta_{MQ})\, j_{-22}(\omega). \end{aligned} \tag{62}$$

For ^{2}H relaxation the spectral densities $J^{QQ}(0)$, $J^{QQ}(\omega_D)$ and $J^{QQ}(2\omega_D)$, together with the magnitude of the quadrupolar interaction, determine the experimentally measured relaxation rates ^{2}H T_1 and T_2 according to standard expressions for NMR spin relaxation [28,29]. Equation (62) applies to cases when the quantum number M is equal to zero.

3.4. Collective motions

The analysis of collective behavior is based on conformational fluctuations in the protein. Collective coordinates are mainly used to single out functionally relevant motions and to elucidate protein energy landscapes. The simplest approach of this kind is the Gaussian network model (GNM) [27], which pertains to the coarse-grained elastic network category. GNM predicts both localized modes, which have been associated primarily with structural features, and collective modes, which have been associated in many cases with biological function.

Methods for treating collective internal motions include normal mode analysis (NMA) [99], molecular dynamics in the context of principal component analysis (PCA) [100], essential dynamics analysis (EDA) [101], combined PCA and NMA based on jumping among minima (JAM) [102], and various elastic network models [27,103,104]. A combined contact and elastic-network-model-based approach has also been developed [105]. Approaches where the Langevin equation is applied in the context of independent damped oscillators have been set forth [106].

MD techniques based on simplifications of the empirical potential energy functions, or advanced sampling techniques, can be included in the present section (e.g., see Ref. [107] and relevant papers cited therein). Recourse to low-dimensional sub-spaces, where significant motions occur, and considering parts of the protein as quasi-rigid bodies, are common strategies [108]. In general, a relatively small number of dominant independent collective modes are determined.

Several predictive structure-based methods have been integrated with MF analysis [109–111].

The network of coupled rotators (NCR) [112–115] is among the most sophisticated structure-based approaches. Internal dynamics is described in terms of bond vectors coupled by pair-potentials, within the scope of analytical time correlation functions. Order parameters are derived, and conformational entropy is calculated. Unlike the simpler models, NCR solves the Langevin equation at each N–H site. It captures the important aspect of local structural asymmetry. The local geometry is encoded. NCR shares some common features with contact-based approaches [116–118] and elastic network models [27,103,104,119].

Brüschweiler and Prompers developed the isotropic reorientational eigenmode dynamics (iRED) approach [25,26]. In this method, the snapshots derived from the MD trajectory are treated analytically to yield an isotropic ensemble from which a covariance matrix is computed. A geometric “separability” parameter, which singles out the five largest eigenvalues associated with the global motion, is defined. Non-separability does not account for correlations between the rotational degrees of freedom of the protein and the probe. However, iRED treats correlated motions along the polypeptide chain; it is applicable to partially unfolded and unfolded proteins.

We include in this section the method of Vugmeyster et al. [120]. This approach assumes that $C(t) = C^{C}(t) \times C^{L}(t)$, belonging thus to the mode-decoupling limit. It associates dynamical coupling with comparable values of τ_e and τ_m.

“Diffusive mode-coupling” approaches [121,122] treat the effect of fast local bond-vector fluctuations on the global diffusion tensor, i.e., on the shape of the protein. The method of Perico and co-workers [121] recovers the original MF formula. The agreement with the experimental NMR data is not satisfactory. Caballero-Manrique et al. [122] developed an enhanced approach and used it to calculate experimental relaxation parameters; here the agreement between theoretical and experimental relaxation parameter is good.

There is ample literature on Markov chain dynamics [123–127] and lipid dynamics [128–130].

4. Future directions

The SRLS model as described in this review article has served as a working model in several analyses of NMR spin relaxation data from proteins [19,20,34,35,46–50]. We have found that for N–H bonds located in flexible regions of the protein structure, and for methyl groups, this

model provides a new and insightful picture of protein dynamics, with a level of parameterization of the model sufficient in most cases to provide consistent analyses of the available experimental data. The analysis of a "rigid" N–H bond can be improved by including inertial effects (see below).

This modeling can be improved in a number of ways. For example, from the viewpoint of an ^{15}N–^{1}H bond located in a mobile domain or flexible loop, one perhaps expects three types of motions including the local motion of the N–H bond, the motion of the flexible moiety housing it, and the overall tumbling of the protein. A natural extension of our current 2-body Smoluchowski SRLS model would be a 3-body Smoluchowski SRLS model to incorporate all three kinds of motion; one such example is developed in Ref. [16]. One can also account for rotamer jumps around side-chain χ angles [17]. However, this would yield additional parameters to fit, an issue on which we comment further below.

The analysis of "rigid" N–H bond dynamics has been problematic in some cases, as pointed out in Appendix A. This can be rationalized by recognizing that in the presence of strong local potentials rapidly moving N–H bonds are expected to experience torsional oscillations which are not included in the overdamped diffusive or Smoluchowski limit. One must therefore account for inertial effects via explicit inclusion of the respective angular momentum degrees of freedom. This leads to the Fokker-Planck-Kramers (FPK) SRLS model, which has been previously described in detail by Polimeno and Freed [16]. The methodology is somewhat more complex, but tractable. The additional physical parameters needed are the moments of inertia of the bodies, which can be inferred from structural considerations. For local motions occurring in strong potentials, this can lead to a reasonable modeling of (under-damped) torsional oscillations. The implementation of the FPK SRLS model to NMR spin relaxation in proteins is in progress.

Another limitation of the Smoluchowski equation is in the back-reaction, due to the coupling potential, on the heavy body, i.e., the overall protein motion, which is rigorously required for "detailed-balance"; this back-reaction was ignored in the early Born-Oppenheimer-type of treatment [15]. In the Smoluchowski SRLS model this leads to significant "mode-coupling" between the local probe motion and the overall protein motion when their diffusive rates become comparable, with the small body "pulling" on the large body. In the FPK-SRLS model, the much larger moment-of-inertia of the whole protein relative to the local probe will greatly suppress this effect, as may be seen in the analysis provided in Ref. [16]. Thus, to treat this limit, it will be appropriate to replace the Smoluchowski equation with the more complete FPK equation. However, in our extensive analyses of NMR data, we have found that such cases of slow local motions are typically associated with mobile domains or relatively large loops; for these heavier probes, Smoluchowski SRLS is reasonable adequate.

One may also ask whether it is useful to compare the results of SRLS analyses of the experimental data with the results of MD simulations. Currently comparisons are made between results from MF analyses of the NMR data and MD [36,70,131–135]. We argue in this review that the results of a SRLS analysis are more physically relevant than those from MF, so it would be appropriate to make comparisons between SRLS and MD. Once the SRLS analysis is completed, producing the best-fit values of the parameters which define the local potential, the diffusion tensors, and the geometric factors (i.e., relative frame orientations), relevant time correlation functions of the $D^{2}_{MK}(\Omega)$ (cf. Eqs. (56) and (56a)) can readily be computed. In would then be of interest to calculate the equivalent correlation functions from the MD trajectories and compare with their SRLS counterparts.

In practice the comparison between NMR/MF and MD is carried out as follows. Based on the assumption that $C(t) = C^{C}(t) \times C^{L}(t)$, the global motion is first eliminated from the MD

trajectory by frame superimposition onto a reference structure. Based on the form of Eq. 34, S^2 MD is typically derived as the value of $C^L(t)$ at long times. In some cases least-squares fitting of the $C^L(t)$ MD to Eq. 34 was carried out. In a very few cases $C^L(t)$ was computed as the time correlation function of $P_2(\cos\beta_{CD})$, where D is the magnetic dipolar frame and C is the protein-fixed frame matching the reference structure (a thorough discussion of these matters appears in Appendix B). Clearly none of these methods provide the correlation functions of the $D^2_{MK}(\Omega)$.

Progress on how such correlation functions may be obtained from MD simulations is illustrated in Refs. [136,137]. It was found that in extracting information on rotational reorientation from MD trajectories, it is more convenient to work with quaternions rather than Euler angles [136]. It is then possible to transform an analysis based upon quaternions into the $D^2_{MK}(\Omega)$. []. In addition, efforts were made in Ref. [136] to model the MD trajectories as Markov chain processes to overcome the need for very long trajectories, and the need to obtain enough trajectories to provide adequate ensemble averages.

An MD approach based on these techniques has been successfully applied to simulate complex ESR line-shapes over a 20-fold range in frequencies [43,136,138–140]. The ESR spectra calculated with MD agreed very well with their counterparts calculated with SRLS and with experiment. The reproduction of ESR line-shapes with MD represents an even greater challenge than the reproduction of the NMR relaxation parameters (typically T_1, T_2 and heteronuclear *NOE*), which only require time correlation functions for their evaluation. The techniques developed in these ESR studies could be adapted to help calculate from the MD trajectories the expressions for the experimental NMR spin relaxation parameters, in analogy to the calculation of ESR line-shapes.

As noted above, in its present implementation SRLS does not treat explicitly the correlated N–H bond vector motions along the polypeptide chain, or such correlations for domain motion. More advanced modeling would be required to achieve this. Polimeno, Barone and co-workers have developed an integrated approach that combines stochastic models, molecular dynamics, quantum-chemical calculations and hydrodynamics-related methods [141–145]. This approach has been applied successfully to small molecules in the context of both ESR [141–145] and NMR [146]. Current efforts are directed toward its application to bio-macromolecules.

5. Conclusions

Experimental NMR spin relaxation data from proteins can be used to obtain unique information on mode-coupling, local potentials, local ordering, conformational distributions, global and local motional rates, associated activation energies, and features of local geometry. For local potentials which are not so strong as to invalidate the overdamped limit, and time scale separations, R^C/R^L, which are apreciably smaller than unity, the Smoluchowski SRLS equation provides an appropriate tool for extracting this information. The generality of its solution makes it possible to determine, for each case, the parameter combination that conforms to the sensitivity of the experimental data. When the conditions mentioned above are not fulfilled, then analogous FPK equations are appropriate; their development is currently near completion.

In the Smoluchowski limit the main factors that affect protein dynamics include mode-coupling, the asymmetry of the local potential, and the fact that in the presence of a local potential the eigenfunctions of the (axial) local motional diffusion operator are no longer simple. For amide bonds located in well-structured regions of the protein structure the dominant factor is the asymmetry of the local potential. For amide bonds located in mobile domains and flexible loops, all of the factors mentioned above are important. For methyl dynamics, mode-coupling is typically a small effect, but the other factors are important.

N–H bonds reorient primarily about the $C^{\alpha}_{i-1} - C^{\alpha}_{i}$ axis with *ps* correlation times when located in well-structured regions, and with *ns* correlation times when located in mobile domains or flexible loops. For "rigid" (flexible) N–H bonds, the local potential is strong (of moderate strength) and highly rhombic when the main ordering axis is defined to lie along the instantaneous N–H orientation. When the main ordering axis is defined to lie along $C^{\alpha}_{i-1} - C^{\alpha}_{i}$ then the local ordering is strong at both "rigid" and flexible N–H sites, with different degrees of rhombicity.

The local ordering at methyl sites in proteins is rhombic, with the main local ordering axis lying along the C–CH_3 bond. The rate of the local motion is typically fast relative to the rate of the global motion. The local potential is weak and highly rhombic. The diversity of the potential at different sites represents in a simple, economical and physically reasonable manner the effect of the structure surrounding methyl groups on their motion.

The model-free approach does not feature key elements that are found to be important by the SRLS model. In view of the oversimplifications inherent in the MF method the experimental data are force-fitted, and the best-fit parameters are often not appropriate for physical interpretation. Their problematic nature is intensified by simplified constructs (e.g., see the expression for S^2) or mathematical definitions (e.g., see the expression for τ_e, based on the theory of moments) whose meanings are physically vague, and by the utilization of spectral densities which do not represent a physical scenario (e.g., see the MF formula for methyl dynamics [36]). There is ample evidence for adverse implications of parameterization and for not abiding by the assumptions underlying the equations employed.

In the limit of large time scale separation one may express the total time correlation function as $\exp(-t/\tau_m) \times C^L(t)$. Replacing the simple MF forms of $C^L(t)$ with more elaborate analytical functions is not usually possible because the time correlation functions for restricted motions in the presence of mean-field potentials lead to intricate numerical solutions – cf. Section 3.1.1.

Acknowledgments

The work reported herein could not have been carried out without the contribution of Dr. Mirco Zerbetto of the University of Padova, Dr. Zhichun Liang of Cornell University, Dr. Vitali Tugarinov of the University of Maryland, Dr. Edith Kahana of Bar-Ilan University, and Drs. M. A. Sinev and E. V. Sineva, formerly of Bar-Ilan University. We also wish to acknowledge people who generously provided their experimental data: Prof. Lewis E. Kay of the University of Toronto, Prof. A. G. Palmer III of Columbia University, Prof. Erik R. P. Zuiderweg of the University of Michigan, Ann Arbor, and Prof. G. Wagner of Harvard Medical School. EM thanks Prof. Zeev Luz and Prof. Shimon Vega of the Weizmann Institute, Israel, for numerous fruitful and inspiring discussions. EM gratefully acknowledges the hospitality of the Department of Computational Biology, University of Pittsburgh School of Medicine, where she spent her sabbatical year 2009/2010, in the course of which this work was finalized.

This work was supported by the Israel Science Foundation (Grant No. 347/07 to E.M.), the Binational Science Foundation (Grant No. 2006050 to E.M. and J.H.F.), the German-Israeli Science Foundation for Scientific Research and Development, grant no. 928-190.0/2006, and the Damadian Center for Magnetic Resonance at Bar-Ilan University, Israel. E.M. This work was also supported by the National Center for Research Resources of the National Institutes of Health (Grant No. P41-RR016292 to J.H.F.). A.P. acknowledges support provided by Ministero dell'Istruzione, Universita e Ricerca (MIUR), grant PRIN 2006 (2006033728), by the Consorzio Interuniversitario per la Scienza e la Tecnologia dei Materiali (INSTM), grant PROMO 2009 and by the University of Padova, grant "Progetto Strategico" HELIOS 2009.

Abbreviations

AK	adenylate kinase
AKeco	adenylate kinase from *Escherichia coli*
B.-O	Born-Oppenheimer approximation

CaM	Ca^{2+}-calmodulin
CSA	chemical shift anisotropy
3D GAF	3-dimensional Gaussian axial fluctuations
DNA	deoxyribonucleic acid
EDA	essential dynamics analysis
EMF	extended model-free
ESR	electron spin resonance
FPK	Fokker-Planck-Kramers
GB3	the B3 immunoglobulin-binding domain of streptococcal protein G
GNM	Gaussian network model
HP36	chicken villin headpiece subdomain protein
iRED	isotropic reorientational eigenmode dynamics
JAM	jumping among minima
LC	liquid crystal
MD	molecular dynamics
MF	model-free
MOMD	microscopic order macroscopic disorder
NCR	network of coupled rotators
NMA	normal mode analysis
NMR	nuclear magnetic resonance
NOE	nuclear Overhauser enhancement
PCA	principal component analysis
protein L	the B1 immunoglobulin binding domain of *Peptostreptococcal* protein L
RDC	residual dipolar coupling
RNA	ribonucleic acid
SLE	stochastic Liouville equation
SRLS	slowly relaxing local structure

References

1. Ishima R, Torchia DA. Nat Struct Biol 2000;7:740. [PubMed: 10966641]
2. Case D. Acc Chem Res 2002;35:325. [PubMed: 12069616]
3. Brüschweiler R. Curr Opin Struct Biol 2003;13:175. [PubMed: 12727510]
4. Palmer AG. Chem Rev 2004;104:3623. [PubMed: 15303831]
5. Mittermaier A, Kay LE. Science 2006;312:224. [PubMed: 16614210]
6. Igumenova TI, Frederick KK, Wand JA. Chem Rev 2006;106:1672. [PubMed: 16683749]
7. Kitao A, Wagner G. Mag Reson Chem 2006;44:S130.
8. Jarymowycz VA, Stone MJ. Chem Rev 2006;106:1624. [PubMed: 16683748]
9. Nodet G, Abergel D. Eur Biophys J Biophys Lett 2007;36:985.
10. Markwick PRL, Malliavin T, Nilges M. PLoS Comput Biol 2008;4:1.

11. Lipari G, Szabo A. J Am Chem Soc 1982;104:4546.
12. Lipari G, Szabo A. J Am Chem Soc 1982;104:4559.
13. Clore GM, Szabo A, Bax A, Kay LE, Driscoll PC, Gronenborn AM. J Am Chem Soc 1990;112:4989.
14. Polnaszek CF, Freed JH. J Phys Chem 1975;79:2283.
15. Freed JH. J Chem Phys 1977;66:4183.
16. Polimeno A, Freed JH. Adv Chem Phys 1993;83:89.
17. Polimeno A, Freed JH. J Phys Chem 1995;99:10995.
18. Liang Z, Freed JH. J Phys Chem B 1999;103:6384.
19. Tugarinov V, Liang Z, Shapiro YuE, Freed JH, Meirovitch E. J Am Chem Soc 2001;123:3055. [PubMed: 11457016]
20. Meirovitch E, Shapiro YuE, Polimeno A, Freed JH. J Phys Chem A 2006;110:8366. [PubMed: 16821820]
21. Lin W-J, Freed JH. J Phys Chem 1979;83:379.
22. Muhandiram DR, Yamazaki T, Sykes BD, Kay LE. J Am Chem Soc 1995;117:11536.
23. Millet O, Muhandiram DR, Skrynnikov NR, Kay LE. J Am Chem Soc 2002;124:6439. [PubMed: 12033875]
24. Srynnikov NR, Millet O, Kay LE. J Am Chem Soc 2002;124:6449. [PubMed: 12033876]
25. Prompers JJ, Brüschweiler R. J Am Chem Soc 2001;123:7305. [PubMed: 11472158]
26. Prompers JJ, Brüschweiler R. J Am Chem Soc 2002;124:4522. [PubMed: 11960483]
27. Bahar I, Atilgan AR, Erman B. Fold Des 1997;2:173. [PubMed: 9218955]
28. Abragam, A. The Principles of Nuclear Magnetism. Oxford University Press (Clarendon); Oxford: 1961.
29. Peng, JW.; Wagner, G. Methods in Enzymology. James, TL.; Oppenheimer, NJ., editors. Vol. 239. Academic Press; New York: 1994. p. 563-595.
30. Nordio PL, Busolin P. J Chem Phys 1971;55:5485.
31. Polnaszek CF, Bruno GV, Freed JH. J Chem Phys 1973;58:3185.
32. Emsley, JW., editor. NMR of Liquid Crystals. Riedel; Dorbrecht: 1983.
33. Luckhurst, GR.; Veracini, CA., editors. The Molecular Dynamics of Liquid Crystals. Kluwer Academic Publishers; The Netherlands: 1994.
34. Meirovitch E, Polimeno A, Freed JH. J Phys Chem B 2006;110:20615. [PubMed: 17034251]
35. Meirovitch E, Shapiro YuE, Polimeno A, Freed JH. J Phys Chem B 2007;111:12865. [PubMed: 17941658]
36. Chatfield DC, Szabo A, Brooks BR. J Am Chem Soc 1998;120:5301.
37. Henry E, Szabo A. J Chem Phys 1985;82:4753.
38. Avitabile J, London RE. J Am Chem Soc 1978;100:7159.
39. Polimeno A, Moro GJ, Freed JH. J Chem Phys 1996;104:1090.
40. Meirovitch E, Shapiro YuE, Liang Z, Freed JH. J Phys Chem B 2003;107:9898.
41. Pilar J, Labsky J, Marek A, Budil DE, Earle KA, Freed JH. Macromolecules 2000;33:4438.
42. Borbat PP, Costa-Filho AJ, Earle KA, Moscicki JK. JH Freed Science 2001;291:266.
43. Sezer D, Freed JH. B Roux J Am Chem Soc 2009;131:2597.
44. Liang Z, Freed JH, Keyes RS, Bobst AM. J Phys Chem B 2000;104:5372.
45. Liang Z, Lou Y, Freed JH, Columbus L, Hubbell WL. J Phys Chem B 2004;108:17649.
46. Tugarinov V, Shapiro YuE, Liang Z, Freed JH, Meirovitch E. J Mol Biol 2002;315:171. [PubMed: 11779237]
47. Shapiro, YuE; Kahana, E.; Tugarinov, V.; Liang, Z.; Freed, JH.; Meirovitch, E. Biochemistry 2002;41:6271. [PubMed: 12009888]
48. Meirovitch E, Shapiro YuE, Tugarinov V, Liang Z, Freed JH. J Phys Chem B 2003;107:9883.
49. Shapiro, YuE; Meirovitch, E. J Phys Chem B 2006;110:11519. [PubMed: 16771428]
50. Shapiro, YuE; Kahana, E.; Polimeno, A.; Meirovitch, E. J Phys Chem B 2009;113:12050. [PubMed: 19673471]

51. Kinosita K, Kawato S, Ikegami A. Biophys J 1977;20:289. [PubMed: 922121]
52. Szabo A. J Chem Phys 1980;72:4620.
53. Brink, DM.; Satchler, GR. Angular Momentum. Clarendon Press; Oxford: 1968.
54. Frederick KK, Sharp KA, Warischalk N, Wand AJ. J Phys Chem B 2008;112:12095. [PubMed: 18759409]
55. Akke M, Brüschweiler R, Palmer AG III. J Am Chem Soc 1993;115:9832.
56. Li Z, Raychaudhuri S, Wand AJ. Protein Sci 1996;5:2647. [PubMed: 8976574]
57. Yang D, Kay LE. J Mol Biol 1996;263:369. [PubMed: 8913313]
58. Li D-W, Brüschweiler R. Phys Rev Lett 2009;102:118108. [PubMed: 19392246]
59. Woessner DE. J Chem Phys 1962;36:1.
60. Brainard JR, Szabo A. Biochemistry 1981;20:4618. [PubMed: 7197547]
61. Prabhu NV, Lee AL, Wand AJ, Sharp KA. Biochemistry 2003;42:562. [PubMed: 12525185]
62. Mitternmaier A, Kay LE. J Am Chem Soc 2001;123:6892. [PubMed: 11448195]
63. Okamura H, Makino K, Nishimura Y. J Mol Biol 2007;367:1093. [PubMed: 17313959]
64. Tugarinov V, Kay LE. J Biomol NMR 2004;29:369. [PubMed: 15213435]
65. Lienin SF, Bremi T, Brutscher B, Brüschweiler R, Ernst RR. J Am Chem Soc 1998;120:9870.
66. Blackledge M. Prog Nucl Magn Reson Spectrosc 2005;46:26.
67. Daragan VA, Mayo KH. Prog Nucl Magn Reson Spectrosc 1997;31:63.
68. Mittermaier A. LE Kay J Biomol NMR 2002;23:35.
69. Chou JJ, Case DA, Bax A. J Am Chem Soc 2003;125:8959. [PubMed: 12862493]
70. Hu H, Hermans J, Lee AL. J Biomol NMR 2005;32:151. [PubMed: 16034666]
71. Best RB, Clarke J, Karplus M. J Mol Biol 2005;349:185. [PubMed: 15876377]
72. Li D-W, Meng D, Bruschweiler R. J Am Chem Soc 2009;131:15853. [PubMed: 19821582]
73. Szabo A. J Chem Phys 1984;81:150.
74. Wang CC, Pecora R. J Chem Phys 1980;72:5333.
75. Batchelder LS, Niu CH, Torchia DA. J Am Chem Soc 1983;105:2228.
76. Vugmeyster L, Ostrovsky D, Ford JJ, Burton SD, Lipton AS, Hoatson GL, Vold RL. J Am Chem Soc 2009;131:13651. [PubMed: 19772361]
77. Wittebort RJ, Szabo A. J Chem Phys 1978;69:1722.
78. Bremi T, Brüschweiler R. J Am Chem Soc 1997;119:6672.
79. Wallach D. J Chem Phys 1967;47:5258.
80. Woessner DE. J Chem Phys 1962;37:647.
81. LeMaster DM. J Am Chem Soc 1999;121:1726.
82. Korzhnev DM, Billeter M, Arseniev AS, Orekhov VY. Prog Nucl Magn Reson Spectrosc 2001;38:197.
83. Atkinson RA, Kieffer B. Prog Nucl Magn Reson Spectrosc 2004;44:141.
84. Morse, PM.; Feshbach, H. Methods of Theoretical Physics. Vol. Ch 12. McGraw-Hill; NY: 1953.
85. Zare, RN. Angular Momentum. Wiley-Interscience; NY: 1988.
86. Silver, BL. Irreducible Tensor Methods. Academic Press; New York: 1976.
87. Halle B, Wennerström H. J Chem Phys 1981;75:1928.
88. Lipari G, Szabo A. Biophys J 1980;30:489. [PubMed: 7260284]
89. Lipari G, Szabo A. J Chem Phys 1981;75:2971.
90. Zerbetto M, Polimeno A, Meirovitch E. J Phys Chem B 2009;113:13613. [PubMed: 19775101]
91. Xu J, Xue Y, Srynnikov NR. J Biomol NMR 2009;45:57. [PubMed: 19582374]
92. Mason RP, Polnaszek CF, Freed JH. J Phys Chem 1974;78:1324.
93. Moro GJ, Freed JH. J Chem Phys 1981;74:3757.
94. Moro, GJ.; Freed, JH. Large-Scale Eigenvalue Problems, Math Studies Series. Cullum, J.; Willough, R., editors. Vol. 127. North Holland: 1986. p. 143

95. Fischer MWF, Zang L, Pang Y, Hu W, Majumdar A, Zuiderweg ERP. J Am Chem Soc 1997;119:12629.
96. Mandel AM, Akke M, Palmer AG III. J Mol Biol 1995;246:144. [PubMed: 7531772]
97. Fushman D, Cahill S, Cowburn D. J Mol Biol 1997;266:173. [PubMed: 9054979]
98. Barone V, Zerbetto M, Polimeno A. J Comput Chem 2009;30:2. [PubMed: 18496840]
99. Brooks B, Karplus M. Proc Natl Acad Sci USA 1983;80:6571. [PubMed: 6579545]
100. Karplus M, McCammon JA. Nat Struct Biol 2002;9:646. [PubMed: 12198485]
101. Amadei A, Linssen AB, Berendsen HJ. Proteins 1993;17:412. [PubMed: 8108382]
102. Kitao A, Wagner G. Proc Natl Acad Sci 2000;97:2064. [PubMed: 10688878]
103. Feng Y, Yang L, Kloczkowski A, Jernigan RL. Proteins 2009;72:551. [PubMed: 19507242]
104. Chu J. Biophys J 2009;96:427a.
105. Zheng W, Brooks BR, Hummer G. Proteins 2007;69:43. [PubMed: 17596847]
106. Lamm G, Szabo A. J Chem Phys 1986;85:7334.
107. Chen J, Im W, Brooks ChL III. J Am Chem Soc 2004;126:16038. [PubMed: 15584737]
108. Plaku E, Stamati H, Clementi C, Kavrati LE. Proteins 2007;67:897. [PubMed: 17380507]
109. Brüschweiler R, Case DA. Phys Rev Lett 1994;72:940. [PubMed: 10056573]
110. Prompers JJ, Brüschweiler R. Prot Struct Funct Gen 2002;46:177.
111. Horstink LM, Abseher R, Nilges M, Hilbers CW. J Mol Biol 1999;287:569. [PubMed: 10092460]
112. Abergel D, Bodenhausen G. J Chem Phys 2004;121:761. [PubMed: 15260602]
113. Abergel D, Bodenhausen G. J Chem Phys 2005;123:204901. [PubMed: 16351311]
114. Calandrini V, Abergel D, Kneller GR. J Chem Phys 2008;128:145102. [PubMed: 18412480]
115. Nodet G, Abergel D. ChemPhysChem 2008;9:625. [PubMed: 18324719]
116. Zhang F, Brüschweiler R. J Am Chem Soc 2002;124:12654. [PubMed: 12392400]
117. Ming D, Brüschweiler R. J Biomol NMR 2004;29:363. [PubMed: 15213434]
118. Ming D, Brüschweiler R. Biophys J 2006;90:3382. [PubMed: 16500967]
119. Cui G, Merz KM Jr. Biophys J 2008;94:3769. [PubMed: 18227134]
120. Vugmeyster L, Raleigh DP, Palmer AG II, Vugmeister BE. J Am Chem Soc 2003;125:8400. [PubMed: 12837113]
121. La Penna G, Fausti S, Perico A, Ferretti JA. Biophys J 2000;54:89.
122. Caballero-Manrique E, Bray JK, Deutschman WA, Dahlquist FW, Guenza MG. Biophys J 2007;93:4128. [PubMed: 17766356]
123. Nordio, PL.; Ferrarini, A.; Moro, G. Chemical Reactivity in Liquids, Fundamental Aspects. Moreau, M.; Turq, P., editors. Plenum; N. Y: 1988.
124. Ferrarini A, Moro GJ, Nordio PL, Polimeno A. Chem Phys Lett 1988;151:531.
125. Moro, GJ.; Ferrarini, A.; Polimeno, A.; Nordio, PL. Reactive Flexible Molecules in Liquids. Dorfmuller, Th, editor. Kluwer; Berlin: 1989.
126. Cassol R, Ferrarini A, Nordio PL. J Phys Chem 1993;97:2033.
127. Cassol R, Ge MT, Ferrarini A, Freed JH. J Phys Chem B 1997;101:8782.
128. Nevzorov AA, Trouard TP, Brown MF. Phys Rev E 1997;55:3276.
129. Pastor RW, Venable RM. Acc Chem Res 2002;35:438. [PubMed: 12069629]
130. Scheidt H, Huster D. Biophys J 2009;96:3663–3672. [PubMed: 19413971]
131. Fushman D, Ohlenschlager O, Ruterjans H. Biomol Struct Dynamics 1994;11:1377.
132. Pfeiffer S, Fushman D, Cowburn D. J Am Chem Soc 2001;123:3021. [PubMed: 11457013]
133. Trbovic N, Kim B, Friesner RA, Palmer AG III. Proteins 2007;71:684. [PubMed: 17975832]
134. Nederveen AJ, Bonvin AMJJ. J Chem Theory Comput 2005;1:363.
135. Maragakis P, Lindorf-Larssen K, Eastwood MP, Dror RO, Klepeis JL, Arkin IT, Jensen MO, Xu H, Trbovic N, Friesner RA, Palmer AG III, Shaw DE. J Phys Chem B 2008;112:6155. [PubMed: 18311962]
136. Sezer D, Freed JH, Roux B. J Chem Phys 2008;128:165106. [PubMed: 18447510]
137. Lynden-Bell AJ, Stone RM. Mol Simul 1989;3:271.

138. Sezer D, Freed JH, Roux B. J Phys Chem B 2008;112:11014. [PubMed: 18698714]
139. Sezer D, Freed JH, Roux B. J Phys Chem B 2008;112:5755. [PubMed: 18412413]
140. Zhang Z, Fleissner M, Tipikin D, Liang Z, Moscicki JK, Earle K, Hubbell W, Freed JH. A multifrequency Electron Spin Resonance Study of the dynamics of T4 lysozyme. J Phys Chem B. submitted.
141. Barone V, Polimeno A. Phys Chem Chem Phys 2006;8:4609. [PubMed: 17047758]
142. Barone V, Brustolon M, Cimino P, Polimeno A, Zerbetto M, Zoleo A. J Am Chem Soc 2006;128:15865. [PubMed: 17147399]
143. Zerbetto M, Carlotto S, Polimeno A, Corvaja C, Franco L, Toniolo C, Formaggio F, Barone V, Cimino P. J Phys Chem B 2007;111:2668. [PubMed: 17311450]
144. Carlotto S, Cimino P, Zerbetto M, Franco L, Corvaja C, Crisma M, Formaggio F, Toniolo C, Polimeno A, Barone V. J Am Chem Soc 2007;129:11248. [PubMed: 17705490]
145. Barone V, Polimeno A. Chem Soc Rev 2007;36:1724. [PubMed: 18213981]
146. Zerbetto M, Polimeno A, Kotsyubynskyy D, Ghalebani L, Kowalewski J, Meirovitch E, Olsson U, Widmalm G. J Chem Phys 2009;131:234501. [PubMed: 20025329]
147. Yao L, Vogeli B, Ying J, Bax A. A J Am Chem Soc 2008;130:16518.
148. Damberg P, Jarvet J, Graslund A. J Am Chem Soc 2004;127:1995. [PubMed: 15701036]
149. Cornilescu G, Bax A. J Am Chem Soc 2000;122:10143.
150. Spiegel, MR.; Liu, J. Mathematical Handbook of Formulas and Tables Schaum's Outline Series. 2. McGraw-Hill; New York: 1999. p. 266
151. Tjandra N, Szabo A, Bax A. A J Am Chem Soc 1996;118:6986.
152. Clore GM, Schwieters CD. J Mol Biol 2006;355:879. [PubMed: 16343537]
153. Budil DE, Lee S, Saxena S, Freed JH. J Magn Res A 1996;120:155.
154. Moro GJ, Polimeno A. Chem Phys 1989;131:281.
155. Levy RM, Karplus M, Wolynes P. J Am Chem Soc 1981;103:5998.
156. Karplus M, Ichiye T. J Mol Biol 1996;263:120. [PubMed: 8913294]
157. Johnson E, Showalter SA, Brüschweiler R. J Phys Chem B 2008;112:6203. [PubMed: 18376887]
158. Showalter SA, Johnson E, Rance M, Brüschweiler R. J Am Chem Soc 2007;129:14146. [PubMed: 17973392]
159. Johnson E, Chazin W, Rance M. J Mol Biol 2006;357:1237. [PubMed: 16476440]
160. Showalter SA, Brüschweiler R. J Chem Theory Comput 2007;3:961.
161. Emsley JW, Luckhurst GR, Stockley CP. Proc R Soc London Ser A 1982;381:117.
162. Dingemans T, Photinos DJ, Samulski ET, Terzis AF, Wutz C. J Chem Phys 2003;118:7046.
163. Wong V, Case DA. J Phys Chem B 2008;112:6013. [PubMed: 18052365]
164. Tjandra N, Kuboniwa H, Ren H, Bax A. Eur J Biochem 1995;230:1014. [PubMed: 7601131]
165. Lee AL, Flynn PE, Wand AJ. J Am Chem Soc 1999;121:2891.
166. Brüschweiler R, Liao X, Wright PE. Science 1995;268:886. [PubMed: 7754375]
167. Hall JB, Fushman D. J Biomol NMR 2003;27:261. [PubMed: 12975584]
168. Trbovic N, Cho J-H, Abel R, Friesner RA, Rance M, Palmer AG III. J Am Chem Soc 2009;131:615. [PubMed: 19105660]
169. Lindorf-Larssen K, Best RB, DePristo MA, Dobson CM, Vendruscolo M. Nature 2005;433:128. [PubMed: 15650731]
170. Salvatella X, Richter B, Vendruscolo M. J Biomol NMR 2008;40:71. [PubMed: 18030429]
171. Clore GM, Schwieters CD. J Am Chem Soc 2004;126:2923. [PubMed: 14995210]
172. Clore GM, Schwieters CD. Biochemistry 2004;41:10678. [PubMed: 15311929]
173. Meiler J, Prompers JJ, Peti W, Griesinger C, Brüschweiler R. J Am Chem Soc 2001;123:6098. [PubMed: 11414844]
174. Peti W, Meiler J, Brüschweiler R, Griesinger C. J Am Chem Soc 2002;124:5822. [PubMed: 12010057]
175. Lange OF, Lakomek NA, Fares C, Schroder GF, Walter KFA, Becer S, Meiler J, Grübmuller H, Griesinger C, de Groot BL. Science 2008;320:1471. [PubMed: 18556554]

176. Lakomek NA, Walter KFA, Fares C, Lange OF, de Groot BL, Grübmuller H, Munk RBA, Becker S, Meiler J, Griesinger C. J Biomol NMR 2008;41:139. [PubMed: 18523727]
177. Lorieau JL, McDermott AE. J Am Chem Soc 2006;128:11505. [PubMed: 16939274]
178. Sunada S, Go N, Koehl P. J Chem Phys 1996;104:4768.
179. Tombolato F, Ferrarini A, Freed JH. J Phys Chem B 2006;110:26248. [PubMed: 17181283]
180. Tombolato F, Ferrarini A, Freed JH. J Phys Chem B 2006;110:26260. [PubMed: 17181284]
181. Krushelnitsky A, Reichert D. Prog Nucl Magn Reson Spectrosc 2005;47:1.
182. Giraud N, Blackledge M, Goldman M, Bockmann A, Lesage A, Penin F, Emsley L. J Am Chem Soc 2005;127:18190. [PubMed: 16366572]
183. Meirovitch E, Nayeem A, Freed JH. J Phys Chem 1984;88:3454.
184. Huster D, Xiao L, Hong M. Biochemistry 2001;40:7662. [PubMed: 11412120]
185. Meints GA, Karlsson T, Drobny GP. J Am Chem Soc 2001;123:10030. [PubMed: 11592881]
186. Miller PA, Shajani Z, Meints GA, Caplow D, Goobes G, Varani G, Drobny GP. J Am Chem Soc 2006;128:15970. [PubMed: 17165714]
187. Meints GA, Miller PA, Pederson K, Shajani Z, Drobny GP. J Am Chem Soc 2008;130:7305. [PubMed: 18489097]
188. Echodu D, Goobes G, Shajani Z, Pederson K, Meints G, Varani G, Drobny GP. J Phys Chem B 2008;112:13934. [PubMed: 18844399]
189. Yang J, Tasayco ML, Polenova T. J Am Chem Soc 2009;131:13690. [PubMed: 19736935]
190. Chevelkov V, Fink U, Reif B. J Am Chem Soc 2009;131:14018. [PubMed: 19743845]
191. Chevelov V, Zhuravleva AV, Xue Y, Reif B, Skrynnikov NR. J Am Chem Soc 2007;129:12594. [PubMed: 17902660]
192. Agarwal V, Xue Y, Reif B, Skrynnikov NR. J Am Chem Soc 2008;130:16611. [PubMed: 19049457]
193. Tamura A, Matsushita M, Naito A, Kojima S, Miura KI, Akasaka K. Protein Science 1996;5:127. [PubMed: 8771205]
194. Ge M, Freed JH. Biophys J 1993;65:2106. [PubMed: 7507719]
195. Tjandra N, Bax A. Science 1997;278:1111. [PubMed: 9353189]
196. Tolman RJ, Al-Hashimi H, Kay LE, Prestegard JH. J Am Chem Soc 2001;123:1416. [PubMed: 11456715]
197. Tolman JR. J Am Chem Soc 2002;124:12020. [PubMed: 12358549]
198. Tolman JR. K Ruan Chem Rev 2006;106:1720.
199. Vugmeyster L, Trott O, Might CJ, Raleigh DP, Palmer AG III. J Mol Biol 2002;320:841. [PubMed: 12095260]
200. Korchuganov DS, Gagnidze IE, Tkach EN, Schulga AA, Kirpichnikov MP, Arseniev AS. J Biomol NMR 2004;30:43.
201. Wang T, Cai S, Zuiderweg ERP. J Am Chem Soc 2003;125:8639. [PubMed: 12848571]
202. Kay LE, Torchia D, Bax A. Biochemistry 1989;28:8972. [PubMed: 2690953]
203. Pawley NH, Wang C, Koide S, Nicholson LK. J Biomol NMR 2001;20:149. [PubMed: 11495246]
204. Lee LK, Rance M, Chazin WJ, Palmer AG III. J Biomol NMR 1997;9:287. [PubMed: 9204557]
205. de la Torre JG, Huertas ML, Carasco B. J Magn Res 2000;147:138.
206. Ortega A, de la Torre JG. J Am Chem Soc 2005;127:12764. [PubMed: 16159246]
207. Ryabov YE, Geraghty C, Varshney A, Fushman D. J Am Chem Soc 2006;128:15432. [PubMed: 17132010]
208. Osborne MJ, Wright PE. J Biomol NMR 2001;19:209. [PubMed: 11330809]
209. Copié V, Tomita Y, Akiyama SK, Aota A, Yamada KM, Venable RM, Pastor RW, Krueger S, Torchia DA. J Mol Biol 1998;277:663. [PubMed: 9533887]
210. Ulmer TS, Ramirez BE, Delaglio F, Bax A. J Am Chem Soc 2003;125:9179. [PubMed: 15369375]
211. Noda, L. The Enzymes. 3. Boyer, PD., editor. Vol. 8. Academic Press; London: 1973. p. 279-305.
212. Müller CW, Schlauderer GJ, Reinstein J, Schulz G. Structure 1996;4:147. [PubMed: 8805521]
213. Richard JP, Frey PA. J Am Chem Soc 1978;110:7757.

214. Aden J, Wolf-Watz M. J Am Chem Soc 2007;129:14003. [PubMed: 17935333]
215. Müller CW, Schulz G. J Mol Biol 1992;224:159. [PubMed: 1548697]
216. Müller-Dickerman H-J, Schulz GE. J Mol Biol 1995;246:522. [PubMed: 7877173]
217. Kraulis PJ. J Applied Crystall 1991;24:946.
218. Lou H, Cukier RI. J Phys Chem B 2006;110:12796. [PubMed: 16800615]
219. Kubitzki M, de Groot B. Structure 2003;16:1175. [PubMed: 18682219]
220. Elamrani S, Berry MB, Phillips GN Jr, McCammon JA. Proteins 1996;25:79. [PubMed: 8727320]
221. Bae E, Phillips GN Jr. Proc Natl Acad Sci USA 2005;103:2132. [PubMed: 16452168]
222. Lou H, Cukier RI. J Phys Chem B 2006;110:24121. [PubMed: 17125384]
223. Pontiggia F, Zen A, Micheletti C. Biophys J 2008;95:5901. [PubMed: 18931260]
224. Yuan W, Yang J, Kopecekova P, Kopecek J. J Am Chem Soc 2008;130:15760. [PubMed: 18980321]
225. Jacobs DJ, Rader AJ, Kuhn LA, Thorpe MF. Proteins 2001;44:150. [PubMed: 11391777]
226. Temiz A, Meirovitch E, Bahar I. Proteins 2004;57:468. [PubMed: 15382240]
227. Maragakis P, Karplus M. J Mol Biol 2005;352:807. [PubMed: 16139299]
228. Whitford PC, Miyashita O, Levy Y, Onuchic JN. J Mol Biol 2007;366:1661. [PubMed: 17217965]
229. Chu J-W, Voth GA. Biophys J 2007;93:3860. [PubMed: 17704151]
230. Yang L, Song G, Jernigan RL. Proc Natl Acad Sci USA 2009;106:12211. [PubMed: 19622742]
231. Pontiggia FF, Zen A, Micheletti C. Biophys J 2008;95:5901. [PubMed: 18931260]
232. Potestio R, Pontiggia F, Micheletti C. Biophys J 2009;96:4993. [PubMed: 19527659]
233. Arora K, Brooks CL III. Proc Natl Acad Sci USA 2007;104:18496. [PubMed: 18000050]
234. Sinev MA, Sineva EV, Ittah V, Haas E. Biochemistry 1996;35:6425. [PubMed: 8639589]
235. Sinev MA, Sineva EV, Ittah V, Haas E. FEBS Lett 1996;397:273. [PubMed: 8955362]
236. Hanson JA, Duclerstacit K, Watkins LP, Bhattacharyya S, Brokaw J, Chu J-W, Yang H. Proc Natl Acad Sci USA 2007;104:18055. [PubMed: 17989222]
237. Wolf-Watz M, Thai V, Henzler-Wildman KA, Hadjipavlou G, Eisenmesser EZ, Kern D. Nat Struct & Mol Biol 2004;11:945. [PubMed: 15334070]
238. Kumar S, Sham YY, Tsai C-J, Nussinov R. Biophys J 2001;80:2439. [PubMed: 11325743]
239. Ruan Q, Ruan K, Balmy C, Glaser M, Mantulin WW. Biochemistry 2001;40:14706. [PubMed: 11724585]
240. Henzler-Wildman KA, Lei M, Thai V, Kerns SJ, Karplus M, Kern D. Nature 2007;450:913. [PubMed: 18026087]
241. Shapiro, YuE; Sinev, MA.; Sineva, EV.; Tugarinov, V.; Meirovitch, E. Biochemistry 2000;39:6634. [PubMed: 10828981]
242. Shapiro, YuE; Meirovitch, E. J Phys Chem B 2009;113:7003. [PubMed: 19385637]
243. Barnes JP, Freed JH. Biophys J 1998;75:2532–2546. [PubMed: 9788949]
244. Kroenke CD, Rance M. AG Palmer J Am Chem Soc 1999;121:10119.
245. Mandel AM, Akke M, Pamer AG III. Biochemistry 1996;35:16009. [PubMed: 8973171]
246. Ikura M, Barbato G, Kay LE, Pastor RW, Bax A. Biochemistry 1992;31:5269. [PubMed: 1606151]
247. Tjandra N, Kuboniwa H, Ren H, Bax A. Eur J Biochem 1995;230:230.
248. Baber JL, Szabo A, Tjandra N. J Am Chem Soc 2001;123:3953. [PubMed: 11457145]
249. Chang S-L, Szabo A, Tjandra N. J Am Chem Soc 2003;125:11379. [PubMed: 16220961]
250. Babu YS, Bugg CE, Cook WJ. J Mol Biol 204:1988.
251. Pang Y, Buck M, Zuiderweg ERP. Biochemistry 2002;41:2655. [PubMed: 11851412]
252. Levy RM, Karplus M, Wolynes PG. J Am Chem Soc 1981;103:5998.
253. Sampedro JG, Munoz-Clares RA, Uribe SJ. Bacteriology 2002;184:4384.
254. Peinelt C, Apell H-J. Biophys J 2004;86:815. [PubMed: 14747317]
255. Chen K, Tjandra N. J Am Chem Soc 2008;130:12745. [PubMed: 18761455]
256. Ryabov YE, Fushman D. Proteins 2006;63:787. [PubMed: 16609980]
257. Ryabov YE, Fushman D. J Am Chem Soc 2007;129:3315. [PubMed: 17319663]

258. Wong V, Case DA. A Szabo Proc Natl Acad Sci USA 2009;106:11016.
259. Chen K, Tjandra N. J Am Chem Soc 2008;130:12745. [PubMed: 18761455]
260. Zhang Q, Sun X, Watt EO, Al-Hashimi HM. Science 2006;311:653. [PubMed: 16456078]
261. Hansen AL, Al-Hashimi HM. J Am Chem Soc 2007;129:16072. [PubMed: 18047338]
262. Lee A, Sharp KA, Kranz JK, Song XJ, Wand AJ. Biochemistry 2002;41:13814. [PubMed: 12427045]
263. Li DW, Brüschweiler R. Phy Rev Lett 2009;102:118108.
264. Johnson E, Palmer AG III, Rance M. Proteins 2007;66:796. [PubMed: 17173286]
265. Fuentes EJ, Gilmore SA, Mauldin RV, Lee AL. J Mol Biol 2006;364:337. [PubMed: 17011581]
266. Clarkson MW, Gilmore SA, Edgell MH, Lee AL. Biochemistry 2006;45:7693. [PubMed: 16784220]
267. Law AB, Fuentes EJ, Lee AL. J Am Chem Soc 2009;131:6322. [PubMed: 19374353]
268. Xue Y, Pavlova MS, Ryabov YE, Reif B, Skrynnikov NR. J Am Chem Soc 2007;129:6827. [PubMed: 17488010]
269. Chatfield DC, Augusten A, D'Cunha C. J Biomol NMR 2004;29:377. [PubMed: 15213436]

6. Appendices

Appendix A: Typical data fitting scenarios

Let us denote N–H bonds located in well-structured regions of the protein, notably elements of secondary structure, as "rigid", and those located in mobile domains, loops, end-chain segments, etc., as "flexible". In many cases the MF analysis of "rigid" N–H bonds (and in some cases of "flexible" N–H bonds) requires the inclusion of conformational exchange (R_{ex}) contributions (added to the expression for $1/T_2$ given in Eq. 64). The fitting of the experimental data by the program SRLS/C++OPPS in terms of motion of these three types of N–H bond is illustrated below [90]. We selected as an example ^{15}N relaxation parameters of *E. coli* adenylate kinase (AKeco) acquired at 14.1 and 18.8T, and 303K [46,47]. The global motional correlation time at this temperature is 14.9 ns [50].

The expressions for ^{15}N $1/T_1$, $1/T_2$ and ^{15}N–{^{1}H} *NOE* are given by [29]:

$$1/T_1=d^2[\,J^{DD}(\omega_H-\omega_N)+3\,J^{DD}(\omega_N)+6\,J^{DD}(\omega_H+\omega_N)]+c^2J^{CC}(\omega_N), \tag{63}$$

$$1/T_2=1/2d^2[\,4\,J^{DD}(0)+J^{DD}(\omega_H-\omega_N)+3\,J^{DD}(\omega_N)+6\,J^{DD}(\omega_H)+6\,J^{DD}(\omega_H+\omega_N)]+c^2/6[\,4\,J^{CC}(0)+3\,J^{CC}(\omega_N)], \tag{64}$$

and

$$NOE=1+\{(\gamma_H/\gamma_N)d^2[\,6J^{DD}(\omega_H+\omega_N)-J^{DD}(\omega_H-\omega_N)]\,T_1\}, \tag{65}$$

where $d^2=\gamma_H^2\gamma_N^2h^2/(40\pi^2)\langle 1/r_{NH}^3\rangle^2$, $c^2=(2/15)\gamma_N^2B_0^2(\sigma_\parallel-\sigma_\perp)^2$, r_{NH} is the ^{15}N–^{1}H internuclear distance in Å, B_0 is the magnetic field strength, and $\sigma_\parallel$ and $\sigma_\perp$ are the parallel and perpendicular components of the axially symmetric ^{15}N chemical shift tensor. $J^{DD}(\omega)$ and $J^{CC}(\omega)$ are obtained using Eq. (56a) with μ representing the ^{15}N–^{1}H dipolar interaction and the ^{15}N CSA interaction, respectively. The magnetic interaction parameters used in the calculations presented below are $r_{NH(eff)}$ = 1.015 Å [147], $\Delta\sigma$ = −169 ppm [148] and β_D = 17° [149].

L_{max} (the quantum number which determines how many terms need to be preserved in Eq. (61) and similar equations) of 24 was always found to suffice in these calculations. In our previous implementation of SRLS [20] the principal values of the global and local diffusion tensors, $\boldsymbol{R}^{\mathbf{C}}$ and $\boldsymbol{R}^{\mathbf{L}}$, are given in units of R^{L} or $R_{\perp}^{L}$. In the SRLS/C++OPPS program they are given in units of s^{-1}. We use the same notation in both cases.

For axial local potentials we also show below the results of the MF analyses corresponding to the SRLS analyses carried out. Corresponding calculations feature the same number of formally analogous variables; hence, the differences arise from the manner in which the time correlation functions (spectral densities) are calculated.

The MF parameter S^2 is formally analogous to $(S_0^2)^2$ in SRLS. For high axial local ordering τ_e agrees with $\tau_{ren}=2\tau/c_0^2$ [14,20,31,40]. The MF parameters τ_f and τ_s are formally analogous to $\tau_{\|}=1/(6R_{\|}^{L})$ and $\tau_{\perp}=1/(6R_{\perp}^{L})$, respectively, in SRLS. The parameters S_f^2 and S_s^2 can be expressed in terms of $(S_0^2)^2$ and $(S_2^2)^2$ [20,40].

Example 1: “Rigid” residue with axial local ordering

Data for the ^{15}N–^{1}H bond of the aspartic acid residue D197 of the CORE domain of AKeco were analyzed with the MF program DYNAMICS [97]. MF model 2, where S^2 and τ_e are varied, was selected. It led to the best-fit values of $S^2 = 0.84$ (corresponding to the coefficient $c_0^2=12.4$ of the potential u given (in units of k_BT) by the axial version of Eq. 52, calculated assuming that $S^2 \rightarrow (S_0^2)^2=\langle D_{00}^2\rangle^2$) and τ_e = 12.7 ps (corresponding to τ = 78 ps using the expression for τ_{ren} given above), with χ^2 = 2. In analogy, we allowed c_0^2 and τ to vary in the SRLS calculation. We fixed the angle β_{MD} at 0°, in accordance with its implicit value in MF. This led to $c_0^2=11.6$ ($(S_0^2)^2=0.83$) and τ = 69 ps, with χ^2 = 0.6. The SRLS calculation lasted 19 s. These results are shown in Table 1, rows 1 and 2.

The differences between the SRLS and MF results are 1.2% for the squared order parameter, 13% for the local motional correlation time, and 6.9% for the potential coefficient, c_0^2. Although χ^2 = 0.6 in the SRLS calculation and χ^2 = 2 in the MF calculation, both are considered appropriate since both values lie below 5.99, which is the percentile value for χ^2 distribution for 4 degrees of freedom (six data points and two variables) for a commonly used 5% threshold (Table 39 of Ref. [150]).

The differences stem from (1) accounting in SRLS for the frame transformation between the ^{15}N–^{1}H dipolar and ^{15}N CSA frames [20] (Figure 1), and (2) possible deviations in MF from the single-decay approximation for the local motion [20]. As pointed out above, in the presence of local motions the transformation from the ^{15}N–^{1}H dipolar frame to the ^{15}N CSA frame requires besides $j_{00}(\omega)$ the time correlation functions $j_{11}(\omega)$ and $j_{22}(\omega)$, which do not exist in MF. This frame transformation is required to calculate $J^{CC}(\omega)$, as well as the cross-correlated spectral density, $J^{DC}(\omega)$.

When the local motion is in the extreme motional narrowing limit the functions $j_{11}(\omega)$ and $j_{22}(\omega)$ are negligible in comparison to $j_{00}(\omega)$. Hence MF can calculate $J^{CC}(\omega)$ and $J^{DC}(\omega)$ adequately only in this limit. This is stated explicitly in Ref. [151] in the context of $J^{DC}(\omega)$. SRLS can treat cross-correlated relaxation, as well as provide $J^{CC}(\omega)$, over the entire parameter range relevant for folded proteins. It is therefore recommended to use SRLS even in cases in which the local potential is axially symmetric.

Example 2: “Rigid” residue with rhombic local ordering

The leucine residue L209 of AKeco is also a “rigid” residue. In this case the MF calculation did not pass the Goodness-Of-Fit (GOF) criteria of the program DYNAMICS [97]. The best results generated by this program, obtained with model 3 MF, are $S^2 = 0.78$ (c_0^2=9), $\tau_e = 9.3$ ps ($\tau = 41.7$ ps) and $R_{ex} = 4.35\ s^{-1}$. The χ^2 value is 8.8, which is higher than the relevant threshold of 7.81 (Table 39 of Ref. [150]). By using as variables c_0^2, R^L and R_{ex} (in analogy with the MF variables), and setting $\beta_{MD} = 0°$, we obtained with SRLS c_0^2=10.1 ($(S_0^2)^2$=0.805), $\tau = 30.9$ ps and $R_{ex} = 3.56\ s^{-1}$. The χ^2 value is 5.8, which is below the relevant threshold. These results are shown in Table 1, rows 3 and 4.

As pointed out above, R_{ex} can absorb the rhombicity of the local potential [40]. With this in mind we set $\beta_{MD} = 101.3°$ and $\alpha_{MD} = 90°$. This is consistent with rhombic local ordering with $C^{\alpha}_{i-1} - C^{\alpha}_{i}$ (rather than N–H, as implied by axial ordering and $\beta_D = \alpha_D = 0°$) being the main local ordering/local diffusion axis [20,46–50,65,78]. Within the scope of this geometry we allowed c_2^2 to vary and set R_{ex} equal to zero. To obtain good statistics and effective convergence we had to set $R^L_{\perp}=R^C$ and allow $R^L_{\parallel}$ to vary.

The results of this calculation are shown in Table 1, row 5. The potential coefficients are $c_0^2 = -15.9$ and $c_2^2 = -3.4$. The Cartesian tensor components calculated from these coefficients (e.g., see Ref. [20]) are $S_{xx} = -0.401$, $S_{yy} = +0.874$ and $S_{zz} = -0.473$.[2] Viewed in the context of $\alpha_{MD} = 90°$ and $\beta_{MD} = 101.3°$, the fact that $S_{yy} = +0.874$ means that relatively high ordering prevails along the $C^{\alpha}_{i-1} - C^{\alpha}_{i}$ axis. The anisotropy of the local ordering *around* $C^{\alpha}_{i-1} - C^{\alpha}_{i}$ is given by $(S_{xx} - S_{zz})/S_{yy} = 0.082$.

The value of $R^L_{\parallel}=1.3 \times 10^{10}\ s^{-1}$ corresponds to $\tau = 12.8$ ps. This represents fast fluctuations of the N–H bond. Setting $R^L_{\perp}$ equal to $R^C = 1.117\times10^7\ s^{-1}$ (14.9 ns) means that we cannot detect backbone motions which based on geometric considerations are associated with $R^L_{\perp}$. Thus, the combined two-field data from the “rigid” N–H bond of residue L209 makes it possible to determine the magnitude and symmetry of the local ordering, the form of the potential in terms of which the order parameters S_0^2 and S_2^2 (or S_{xx}, S_{yy} and S_{zz}) are defined, and the rate of the N–H fluctuations.

Note that not accepting the simple scenario of an axial potential and locating the main local ordering/local diffusion axis along the N–H bond, i.e., $\beta_{MD} = 0°$, was motivated by physical considerations. If only statistical criteria were considered, we would have accepted the results shown in Table 1, row 4. At present the local geometry associated with residue L209 is fixed at $\alpha_{MD} = 90°$ and $\beta_{MD} = 101.3°$, and $R^L_{\perp}=R^C$ is fixed. The analysis of data combined from three B_0 values, concerted analysis of temperature-dependent data, or combined analysis of several probes with their equilibrium orientation lying within the peptide plane, might allow for a large number of variables, including $R^L_{\perp}$ (this discussion is limited to the overdamped Smoluchowski limit).

The time required to complete the calculation illustrated in Table 1, row 5, was approximately one hour. The local potential determined is high ($c_0^2 = -15.9$), the local ordering is high ($S_{yy} = +0.874$), and the time scale separation between $R^L_{\parallel}$ and R^C is large (0.00087). The L_{max} value required was 24. Higher potentials do not require much larger L_{max} values, and the time scale separation has already reached a limiting value for which a robust fitting calculation should stop. Therefore, this example may be considered represent a typical long fitting calculation.

Example 3: "Flexible" residue with rhombic local ordering

The glycine residue G46 of AKeco is located in the mobile domain AMPbd. The program DYNAMICS [97] selected model 7 but the calculation did not pass the GOF criteria. The best results are S^2=0.778 (c_0^2=8.9), S_f^2 = 0.87 (corresponding to β_{MD} = 12.2°, according to $S_f^2 = (1.5\cos^2\beta_{MD} - 0.5)^2$ – see Ref. [19]), τ_s = 0.91 ns, τ_f = 0.0 ps and R_{ex} = 1.8 s^{-1}. The χ^2 value is 5.1. By using SRLS with axial potentials and assuming that $R_{\|}^{L} \gg R_{\perp}^{L}$ [19], in analogy with $\tau_s \gg \tau_f$ in MF, we obtained c_0^2=3.6 ($(S_0^2)^2$=0.448), β_{MD} = 21.4°, $\tau_\perp$ = 7.12 ns and $\tau_{\|}$ = 0.004 ns [46]. These results are shown in Table 1, rows 6 and 7.

As reported previously [46], the SRLS and MF results differ significantly mainly because mode-coupling is not accounted for in MF. However, the SRLS results shown in Table 1, row 7, are also problematic because c_0^2=3.6 represents too weak a potential inside a folded protein, and a 21.4° tilt from the N–H bond does not identify a structural element which can serve as the main local ordering/local diffusion axis [20].

Row 8 of Table 1 shows the results obtained with SRLS/C++OPPS by allowing the local potential to be rhombic and the local diffusion tensor, $\boldsymbol{R}^{\mathbf{L}}$, to be axially symmetric. The angles α_D and β_D were set equal to 90° and 101.3°, respectively. The best-fit values of the potential coefficients are c_0^2= − 6.8 and c_2^2= − 4.40, and the corresponding Cartesian tensor components are S_{xx} = −0.426, S_{yy} = +0.876 and S_{zz} = −0.450. The anisotropy of the local ordering *around* $C_{i-1}^{\alpha} - C_i^{\alpha}$ is given by $(S_{xx} - S_{zz})/S_{yy}$ = 0.027. $R_\perp^L$=4.15 × 10^7 s^{-1} corresponds to $\tau_\perp$ = 4.0 ns, and $R_{\|}^{L}$=8.11 × 10^9 s^{-1}, to $\tau_{\|}$ = 20.6 ps. This calculation was completed in 21 minutes.

The physical picture is as follows. Based on geometric (and other [20,46]) considerations, the perpendicular component, $\tau_\perp$ = 4.0 ns, may be associated with domain motion. In the present case $\tau_\perp$ is 3.7 times faster than the global tumbling. The parallel component, $\tau_{\|}$ = 20 ps, represents fast fluctuations about an axis in close proximity to the equilibrium N–H orientation, and is 1.6 times slower for the "flexible" N–H bond of residue G46 than for the "rigid" N–H bond of residue L209.

Both the "rigid" N–H bond of residue L209 and the "flexible" N–H bond of residue G46 experience comparably high ordering *around* the $C_{i-1}^{\alpha} - C_i^{\alpha}$ axis: we obtained S_{yy} = +0.874 for the former and S_{yy} = +0.876 for the latter. On the other hand, the anisotropy of the local ordering is nearly 3-times higher for the "rigid" site than for the "flexible" site. This is interesting new information. There are controversial views, based largely on order parameters from MF analysis of spin relaxation, on whether proteins prevail in solution as narrow or broad conformational ensembles [152]. The forms of these ensembles bear a direct relationship to the *relative* equilibrium probability density, P_{eq}, determined with SRLS. The P_{eq} function depends on the geometric perspective; this is illustrated in Appendix F, Section 4.

The 3D GAF model [65,78] can also quantify the magnitude and anisotropy of the local ordering. However, it requires the prevalence of fast local motions, the availability of MD trajectories, and it does not provide local potentials (which can be used to calculate thermodynamic quantities).

SRLS/C++OPPS-based ^{15}N spin relaxation analysis of an entire protein: estimate of efficiency

Let us consider a representative protein comprising 300 residues, and assume that 10% of the residues are "flexible". Example 3 above describes the analysis of a "flexible" residue of AKeco; this case may be considered as a paradigm for the analysis of the "flexible" residues

of the representative protein. By analogy it would take about 10.5 hours to least-squares fit the experimental data for 30 “flexible” residues. Example 2 above describes the analysis of a “rigid” residue of AKeco; this case may be considered as a paradigm for the analysis of the “rigid” residues of the representative protein. By analogy it would take about 270 hours to least-squares fit the experimental data for 270 “rigid” residues. Let us multiply this time by 1.5, to account for the possibility that 50% of the “rigid” residues require a second trial of starting parameters. Based on these considerations it would take 405 hours to least-squares fit the experimental data for 270 “rigid” residues, and about 17 days to analyze all the residues of this protein.

This estimate is based on calculations carried out on a portable HP computer equipped with an Intel 2.7 GHz Dual Core CPU and 4GB RAM. On a Quad-Core i7 Extreme CPU with a 3.2 GHz clock speed, 1600 MHz 8 MB cache, and 24 GB of 1300 MHz CL6 RAM, the analysis of the 300 residue protein selected as example will be completed in 4 – 5 days. Utilization of the parallelized version of C++OPPS in the context of a computer cluster will reduce the running time significantly.

Problems encountered in some cases and prospects

The present data-fitting scheme of the C++OPPS package features the publicly available MINPACK minimization package. The pertinent minimizer has not been adapted/optimized, and other minimizers have not been yet implemented/examined. With “rigid” N–H bonds we encountered in some cases problems associated with the exit criteria of the MINPACK minimizer. In the context of SRLS/ESR the Levenberg-Marquardt minimizer has been adapted/optimized successfully [153]. We might be able to overcome the problem noted by optimizing the MINPACK minimizer, or employing other minimizers. Such efforts are underway.

It is easy to fit the “rigid” N–H bond data that correspond to strong axial potentials, fast isotropic local diffusion, and frequent inclusion of conformational exchange contributions. This is similar to the results obtained with MF analyses. When rhombic potentials or axial local diffusion were allowed for, with $\alpha_{MD} = 90°$ and $\beta_{MD} = 101.3°$, we encountered (in the limited calculations carried out so far) quite a few cases in which the fitting process led to unphysical results. It is known that in the presence of strong local potentials one should use the Fokker-Planck-Kramers (FPK) equation with both orientation and angular momentum included explicitly [16,154]. This will allow the probe to engage in torsional oscillations in the potential well, expected on physical grounds, which in the over-damped Smoluchowski treatment are relaxed instantaneously. Thus, the problems encountered in fitting data for “rigid” N–H bonds might have a physical reason, which could be tackled by solving the corresponding FPK equation. The latter includes inertial effects; the dynamic picture of the well-structured regions of the protein might change by accounting for these effects.

The full two-body FPK model is treated explicitly in Ref. [16]. Efforts to implement it for ^{15}N spin relaxation in proteins are underway. The additional parameters required are moments of inertia, which can be derived from 3D structures.

Appendix B: NMR parameters calculated with molecular dynamics methods

NMR relaxation of natural abundance ^{13}C has been treated already in early MD work [155]. Relatively simple models were developed to interpret the experimental data. The models considered pertain to the continuous diffusion, restricted diffusion and lattice jump categories. Their accuracy was tested. Stochastic dynamics was used to calculate experimental ^{13}C NMR relaxation parameters of small alkanes. The results obtained were used to predict NMR relaxation in proteins. Since then extensive MD studies of proteins have been carried out in

the context of NMR spin relaxation. At present μs long simulations, which feature explicit solvent and use constantly improving force-fields, can be carried out for small proteins.

In calculating time correlation functions from MD trajectories it is typically assumed that the global and local motions are statistically independent, i.e., $C(t) = C^{C}(t) \times C^{L}(t)$. Based on this assumption the global motion is usually eliminated by superimposing the MD frames onto a reference structure. The time correlation function obtained in this way for internal motion, $C^{L}(t)$, is often least-squares fitted to the form of the MF time correlation function, and in some cases to the Extended Model Free (EMF), reduced EMF, or other variants of the MF formula. This yields order parameters and correlation times that are compared to their MF counterparts. In some cases the squared order parameter is derived directly as the plateau value of the $C^{L}(t)$ function, or calculated using the expression developed in Ref. [37], the isotropic Reorientational Eigenmode Dynamics (iRED) method [25,26], or other methods (see below).

To calculate spectral densities and relaxation parameters with MD the total time correlation function, $C(t)$, is required. One usually determines $C^{C}(t)$ by calculating the global diffusion tensor based on experimental ^{15}N T_1/T_2 ratios. Multiplication by $C^{L}(t)$ (parameterized as outlined above) yields an analytical form of $C(t)$.

To calculate from the MD trajectory $C^{L}(t)$, or S^2 according to Ref. [37], it is necessary to carry out the frame superposition mentioned above. This procedure depends non-negligibly on the choice of the reference structure [132,156]. Frame superposition is not required when order parameters are calculated using the iRED method [25,26].

The network of coupled rotators (NCR) of Abergel et al. [112–115] provides order parameters, as well as local motional correlation times. NCR is based on interesting physical ideas; it provides implicitly information on the asymmetry of the local ordering. However, it pertains to the large time scale separation limit, the local geometry is encoded, and the local motion is intrinsically isotropic.

Methods for calculating order parameters based on harmonic approximations, such as Normal Mode Aanalysis (NMA) [99] and Gaussian Network Model (GNM) [27], have been developed. Contact models for calculating order parameters based on parameterization of the local structure have been developed by Brüschweiler and coworkers [116–118].

Several representative MD studies, where results are compared with MF analyses of NMR spin relaxation data, are presented below. The extent of agreement between order parameters, spectral density values and relaxation parameters obtained with MD and NMR/MF is discussed.

Chatfield et al. [36] used the force field CHARMM and the TIP3P model for water to generate a trajectory of 18 ns in length for liganded and 3.75 ns in length for unliganded SNase. Order parameters were calculated using the expression developed in Ref. [37]. For N–H and C^{α}–H the agreement between S^2(MD) and S^2(MF) was found to be reasonably good. On the other hand, large discrepancies were found between S^2(MD) and S^2(MF) for the C^{α}–C^{β} bond of alanine. While MD yields comparable squared order parameters for C^{α}–H and C^{α}–C^{β}, as one would expect, MF yields $S^2(C^{\alpha}–C^{\beta})$ approximately 30% smaller than $S^2(C^{\alpha}$-H). This discrepancy has not been resolved over the years. The S_{axis}^2 order parameters of eglin c are still much smaller as compared to their MD-derived counterparts [70].

Showalter et al. [157] used the improved AMBER99SB force field to simulate $^{13}CDH_2$ methyl dynamics in calbindin Dk_9. After eliminating the global motion, the time correlation function calculated from the MD trajectory was parameterized according to:

$$C^{L}(t)=C_{CC}(t)\times C_{CH3}(t)=C_{CC}(t)\times[0.1+0.9\exp(-t/\tau_{CH3})]. \quad (66)$$

$C_{CH3}(t)$ represents the motion about the C–CH_3 axis and $C_{CC}(t)$ the motion of the C–CH_3 axis. $C_{CC}(t)$ was parameterized with a sum of 5 exponentials and an offset [65]. The differences between corresponding simulated and experimental values of $J(0)$, $J(\omega_D)$ and $J(2\omega_D)$, obtained previously [158] and analyzed with MF, were minimized allowing τ_{CH3} to vary. Good agreement was obtained for $J(\omega_D)$ and $J(2\omega_D)$ and poorer agreement for $J(0)$, with the values obtained with MF analysis of the experimental data [158] smaller than the corresponding MD values. This is due partly to having varied τ_{CH3}, which affects to a larger extent the higher frequency values of $J(\omega)$ [157].

Additional parameterization schemes have been used: (1) $C_{CC}(t)$ was parameterized using Eq. (34) with $C_{CH3}(t)$ taken as shown in Eq. (66), and (2) $C^{L}(t)$ was parameterized using Eq. (43). The first protocol led to better agreement between MD and MF; in particular, the differences between corresponding squared order parameters were less systematic. This indicates that allowing for two separate local motions for the methyl group is a better approximation to the actual scenario than Eq. (43), in agreement with the latter not representing intrinsically a physical scenario (cf. Section 3.2.3.) whereas Eq. (66) might represent one in simple limits.

In general, the agreement between MD and NMR/MF is better using the improved AMBER99SB force-field [157]. In particular, the agreement between corresponding MD and NMR/MF methyl-related squared order parameters is still significantly worse than the agreement between corresponding MD and NMR/MF N–H-related squared order parameters [160].

Pfeiffer et al. [132] used the AMBER 5.0 force field and the TIP3 model for water to generate a 7.6 ns trajectory for the β-adrenergic pleckstrin homology (PH) domain of the β-adrenergic receptor kinase-1. The objective was to study N–H bond dynamics. The global motion was treated as in Ref. [157]. The time correlation function for local motion was least-squares fit to a MF-type time correlation function featuring three decoupled local motions. This implies three squared order parameters and three local motional correlation times entering $C^{L}(t)$. The generalized order parameter, S^2, given by the product of these three squared order parameters, was calculated according to Ref. [37]; it was then used as a restraint in the fitting process.

For the core of the protein $J(0)$ and $J(\omega_N)$ from MD were found to be on average lower by 6% than their MF counterparts. On the other hand, $J(0.87\ \omega_H)$ from MD was found to be lower by 21% than $J(0.87\ \omega_H)$ from MF. The value of $J(0.87\ \omega_H)$ represents $J(\omega_H+\omega_N)$, $J(\omega_H)$ and $J(\omega_H-\omega_N)$ combined into a single spectral density value within the scope of the Reduced Spectral Density strategy (e.g., see Ref. [8]). The value of S^2 from MD was 1% (6%) lower than S^2 from MF for all the N–H bonds (the N–H bonds in the protein core).

This pattern is opposite to the pattern determined by Showalter et al. [157] for methyl dynamics. This is likely to be associated with using different parameterization schemes, in the context of different parameter ranges dominated by different factors. Thus, the local ordering is strong for “rigid” N–H bonds [132]; in this limit the Wigner functions are relatively good approximations to the eigenfunctions of the local diffusion operator [14,20]. On the other hand, the local ordering is weak at methyl sites; as shown in Appendix G, even very weak potentials render the Wigner functions to be poor approximations to the eigenfunctions of the local diffusion operator.

Reference [160] also employed the improved AMBER99SB force field to study N–H bond dynamics in ubiquitin. In that study, the MD time correlation function for internal motion was

parameterized according to Eq. (2), the squared order parameters were calculated with the iRED method [26], and an axial global diffusion tensor was determined independently based on ^{15}N T_1/T_2 data. Good agreement was obtained with this parameterization scheme between relaxation parameters from MD and MF. On the other hand, the agreement between values of the corresponding squared order parameters was less satisfactory. A similar picture emerges from Table 1 below. We found repeatedly that experimental relaxation parameters could be fit equally well from a statistical point of view with formally analogous SRLS and MF spectral densities, albeit with different best-fit parameters.

The reason for better agreement between corresponding MD and NMR/MF relaxation parameters as compared to order parameters is that the principal quantities are the $j_{KK'}(\omega)$ functions. They comprise intrinsically the best-fit parameters. Agreement between corresponding best-fit parameters means good reproduction of the actual physical scenario. Agreement between relaxation parameters means statistical reproduction of the $J^{XY}(\omega)$ or $J^{XX}(\omega)$ functions. If the former type of agreement is worse that the latter type, this is an indication that the force-field is largely accurate, whereas the MF analysis is relatively inaccurate.

Parameterization renders the derivation of consistent information problematic. Results with different characteristics are obtained even when the same force-field is used – cf. Refs. [157] and [160]. It would be useful to calculate the MD counterparts of the SRLS $C_{KK'}(t)$ functions instead of parameterizing the MD trajectory in various ways. Deriving consistent physical information from calculations of the (artificial) generalized order parameter, using various parameterizing techniques [160], is also problematic. There exist established methods for calculating potentials in terms of which physical order parameters are defined [161,162]. It would be useful to apply these methods to study local ordering in proteins.

Discrepancies between corresponding MD and MF-derived order parameters, spectral density values, and relaxation parameters have been ascribed to force-field imperfections, insufficient length of the MD trajectories, problematic aspects of the MD protocols, and/or motions affecting the MD trajectory but not affecting the experimental data [132,133,157,163]. We suggest adding to this list the oversimplification inherent in MF.

Trbovic et al. [133] used the improved AMBER ff99sb, AMBER ff03 and OPLS AA force fields to study N–H bond dynamics of the B3 immunoglobulin-binding domain of streptococcal protein G (GB3). Thirteen trajectories of 2.4 ns generated using OPLS AA were subjected to simulation using AMBER ff99SB and ff03. The global motion was eliminated from the MD trajectory. $C^{L}(t)$ was calculated as the time correlation function of the Legendre polynomial of rank 2, and order parameters were calculated according to Ref. [37]. Final time correlation functions and order parameters were obtained as averages over multiple trajectories.

Squared order parameters from MD were compared with their MF counterparts. In many cases S^2(MD) was found to be smaller than S^2(MF). This was associated primarily with imbalance between the description of hydrogen bonding and other terms in the force fields employed [133]. However, the parameterization strategies used in the MD and MF protocols are not the same; this may also influence the results.

Maragakis et al. [135] generated recently a 1.2 μs trajectory of ubiquitin using the improved OPLS–AA/SPC force field. After eliminating the global motion S^2 was obtained as C^{L} (100 ns) (method 1) or according to Ref. [37] (method 2). The parameter S^2 was also calculated from the original MD trajectory by least-squares fitting the MD time correlation function for internal motion to the reduced extended MF formula (method 3).

It was found that in loop regions the correspondence between S^2(MD) and S^2(MF) is significantly better using method 3. This was ascribed to the global motion, which is preserved in method 3, decorrelating local motions slower than it. Thereby the simulated time correlaton function is brought into better agreement with the experimental time correlation function which is only affected by local motions comparable to, or faster than, the global motion.

The MD simulations led to τ_m = 1.98 ns; the experimental τ_m value of ubiquitin at the relevant temperature is 4.1 ns [164,165]). Accurate determination of the global diffusion from MD trajectories is notoriously difficult because the rate constant for the rotational reorientation of water is overestimated even in the most advanced models for water. It was shown in Ref. [135] that S^2(MD) and S^2(MF) agree; then τ_s, S_s^2 and/or S_f^2 must differ to overcome the differences in τ_m. Again, an improved treatment of the spin relaxation might be useful.

Wong and Case [163] studied ubiquitin, binase, GB3 and lysozyme using the AMBER99sb force field with the TIP4P/EW or SPC/E models for water. Trajectories 6 – 60 times as long as the mean experimental τ_m value were generated. For the first time a method for determining the global diffusion tensor from the MF trajectory was set forth. Site-specific global-motional correlation times, $\tau_m(i)$, were calculated based on the method of Ref. [166], which is applicable to $R_{\|}^{C}/R_{\perp}^{C} \leq 2$. The trace of the $\boldsymbol{R}^{\mathbf{C}}$ tensor was 6.6 – 24.6% smaller as compared to its MF counterpart.

This provided $C^C(t)$. The time correlation function $C^L(t)$ was calculated from the MD trajectory assuming reorientation of the probe with respect to a “frozen” protein. The fact that $C(t)$ and $C^C(t) \times C^L(t)$ agreed was taken as proof that $C(t)$ may be factorized into $C^C \times C^L(t)$. However, the important point is whether the parameters entering $C^L(t)$ are physically meaningful, or force-fitted quantities. This is examined below.

Table 2 shows the S^2 and τ_e values obtained in Ref. [163] by fitting the MD $C^L(t)$ function to the MF time correlation function (Eq. (34)), along with their MF counterparts. The MD parameters are in most cases different from the corresponding MF parameters. This is ascribed in Ref. [163] to local motions slower than the global motion affecting the MD trajectory but not affecting the NMR relaxation parameters. However, the local motions detected are on the order of 2 ns and faster; such motions should have been detected with MF. Yet, MF analyses of these proteins yielded (with a few exceptions) τ_e values on the order of several tens of *ps* [164,165,167].

Thus, even a very careful study, which determined the global diffusion tensor from the MD trajectory, used improved force-fields and employed high-quality experimental data, led to best-fit parameters that differ significantly from their MF counterparts.

A recent study used MD methods to investigate structural dynamics of arginine side chains [168]. It was concluded that side-chain flexibility is concealed from ^{15}Nε spin relaxation analyzed with MF due to the persistence of salt bridges, while the aliphatic part of the arginine side chain retains substantial disorder. Improved analysis of the ^{15}Nε relaxation data might be useful.

Best et al. [71] derived order parameters for methyl dynamics from MD trajectories. Non-harmonic effects were shown to be important; transitions among local (rotameric) minima were considered. Hu et al. [70] correlated semi-quantitatively MF S_{axis}^2 for C–CH_3 motion with the populations of rotameric states associated with the preceding χ angle. However, as outlined herein (in particular in Section 3.2.3) and in Refs. [34] and [35], S_{axis}^2 MF is often inaccurate; this is likely to affect the analysis.

Vendruscolo and co-workers [169,170] developed an ensemble refinement method that uses the squared generalized MF order parameter as a restraint. Its calculated counterpart is obtained mostly using the formula of Ref. [37]. Extensive conformational distributions are predicted by this method.

The accuracy of the local ordering derived from the MD trajectory can be improved by developing methods for calculating unambiguously $<D^2_{00}>$ and $<D^2_{02}+D^2_{0-2}>$. The accuracy of the local ordering derived from the experimental NMR data can be improved by calculating S^2_0 and S^2_2 using SRLS. The form of the conformational distributions determined might change when physical order parameters, and consistent frame definitions, are used.

Clore and Schwieters [152,171,172] also derived squared order parameters with MD within the context of ensemble refinement strategies. These authors found narrow conformational distributions both in solution and in polycrystalline enviroments, comprising optimally 4–8 members. This is inconsistent with the extensive conformational distributions found by Vendruscolo and co-workers [169,170] and Griesinger and co-workers (based on values of RDC) [173–176] in solution, as well as the work of Lorieau et al. [177], who detected large-amplitude axial motions for C^{α}, C^{β} and several side-chain carbons in polycrystalline ubiquitin.

The significant differences in the extent of the conformational distributions derived might stem from the way in which P_{eq} is obtained (often implicitly) in the various studies. As pointed out above, since the actual local ordering frame is rhombic, P_{eq} depends on the definition of the ordering frame.

Operating within physically well-defined theoretical scenarios and abiding by the assumptions underlying the equations/expressions used is important in practice. For example, overlooking the premises underlying MF, and considering the limiting expression of Ref. [37] (criticized in Ref. [178]) to be exact, led in Ref. [54] to an altogether oversimplified analysis. Methyl dynamics was modeled in terms of jumps (or diffusive motion) among three unequally populated rotamers. This highly asymmetric motion corresponds necessarily to rhombic local ordering. Yet, a single order parameter – S MF – was used to interpret this ordering scenario, with the objective of proving that this strategy is appropriate. Rhombic ordering is to be treated in the context of properly defined order parameters S^2_0 and S^2_2 [32,33], e.g., as done in Refs. [179,180].

The MD trajectories calculated for proteins are becoming increasingly longer and the force-fields become increasingly better. It is timely to develop methods for extracting from the MD trajectory mesoscopic parameters that can be compared with experimental counterparts based on stochastic models. As pointed out above, this could be accomplished by devising methods for computing the MD analogues of the $C_{KK'}(t)$ functions obtained with SRLS analysis of NMR spin relaxation parameters.

Appendix C: Protein dynamics in the solid state

Reference [181] summarizes this topic until the end of 2004. The main methods include lineshape analysis, T_1 relaxation and exchange experiments, using primarily ^{2}H and ^{13}C. Recent developments are summarized below.

Giraud et al. [182] acquired ^{15}N T_1 data at 293K from a polycrystalline powder of the 21 kDa dimeric Crh protein. The dynamic model used consists of wobble-in-a-cone in the presence of a square-well potential. It includes the time correlation functions for K = 0, 1 and 2, required by the powder averaging. Wobbling correlation times, $1/(6D_w)$, of 50 – 500 ns, and a semi-cone angles of 10 – 15°, were determined.

Qualitative observations on rocking backbone motion in Crh have been reported. To quantify them, and eventually detect additional dynamic and structural features, it would be useful to acquire T_1 data and powder patterns at lower temperatures. Slow-motion lineshapes, affected by motional rates on the order of the magnetic anisotropies, can detect μs motions. T_1 relaxation times can detect motions approximately 10 times faster. Both can be analyzed with the microscopic order macroscopic disorder (MOMD) approach [183], which is the SRLS limit wherein the protein is immobile.

Lorieau and McDermott [177] acquired motionally averaged powder patterns of C^{α}, C^{β} and side-chain carbons from polycrystalline samples of ^{13}C-labeled ubiquitin. These spectra have been analyzed assuming complete axial motional averaging (although some of the patterns observed had a rhombic appearance). Order parameters ranging from 0.44 to 0.94 have been reported. Here too lowering the temperature to enter the slow motional regime will be very useful, in particular to reveal the nature of the rhombic powder patterns. To enter the relevant time-window one can monitor, besides the temperature, the NMR nucleus type, its chemical/magnetic surroundings, and (except for auto-correlated dipolar relaxation) the external magnetic field.

Additional examples of bio-macromolecular dynamics in the solid state studied with NMR appear in Refs. [76,184–193]. Echodu et al. [188] investigated furanose ring puckering in DNA fragments. T_1, and motionally averaged powder patterns from ^2H nuclei within the furanose ring were analyzed in concert. A previously developed model [185] for restricted motion in the presence of a harmonic potential was used. The rate for internal motion was determined to be 1.8×10^7 s^{-1} at 300K, and the coefficient of the axial potential was determined to be 2.5 k_BT.

T_1 from samples labeled with ^{13}C at furanose ring positions was measured in solution [185]. Mode-decoupling, i.e., $C(t) = C^C(t)\times C^L(t)$, was assumed. $C^L(t)$ was taken the same as the time correlation function used to analyze the solid-state ^2H data. $C^C(t)$ was determined with hydrodynamic calculations, which yielded $R_{\perp}^C=3.6\times10^7\ s^{-1}$ and $R_{\|}^C=7.7\times10^7\ s^{-1}$.

The ^{13}C T_1 data [185] could be reproduced satisfactorily in this manner, although the factorization of C(t) into the produc $C^C(t)\times C^L(t)$ requires that $R^L \gg R^C$, while in actual fact $R^L = 1.8\times10^7\ s^{-1}$ and $R^C(\text{eff})=1/3\,(2R_{\perp}^C+R_{\|}^C)=5.0\times10^7\ s^{-1}$. Because the local motional rate, R^L (adopted from the solid-state work) is 2.8 times *smaller* than the global motional rate, the overall tumbling (see Figs. 5 – 7 of Ref. [188]) dominates the analysis. Thus, within a good approximation one has $C(t) \sim C^C(t)$.

Skrynnikov, Reif and co-workers carried out conjoint analysis of ^{15}N T_1, T_2 and ^{15}N–{^1H} *NOE* data from glycerol-containing solutions and ^{15}N T_1 data from polycrystalline powders of the SH3 domain of α-spectrin to elucidate N–H bond dynamics [191]. The analysis is based on the hypothesis that the motion in the solid-state is the same as the local motion in solution. The return to equilibrium of the magnetization in the T_1 measurements in the solid state was taken to be mono-exponential.

An enhanced form of the EMF formula, from which the global motional term has been removed, was used [191]. As pointed out in Section 3.2.3., this entails force-fitting. The conjoint analysis yielded markedly unusual results which feature $S_s^2 \sim 1$, $0.77 < S_f^2 < 0.90$, $0 < \tau_f < 31$ ps, $0.7 < \tau_s < 54$ ns and $11.0 < \tau_m < 17.4$ ns. S_s^2 is approximately 1 while τ_s ranges from 0.7 to 50 ns. Adjacent residues are often associated with τ_s values that differ by factors of 50. Mode-coupling is ignored; this is inappropriate when τ_s and τ_m are comparable.

Figure S2 of the Supporting Information of Ref. [191] shows that the solid-state data dominate the analysis. If the solid-state data are excluded, the remaining solution data will be amenable to analysis with the original MF formula [191]. It is very likely that separate analyses would have produced different results, especially given that ^{15}N T_1 values in the solid state are on average 100 times longer than ^{15}N T_1 values in solution. Motions of approximately 10^{-7} s or faster may affect the solid-state data; the liquid-state data may be affected by motions of several *ns* or faster. It is unlikely that N–H motions slower than *ns* do not exist in the polycrystalline samples of the SH3 domain of α-spectrin (also, see the results of Ref. [182]). It is more likely that the analysis conducted did not detect them.

Methyl dynamics of the SH3 domain of α-spectrin were also studied in solution and in the solid-state using ^{13}C T_1 relaxation [192]. One of the valine and leucine methyl groups in deuterated protein samples was labeled with ^{13}C. New experimental methodologies, which constitute a significant advance in the field, were developed. The ^{13}C T_1 values measured in the solid state and in solution were found to be similar [192]. The straightforward implication was that methyl dynamics is the same in the two states of matter; hence conjoint analysis was pursued.

The term $(1 - S^2)\exp(-t/\tau_e)$, obtained by omitting the global motional term from Eq. (34), was used as the time correlation function. This expression does not converge to the appropriate physical limits: when $\tau_e \rightarrow 0$ then $C(t) \rightarrow 0$ and when $S^2 \rightarrow 1$ then $C(t) \rightarrow 0$. The time correlation function given by Eq. (34) does converge to the appropriate physical limits: when $\tau_e \rightarrow 0$ then $C(t) \rightarrow S^2$, and when $S^2 \rightarrow 1$ then $C(t) \rightarrow 1$. This function represents the $K = 0$ component of wobble-in-a-cone in a square-well potential. As pointed out in Ref. [182], where the very same motional model was used, all three time correlation functions corresponding to $K = 0$, 1 and 2 are required to properly analyze T_1 relaxation times from polycrystalline powders.

The average local motional correlation time was determined to be 50 ps. This value agrees with local motional correlation times determined in solution for many proteins using Eq. (43) [6, 8]. It does not agree with other NMR studies of methyl dynamics in the solid state. For example, surface-located methionine methyls groups of the *Streptomyces* subtilisin inhibitor have been studied with ^{2}H NMR in the ligand-free protein, and in its complex with subtilisin. Powder patterns and T_1 relaxation parameters from polycrystalline samples, and ^{2}H spectra from single crystals, were acquired from selectively labeled mutants. All the experimental data were analyzed in concert. Asymmetric motions with correlation times ranging from 100 ps to 10 ns have been detected [193].

An important recent study focuses on a leucine residue of HP36 residing in the core of this protein. Its methyl groups were found to exhibit complex dynamics in the solid state [76]. ^{2}H lineshapes from polycrystalline powders of 5,5,5 d3-leucine-79 of HP36 were acquired in the temperature range of 233–298K. ^{2}H T_1 and T_{1Q} (quadrupolar order) relaxation times were acquired in the temperature range of 112–298K. Combined analysis of all of these data was carried out. The dynamic model determined includes the following components. (1) Woessner-type methyl rotation, with a rate in the extreme motional narrowing limit, occurs about C^{γ}–C^{δ}. (2) Motion of the C^{γ}–C^{δ} bond on an arc in the presence of a potential $U(\varphi) = -\lambda\varphi^2$ occurs at rates ranging from 1.5×10^3 rad/sec at 233.15K to 7.3×10^4 rad/sec at 298.15K. (3) Rotamer jumps of the C^{β} carbon occur at a temperature-independent rate of 4.0×10^4 s^{-1}.

Based on references [76,193], methyl groups do experience slow motions in the solid state. However, temperature-dependent relaxation parameters and temperature-dependent powder patterns from polycrystalline proteins, and eventually NMR spectra from single crystals, are required to elucidate them. A single ^{13}C T_1 data point from a polycrystalline sample [192] does not suffice because the primary motion is still rotation about the C–CH_3 axis, which partially

averages effectively the quadrupolar interaction. All the other motions occur in addition to this motional mode; detecting them requires more extensive experimental evidence and appropriate analysis. Reaching general conclusions about methyl dynamics in the solid state based on scarce data and problematic analysis is premature [192].

We mentioned above the MOMD approach [183] as a general method of NMR lineshape analysis in the solid-state. MOMD was developed for nitroxide ESR applications and applied successfully to liposomes [194], proteins [18,43,45] and DNA fragments [44]. It can be adapted relatively easily to NMR spin relaxation in polycrystalline proteins. In its original form, MOMD treats diffusive motion; specific jump-type or other restricted motional models typically occurring in solids can be implemented as well. Experimental methodologies for obtaining high-quality dynamic NMR lineshapes in the solid state are in the course of being developed [189,190,192]. With a large body of appropriate experimental data available from both solution and solid-state samples, analyses based on SRLS treatment of the former and MOMD treatment of the latter are expected to be useful.

Appendix D: Residual Dipolar Couplings of nuclei in internally mobile proteins

SRLS applied to anisotropic solvents is developed in Refs. [15,17]. The contribution to the spin Hamiltonian from the dipolar interaction between two nuclei, *i* an *j*, is given by the following expression:

$$H_{ij,\mathrm{D}}=\sum_{m,k}<D^{2}_{m,k}(\Omega_{\mathrm{LD}})>F^{(2,k)*}_{ij,\mathrm{D}}T^{(2,m)}_{ij,\mathrm{L}}, \tag{67}$$

where $F^{(2,k)}_{ij,\mathrm{D}}$ denote the components of the magnetic dipolar tensor in the D frame, and $T^{(2,m)}_{L}$ denote the components of the relevant spin operators in the space-fixed laboratory frame, L. We refer below to the particular case in which the nuclei *i* and *j* represent the ^{15}N–^{1}H pair; hence the indexes *ij* will be omitted. For uniaxial media the liquid crystal director (LC) is parallel to the lab frame. The global ordering frame, A, is typically taken the same as the global diffusion frame, C.

In studies of small molecules dissolved in liquid crystals, the emphasis is usually on determining both the ordering tensor and the molecular geometry [161,162]. If the latter is known, i.e., one knows the values of the Euler angles α_{CD} and β_{CD}, five RDCs (between pairs of dipolar-coupled NMR nuclei in the molecule) have to be measured in the general case to determine the molecular alignment tensor.

In the field of protein NMR one is interested primarily in the geometry of the molecule, i.e., the angles α_{CD} and β_{CD} [195]. The following strategy is employed. The global diffusion frame, C, is taken the same as the inertia frame (of the X-ray or NMR structure). The global diffusion tensor, $\boldsymbol{R}^{\mathbf{C}}$, determined predominantly by the shape of the protein, is considered to be independent of the LC medium. On the other hand, the global ordering tensor, $\boldsymbol{A}$, is considered to depend on the medium (and to be affected primarily by electrostatic interactions). Based on experience both $\boldsymbol{R}^{\mathbf{C}}$ and $\boldsymbol{A}$ are rhombic tensors [66,173–176,195–198].

The situation is significantly more complex when the probe experiences restricted local motion. Two additional frames have to be considered: the local ordering/local diffusion frame, M, fixed in the probe, and the local director, C′, fixed in the protein. C′ is taken along the equilibrium orientation of the probe. Local order parameters, S^{2}_{0} and S^{2}_{2}, are defined in terms of a local

potential, $u(\Omega_{C'M})$. Since the M frame is not necessarily the same as the D frame the (time-independent) Euler angles $\Omega_{MD} = (\alpha_{MD},\beta_{MD},0)$ also enter the analysis; they can often be specified based on stereochemical considerations.

Let us assume that all the conditions underlying Eq. (31) are valid. In this case one may carry out separately the averaging over Ω_{LA} to yield a_0^2 and a_2^2, and the averaging over $\Omega_{C'M}$ to yield S_0^2 and S_2^2. In this limit, the contribution to the spin Hamiltonian from the dipolar interaction between two nuclei, *i* and *j* given by eq. (67), is now given as (cf. Fig. 1):

$$H_{ij,D}=\sum_{p,q,r,s}<D^2_{0,p}(\Omega_{LA})>D^2_{p,q}(\Omega_{AC})\,D^2_{q,r}(\Omega_{CC'})<D^2_{r,s}(\Omega_{C'M})>D^2_{s,0}(\Omega_{MD})\,F^{(2,0)*}_{ij,D}T^{(2,0)}_{ij,L} \tag{68}$$

Note that since the global ordering is very small one may assume that $P_{eq}(\Omega_{LA}) = \exp(-u(\Omega_{LA})/<\exp(-u(\Omega_{LA})> \sim 1 - u(\Omega_{LA})/<\exp(-u(\Omega_{LA})>$.

For at least 2-fold symmetry around A and at least 3-fold symmetry around LC the following expression represents the measurable RDC when the moiety comprising the nuclei *i* and *j* is attached rigidly to the protein [14,30–33,66]:

$$D_D(\Omega_{CD})=(\mu_0/4\pi)\gamma_i\gamma_j h/(4\pi^2 r_{ij}{}^3)[\,a_0^2P_2(\cos\beta_{CD})+(3/2)^{1/2}(a_2^2\sin^2(\beta_{CD})\cos(2\alpha_{CD})]. \tag{69}$$

μ_0 is the permeability of vacuum, γ_i and γ_j are the magnetogyric ratios of the nuclei *i* and *j*, *h* is Planck's constant, and r_{ij} is the distance between *i* and *j*. $a_0^2=<D^2_{00}(\Omega_{LA})>$ and $a_2^2=<D^2_{02}(\Omega_{LA})+D^2_{0-2}(\Omega_{LA})>$ are (in irreducible tensor notation) the principal values of the molecular alignment, ***A*** tensor. These parameters are defined in terms of the mean-field potential, $u(\Omega_{LA})$, exerted by the LC onto the protein. The form of this potential is usually given by Eq. (52); the order parameters a_0^2 and a_2^2 are given by Eq. (59) [32,33].

Let us denote the Euler angles that transform the A_i frame, associated with medium *i*, into the C frame by $\Omega_{ACi} = (\alpha_i,\beta_i,\gamma_i)$. Methods for determining $(a_0^2)_i$, $(a_2^2)_i$, α_i, β_i and γ_i have been developed [66]. Once this information is available the angles α_{CD} and β_{CD} can be determined by measuring RDCs in two independent alignment media.

When the moiety comprising the nuclei *i* and *j* is engaged in local motion one has to calculate averages over the trigonometric functions $P_2(\cos\beta_{CD})$ and $(3\ 2)^{1/2}$ $(\sin^2(\beta_{CD})\cos(2\alpha_{CD})$ which appear in Eq. (69) [66] (for non-spherical global diffusion tensors one has to calculate averages over $P_2(\cos\beta_{C'D})$ and $(3\ 2)^{1/2}$ $(\sin^2(\beta_{C'D})\cos(2\alpha_{C'D}))$. The averaging procedure can be deduced for specific cases from Eq. (68). The angles $\Omega_{CC'}$ in Eq. (68) represent the "structural' information inherent in the RDC. It can be seen that the parameters S_0^2, S_2^2, $\alpha_{CC'}$ and $\beta_{CC'}$ are common to RDC – cf. Eq. (68), and SRLS spin relaxation analysis – cf. Eq (58). The eigenmodes which comprise the functions $j_{KK'}(\omega)$ in Eq. (58) depend on c_0^2 and c_2^2; through Eqs. (59) and (52) they depend on S_0^2 an S_2^2. For rhombic global diffusion tensors the eigenmodes also depend on $\alpha_{CC'}$ and $\beta_{CC'}$. The information on global ordering only enters the RDC analysis, and not the NMR relaxation. The latter is normally obtained in isotropic solution, so that the information on global ordering is in principle irrelevant; relaxation in a liquid crystalline medium with 0.001 ordering, as empoyed in RDC studies, would be virtually the same.

Thus, one may combine the two analyses within the scope of the same physically sound framework, as done in the past for small molecules [14,21,32,33]. If the RDC analysis is carried out independently then four different alignment media will be required to determine $\alpha_{CC'}$, $\beta_{CC'}$, S_0^2 and S_2^2.

This paradigm applies to methyl groups, for which the local ordering is weak. It may apply, within a good approximation, to "rigid" N–H bonds, where the local ordering is very strong; this has to be checked. For N–H bonds (and other probes) located in flexible chain regions Eq. (69) is likely to be oversimplified. For local motion much slower than the global tumbling and much faster than the typical RDC (which is on the order of 10 – 20 Hz) the extra reduction in the RDC may be converted into an order parameter provided that these motions can be replaced by an effective axial motion.

A number of methods for calculating RDCs in the presence of local motions have been developed [173–176,196–198]. They are based, in principle, on the rationale outlined above. In practice they differ significantly from the approach described above. Thus, separate averaging over Ω_{LA} and $\Omega_{C'M}$ is considered appropriate for *ps – ms* local motions. The RDC and MF spin relaxation analyses are combined by using the generalized MF order parameter, S(MF). The angle Ω_{MD} is implicitly (0,0,0) in the MF spin relaxation analysis. It is (α_{MD},β_{MD},0) in RDC analyses through the utilization of concepts such as "amplitude of anisotropy" and "direction of anisotropy" [173,174], which require a rhombic M frame. When the M frame has rhombic symmetry, one should have two order parameters, S_0^2 and S_2^2. Yet, only a single order parameter, S(MF), is available. The angles $\Omega_{CC'}$ are (0,0,0) in the MF analysis because in the present context the global diffusion frame, C, is taken as isotropic. In the RDC analysis they are clearly ($\alpha_{CC'}$,$\beta_{CC'}$,0), i.e., the C frame is rhombic, to derive the desired structural information. Finally, a generalized order parameter, S(RDC), analogous to the generalized MF order parameter, S(MF), is used. S(RDC) < S(MF) is interpreted as prevalence of local motions slower than the global motion.

Clearly, there are inconsistencies, and the validity limits of MF-type equations formally analogous to Eq. (68) are exceeded. The RDC-derived dynamic information of interest pertains to the μs – ns time scale, which is outside the scope of both spin relaxation and chemical exchange scenarios. In this time-regime neither $R^L \gg R^C$, nor $R^L \ll R^C$ with on average axial ordering, which are the conditions that underlie Eq. (68), are fulfilled. Therefore the value of S(RDC), derived by ignoring these considerations with equations formally analogous to Eq. (68), might be inaccurate. For example, the large distributions of structural ensembles based on RDC analysis [170,175] might be over-rated.

Appendix E: 15N–1H bond dynamics

1. Geometric effects

In the extreme motional narrowing limit for the local motion, the only difference between SRLS and MF for axial local potentials is the relative orientation of the ^{15}N–^{1}H dipolar and the ^{15}N CSA frames. We utilized a 17° tilt [149]; this angle is implicitly zero in MF. Based on published ^{15}N spin relaxation data of the villin headpiece helical subdomain (VHHS) fitted with the MF model 1 [199], where the local motion is in the extreme motional narrowing limit, we found that MF S^2 underestimates SRLS $(S_0^2)^2$ on average by 4.5% [20]. This should be compared with reported S^2 precision of 1% [200], and in some cases 0.2% [201].

The error in S^2 has significant implications for the accuracy of conformational entropy derived from it. For high ordering typical of N–H bonds located in the protein core 4.5% error in S^2

implies over 20% error in the coefficient, c_0^2, of a Legendre polynomial of rank 2 potential [20] (Table 3). This is due to the functional form of the $(S_0^2)^2$ versus c_0^2 dependence for high $(S_0^2)^2$, illustrated in Fig. 3.

A previous report maintains that the tilt $\Omega_{D-CSA} = (0, \beta_{D-CSA}, 0)$ between the axial D and CSA frames has a negligible effect on the analysis [36]. However, to evaluate this effect one has to calculate $J^{CC}(\omega)$ from $J^{DD}(\omega)$, or assemble it directly from the $j_{KK'}(\omega)$ functions. In both cases the functions $j_{11}(\omega)$ and $j_{22}(\omega)$, which are not provided in MF, are required. Hence, the effect under consideration cannot be evaluated within the scope of MF.

2. Local motional effects

^{15}N relaxation data of some VHHS residues were analyzed in Ref. [199] with MF model 2 which utilizes Eq. (2). Fifteen such residues were also subjected to SRLS analysis using the spectral density formally analogous to model 2 MF [20]. The average SRLS and MF results are shown in Table 3 (along with the model 1 data discussed above).

SRLS yielded $<\tau/\tau_m> = 0.1$ whereas MF yielded $<\tau_e/\tau_m> = 0.02$ (data not shown). Using for SRLS τ_{ren} with $c_0^2=7.5$, which corresponds to $(S_0^2)^2=0.73$, yielded $<\tau_{ren}/\tau_m> = 0.027$, which is significantly different from $<\tau_e/\tau_m>$ determined by MF. S^2 overestimates $(S_0^2)^2$ by nearly 7% in model 2 and underestimates it by approximately 4.5% in model 1 (first row of Table 3). c_0^2(MF) overestimates c_0^2(SRLS) by 20% in model 2 and underestimates it by 23% in model 1 (second row of Table 3).

For $<\tau/\tau_m> = 0.1$, but also for $<\tau_{ren}/\tau_m> = 0.027$, mode-coupling is important [16]. This leads to an actual SRLS spectral density that is significantly more complex than Eq. (2). Ample comparison between SRLS and MF, illustrating the various aspects with regard to which these approaches differ, appears in Ref. [20]. Note that the actual local ordering is rhombic rather than axial [20,48,50]. Therefore, the data shown in Table 3, based on axial potentials, should be considered as merely illustrative. If the asymmetry of the local potential were accounted for, the differences between SRLS and MF would be much larger.

3. Global diffusion

In the extreme motional narrowing limit for the local motion one may determine τ_m from ^{15}N T_1/T_2 ratios [202,203]. N–H bonds located in elements of secondary structure approach this limit at low magnetic fields. Precision can be estimated by scanning the vicinity of τ_m to determine the range in which the χ^2 value is largely preserved. With this strategy, we evaluated the precision of τ_m to be on the order of 5 – 6%. For VHHS the accuracy of τ_m was increased by approximately 4% when SRLS was used instead of MF (Fig. 9 of Ref. [20]).

In MF analyses the global diffusion tensor, $\boldsymbol{R}^{\mathbf{C}}$, is determined from filtered (to eliminate local motional effects) ^{15}N T_1/T_2 data. Different methods for determining $\boldsymbol{R}^{\mathbf{C}}$ have been developed. Traditional approaches are described in Refs. [202,203]. An effective approximate approach is described in Refs. [166,204]. Recently MF fitting schemes have been integrated with hydrodynamics-based approaches for calculating $\boldsymbol{R}^{\mathbf{C}}$ from 3D structures [205,206]. A separate hydrodynamics-based method for calculating $\boldsymbol{R}^{\mathbf{C}}$ was also developed [207]. Our recently developed fitting scheme for SRLS [90] has been integrated with the hydrodynamics-based approach of Barone et al. [98], which determines $\boldsymbol{R}^{\mathbf{C}}$ from 3D structures and can account for internal torsions as well.

^{15}N T_1/T_2 data sets considered free of local motional effects according to MF might comprise significant local motional effects according to SRLS [20]. Unaccounted for local motional effects, in particular the asymmetry of the local ordering, can be absorbed by an apparently axial global diffusion tensor (see below). To ascertain that $\boldsymbol{R}^{\mathbf{C}}$ is a genuine axial tensor the methods outlined in Ref. [204,208,209] are useful (see below).

4. Asymmetry of the local motion

In the literature, this term refers usually to axial or rhombic symmetry of the local diffusion, or to jumps among unequally populated sites (e.g., Ref. [54]). Yet, the symmetry of a restricted local motion is determined by the symmetry of the local potential, or the local ordering tensor [32,33]. We found that the rhombicity of the local potential has a dominant effect on the analysis [20,48,90]. The effect of potential rhombicity versus global diffusion axiality on the ^{15}N relaxation parameters is illustrated below.

Table 4 illustrates the high sensitivity of the analysis to the asymmetry of the local potential. It can be seen that the ^{15}N–{^{1}H} *NOE* value is affected to a particularly large extent when the local potential is rhombic rather than axial, which is most likely because the *NOE* represents a ratio of two relaxation rates [28], each depending intricately (through the $j_{KK'}(\omega)$ functions and their coefficients in the expressions for $J^{DD}(\omega)$) on the local ordering. Note that in MF the local ordering enters the calculation through the factor S^2. In the extreme motional narrowing limit S^2 cancels out in the expression for the *NOE*; for fast local motion its effect on the NOE is expected to be small [20].

The rhombicity of the local ordering, which affects the *NOE* to such a large extent, is quite limited. This can be appreciated by calculating the Cartesian ordering tensor components from c_0^2=8 and c_2^2=4. These components are given by $S_{xx} = -0.382$, $S_{yy} = -0.454$ and $S_{zz} = 0.836$, yielding $(S_{xx} - S_{yy})/S_{zz} = 0.09$ on a scale extending from −1 to +1.

Table 5 illustrates limited sensitivity of the analysis to small global diffusion axiality, given by $N^C = R_{\|}^C / R_{\perp}^C = 1.2$, as one would expect (we show the results of calculations carried out for the extreme values of the angle between the equilibrium N–H orientation and the principal axis of the global diffusion tensor). This is inconsistent with the large effect $N^C = 1.18$ has on the MF analysis of ^{15}N spin relaxation data from DHFR [208]. Fifty percent of the residues of this protein require substantial conformational exchange contributions, R_{ex}, when an isotropic $\boldsymbol{R}^{\mathbf{C}}$ is used instead of an axial $\boldsymbol{R}^{\mathbf{C}}$ with $N^C = 1.18$ [208]. If, however, $\boldsymbol{R}^{\mathbf{C}}$ is allowed to be axial, then the R_{ex} contributions disappear, and the unaccounted for rhombicity of the S tensor is absorbed by an apparent axiality of the R^C tensor [48].

Strong evidence that R_{ex} can also absorb unaccounted for asymmetry of the local potential/local ordering is provided in Ref. [48], where ribonuclease H (RNase H) and AKeco have been studied in this context. It is also shown in that study that using axial potentials instead of the actual rhombic potentials, and an axial global diffusion tensor instead of the actual isotropic global diffusion tensor, imply inaccurate best-fit order parameters obtained with data fitting. The findings of Ref. [48] are based on extensive predictive calculations, and back-calculations of experimental data, carried out in the context of a conjoint analysis of the auto-correlated relaxation parameters ^{15}N T_1, T_2 and ^{15}N–{^{1}H} *NOE*, and the transverse ^{15}N–^{1}H dipolar/^{15}N CSA cross-correlated relaxation rate, η_{xy}. The fact that the experimental value of $1/T_2$ depends on R_{ex}, whilst η_{xy} does not, is a key element in the analysis.

That ^{15}N spin relaxation is sensitive to the asymmetry of the local ordering was also demonstrated by the 3D GAF model [65,78], an elaborate RDC study which provided

anisotropic probability density functions of N–H orientations [210], and MD simulations which revealed asymmetric N–H fluctuations [131].

5. Applications

5.1. E. coli adenylate kinase: domain motion

5.1.1. Background—The 23.6 kDa enzyme *E. coli* adenylate kinase catalyzes the reaction $ATP*Mg^{+2} + AMP \leftrightarrow ADP*Mg^{+2} + ADP$ [211]. AKeco is made of a single chain intertwined into the domains AMPbd, LID and CORE [212]. The domain AMPbd is associated with the binding of the AMP substrate. The domain LID "folds over" the binding site for the $ATP*Mg^{+2}$ substrate, so that the two-substrate binding site becomes sequestered, and the catalytic reaction can take place.

The ligand-free enzyme was crystallized into the "open" conformation 4ake (Fig. 4a). A two-substrate mimic inhibitor, AP_5A, where AMP and ATP are linked by a fifth phosphate group, was prepared. The complex AKeco*AP_5A was shown to be a transition state mimic [213, 214]. The crystal structure of the "closed" AKeco*AP_5A form is 1ake [215] (Fig. 4b). There are clear indications that in the ligand free form (AKeco) the domains AMPbd and LID execute large-amplitude motions, which come to a halt upon substrate binding. These mechanical movements are thought to be associated, in a more or less direct manner by different research groups, with the catalytic event. On the other hand, the CORE domain is preserved structurally in this process [212,216].

The AKeco/AKeco*AP_5A system is considered as paradigm for correlation between dynamic structure, in particular domain motion, and biological function [216]. AKeco and AKeco*AP_5A have been studied extensively with many methods and in many contexts. Straightforward MD [218,219], weighted masses MD [220], the exploration of the roles of the various AKeco domains for stability and catalysis [221], MD/PCA [222], a 100 ns molecular dynamics study of subdomain motion and mechanics [223], hydrogel-mediated translation of substrate recognition into macroscopic motion [224] were used. Graph theory [255], in-parallel SRLS and GNM analysis [226], a plastic network model exploring large-amplitude conformational changes [227], a coarse-grained model that considers ligand interactions approximately [228], various elaborate coarse-grained methods [229–232], and an MD-based method exploring the pathways between the "open" and "closed" states of AKeco at atomic detail [233] have also been employed. Finally, optical methods [234,235], single molecule fluorescence resonance energy transfer [236], ^{15}N relaxation dispersion [237], studies associated with protein folding [238,239] and ^{15}N spin relaxation [20,46,47,240–242] have been used.

From the NMR point-of-view, ligand-free AKeco prevails in solution as a conformational ensemble inter-converting rapidly on the chemical shift time scale [241]. This is consistent with the energy landscape of ligand-free AKeco shown by the dotted barrier-less curve in Fig. 5. According to this picture, conformational interconversion should be detected with spin relaxation methods provided its rate is faster than the global tumbling.

Experimental ^{15}N T_1, T_2 and $^{15}N–\{^1H\}$ *NOE* data acquired at 14.1 and 18.8T and 303K [46] are shown in Fig. 6. It can be seen that the experimental values of the $^{15}N–\{^1H\}$ *NOE* are significantly lower within the AMPbd and LID domains as compared to the CORE domain. This is clear indication that AMPbd and LID, but not CORE, are engaged in *ns* local motions [13]. We focus below on the study of these motions with NMR spin relaxation, which we have pursued for several years [46–50,241].

5.1.2. MF analysis—In our first attempt, we used the model-free method [11] to analyze the experimental data acquired at 14.1T, 303K [241]. The traditional ^{15}N R_2/R_1-based ($R_1 \equiv 1/T_1$, $R_2 \equiv 1/T_2$) analysis [202,203] for determining the global diffusion tensor yielded $R_{\|}^{C}/R_{\perp}^{C}=1.25$ and R^C (eff) = 15.05 ± 0.5 ns. As expected based on the large experimental ^{15}N–{^{1}H} *NOE* values, the N–H bonds of the CORE domain could be analyzed with the MF spectral density of Ref. [11], which is usually used to analyze "rigid" N-H bonds. The latter are typically associated with large S^2 values and small τ_e values. Based on the ^{15}N–{^{1}H} *NOE* pattern shown in Fig. 6, and previous results obtained for flexible loops in proteins [6,8], we expected the N–H bonds of the AMPbd and LID domains to be amenable to analysis with the EMF spectral density of Ref. [13], which is usually used to analyze "flexible" N-H bond. The latter are typically associated with smaller S^2 and S_s^2 values, and τ_s values of several ns.

The expectation concerning the "flexible" N-H bond was not borne out, as shown by the empty circles in Fig. 7. The squared order parameters S^2, obtained mostly with the MF formula, are high throughout the protein backbone; they do not discriminate between AMPbd/LID and CORE. In a few cases, the EMF formula yielded τ_s mostly below 1 ns, not necessarily associated with N–H bonds located within the AMPbd and LID domains. A relatively small number of conformational exchange terms, R_{ex}, was also obtained.

Similar results were obtained for the local motional parameters using combined 14.1 and 18.8T data and taking the global diffusion to be isotropic [46,47]. In this case additional conformational exchange terms, R_{ex}, were obtained. N-H bond dynamics of AKeco and a thermophylic variant of this enzyme were studied recently with the MF method [240]. The overall picture obtained for the local motion is very similar to the picture obtained by us [241]. Instead of $R_{\|}^{C}/R_{\perp}^{C}=1.25$ and quite a few R_{ex} contributions determined by [241], the authors of Ref. [240] determined $R_{\|}^{C}/R_{\perp}^{C}=1.41$ with very few R_{ex} contributions. This scenario is similar to the one described earlier for DHFR [90]. Namely, unaccounted for rhombicity of the local ordering can be absorbed by artificial $\boldsymbol{R}^{\mathbf{C}}$ axiality, and/or artificial R_{ex} terms.

Let us consider the global diffusion tensor from a physical point-of-view. In the absence of rigorous methods for determining $\boldsymbol{R}^{\mathbf{C}}$ in the presence of slow internal motions of large chain segments, taking it to be on average isotropic appears to be a good approximation. Evidence that this is a better approximation than taking the solution structure the same as the crystal structure [240] is given in Ref. [46].

That $\boldsymbol{R}^{\mathbf{C}}$ axiality, as well as R_{ex} terms, can absorb unaccounted for rhombicity of the local potential has been shown not only for DHFR [90], but also for the rigid parts of AKeco and RNase [48]. For the mobile domains of AKeco an additional important factor enters the scene. The experimental ^{15}N–{^{1}H} *NOE* profiles shown in Fig. 6c indicate than the AMPbd and LID domains experience *ns* internal motion. MF does not even single out the domains AMPbd/LID (Fig. 7) because it does not account for mode-coupling, implied by *ns* internal motions, in addition to not accounting for potential rhombicity. The various MF-based analyses of AKeco differ by these important factors having been absorbed by $\boldsymbol{R}^{\mathbf{C}}$ axiality [240], R_{ex} contributions [46,47], or both [241]. The results of these studies differ because differently filtered ^{15}N R_2/R_1 data sets were used to determine $\boldsymbol{R}^{\mathbf{C}}$. When $\boldsymbol{R}^{\mathbf{C}}$ tensors that are nearly isotropic are analyzed as if they were significantly axial, the analysis is very sensitive to the filtering of the ^{15}N R_2/R_1 data [50,90].

With large intertwined chain segments not treated properly (note that common globular proteins have a small number of relatively short flexible loops), severe force-fitting occurs within AMPbd and LID. For isotropic (axial) $\boldsymbol{R}^{\mathbf{C}}$ the statistics are good but the S^2 values are too high, the τ_s value are too small, *and* an artificial conformational exchange contribution

[241] (apparent global diffusion axiality [240]) is obtained. We considered these results unacceptable. To improve the analysis we developed SRLS [19]. The analysis of the experimental data of Fig. 6 with SRLS is discussed in Sections 5.1.3 and 5.1.4.

In contrast to our approach, the authors of Ref. [240] accepted the MF analysis. We show in Fig. 8 their experimental data along with their S^2 values. Both the experimental $^{15}N–\{^1H\}$ *NOE* profiles (Fig. 8a) and the calculated S^2 profile (Fig. 8b) are very similar to our corresponding data (relevant parts of Figs. 6 and 7). Literal interpretation of the force-fitted S^2 profile led to the conclusion that AKeco does not experience domain motion on the *ns* time scale [240]. Somewhat lower than average S^2 values at some of the hinges of the crystal structure [212] were taken to represent *ps* fluctuations which facilitate catalysis-controlling *ms* domain motion in the system where AKeco is Mg^{2+}/nucleotide-saturated and substrate–saturated [237].

The free-energy profile of coexisting AKeco and AKeco*AP_5A (which is a transition state mimic [213,214]) is shown by the solid curve in Fig. 5. It comprises a 12.5 kcal/mol barrier consistent with *ms* domain motion detected with ^{15}N relaxation dispersion from Mg^{2+}/ nucleotide–saturated and substrate–saturated AKeco [237], where both AKeco and the transition state co-exist. The free-energy profile of ligand-free AKeco is shown by the dashed curve in Fig. 5. It consists of a barrier-less curve consistent with *ns* domain motion detected with SRLS-based ^{15}N spin relaxation of ligand-free AKeco [46,47].

5.1.3. SRLS analysis using axial potentials—The fitting scheme for SRLS developed in Ref. [19], based on pre-calculated 2D grids of spectral densities, features (for practical reasons) axial local potentials and assumes that $R_{\|}^{L} \gg R_{\perp}^{L}$. By applying it to the data shown in Fig. 6 we obtained the $(S_0^2)^2$ and $\tau_\perp$ values shown in Fig. 7 (filled circles) [46]. The corresponding MF parameters obtained with the program DYNAMICS [97] are also shown (empty circles). The $\tau_\perp$ values are on average 8 times larger than the corresponding τ_s values; $\tau_\|$ SRLS (not shown) is on average 4 times larger than τ_f MF. The average value of $(S_0^2)^2$ is 0.3 whereas the average value of S_s^2 is 0.97. The local geometry is given by $10° < \beta_{MD} < 20°$, i.e., $0.9 > [P_2(\cos\beta_{MD})]^2 > 0.76$, which corresponds to $0.9 > S_f^2 > 0.85$ ($S_f^2 \rightarrow [P_2(\cos\beta_{MD})]^2$). Clearly, the SRLS and MF results differ substantially.

SRLS detected *ns* $\tau_\perp$ values for all the N–H bonds within AMPbd and LID. The average value is $<\tau_\perp> = 8.2 \pm 1.3$ ns, to be compared with $\tau_m = 15.1 \pm 0.5$ ns. Practically all the N–H bonds within CORE move locally with correlation times below 130 ps, in agreement with the large values of the $^{15}N–\{^1H\}$ *NOE* shown in Fig. 6. It may be concluded (see Ref. [46] for details) that the *ns* correlation time $\tau_\perp$ represents domain motion. With mode-coupling accounted for, the analysis bears out the information imprinted in the experimental $^{15}N–\{^1H\}$ *NOE* profile (Figs. 6 and 7).

However, several features of the SRLS results are problematic from a physical point of view. $(S_0^2)^2$ values between 0.2 and 0.45, and a local ordering/local diffusion axis tilted at 10 – 20° from the N–H bond, were obtained for AMPbd and LID. The $(S_0^2)^2$ values are unduly low, representing a broad distribution of N–H bond vector orientations, unlikely to prevail in tightly packed protein cores. An axis tilted at 10 – 20° from the N–H bond does not correspond to a structural element that might serve as main local ordering/local diffusion axis. Clearly important effects are not accounted for. We proceeded by further improving the analysis as follows.

5.1.4. SRLS analysis using rhombic potentials—Semi-quantitative analysis showed that rhombic potentials prevail at N–H sites in proteins and affect the analysis significantly [48]. To allow for rhombic potentials we developed a fitting scheme for SRLS where the spectral densities are calculated on the fly. The restriction that $R_{\|}^{\mathrm{L}} \gg R_{\perp}^{\mathrm{L}}$ was also removed [20]. In applying this fitting scheme to the experimental data shown in Fig. 6 we varied the potential coefficients c_0^2, c_2^2, the angle β_{MD}, the time scale separation $R_C = \tau_\perp/\tau_m$, and the local diffusion anisotropy, $N = \tau_{\|}/\tau_\perp$. This parameter combination is formally analogous to the parameter combination features by the Extended Model Free formula, except for the extra parameter, c_2^2.

In Table 6 we show the results obtained for residues G46 and K47 of the AMPbd domain. The components of the Cartesian ordering tensor, S_{xx}, S_{yy} and S_{zz}, calculated from the potential coefficients c_0^2 and c_2^2, are also shown. Let us analyze these parameters in terms of the physical picture they provide.

The principal values of a physical ordering tensor specify the extent to which the axes of the coordinate frame in which the ordering tensor is diagonal orient preferentially with respect to the local director frame, C′. As originally defined, the main ordering axis lies along the axial dipolar frame, i.e., Z_M is parallel to Z_D (hence to the instantaneous N–H orientation). It can be seen that the M frame is highly rhombic, and that X_M is the main ordering axis.

This information can also be deduced from the magnitudes and signs of the potential coefficients c_0^2 and c_2^2 [14]; based on details specified in Ref. [14], we determined X_M as the main ordering axis. The best-fit value of β_{MD} is approximately 100°, while the theoretical value of the tilt angle between $C_{i-1}^{\alpha} - C_i^{\alpha}$ and N–H is 101.3° [65]. It may be concluded that X_M lies along $C_{i-1}^{\alpha} - C_i^{\alpha}$, as illustrated in Fig. 9. The S_{xx} values are relatively high, indicating that the ordering is high about $C_{i-1}^{\alpha} - C_i^{\alpha}$, in agreement with the high c_2^2 values.

$N = R_{\|}^{\mathrm{L}}/R_{\perp}^{\mathrm{L}}$ estimates the degree of axiality of the local diffusion tensor. Attempts to derive activation energies from the temperature-dependences of $R_{\|}^{\mathrm{L}}$ and $R_{\perp}^{\mathrm{L}}$ were made. They were mostly unsuccessful. On the other hand, well-defined activation energies were obtained from $R^{\mathrm{L}} = R_{\|}^{\mathrm{L}} = R_{\perp}^{\mathrm{L}}$. Also, the fitting process was very tedious for $N \neq 1$, and significantly more robust for $N = 1$. We interpreted these results to indicate that $N \neq 1$ causes overfitting and proceeded by setting N equal to 1.

In Table 6 presents results obtained with $N = 1$ for the representative residue L35 of AMPbd. Results obtained for all the residues within AMPbd and LID are reported in Ref. [50]; the average value of τ_m/τ is 2.5. The absolute values of the parameters differ for the $N = 1$ and $N \neq 1$ scenarios. However, the overall picture is similar. Thus, high and moderately rhombic ordering prevails about $C_{i-1}^{\alpha} - C_i^{\alpha}$, and the domains move on the *ns* time scale. This description is compatible with the sensitivity of the experimental data used.

The asymmetry of the local ordering plays an important role in various aspects of NMR spin relaxation in proteins. Further insight into this important property is provided by the probability of the main ordering axis having an orientation in the infinitesimal range $\beta_{CM} \pm \Delta\beta_{CM}$ and $\gamma_{CM} \pm \Delta\gamma_{CM}$ for any α_{CM} (since the C′ frame is uniaxial). It is conveniently given by a relative (or unnoormalized) probability as $P_{rel} = \exp(-u)\sin\beta_{CM}\Delta\beta_{CM}\Delta\gamma_{CM}$ [243], plotted as a function of the spherical coordinates $(\beta_{CM}, \gamma_{CM})$. Note u is the actual potential divided by $k_B T$, rendering u dimensionless.

The average rhombic local N–H potential within AMPbd and LID at 302 K is

$$u = -1.5 \times (-4.57) \times (\cos^2\beta_{CM} - 0.5) - \sqrt{3/2} \times 16.11 \times \sin^2\beta_{CM} \times \cos(2\gamma_{CM}).$$

This potential is depicted in Fig. 10c as a function of the coordinates β_{CM} and γ_{CM} in units of radians. Its rhombic symmetry is borne out by the significant difference between the extreme values along the γ_{CM} coordinate. In Fig. 11c we show a representation of the function $P_{rel}(\beta_{CM},\gamma_{CM})$, by plotting $Z_C = R\cos\beta_{CM}$ vs $X_C = R \sin\beta_{CM} \cos\gamma_{CM}$, $Y_C = R \sin\beta_{CM} \sin\gamma_{CM}$, where $R = \exp(-u) \sin\beta_{CM}$. The figure axes have been scaled as indicated by the attached labels to make possible the illustration of this highly peaked drawing (consistent axes scaling in Fig. 11 enables comparison among its various drawings). Fig. 11c exhibits peaks along X_C, in accordance with X_M orienting preferentially perpendicular to Z_C (both $\exp(-u)$ and the solid angle $(\sin\beta_{CM}\,\Delta\beta_{CM}\,\Delta\gamma_{CM})$ are large for this type of ordering).

We show in Fig. 10a the average potential, $u = -4.74\times(1.5\cos^2\beta_{CM} - 0.5)$, obtained with SRLS for AMPbd and LID at 302K using axial potentials ($c_2^2=0$). This potential is weak, as shown by its shape, given by a shallow well. The corresponding P_{rel} function is shown in Fig. 11a. While the ratio between the scaling of the X_C axis and the scaling of the Y_C and Z_C axes is 10 in Fig. 11c, the ratio between the scaling of the Z_C axis and the scaling of the X_C and Y_C axes is 2 in Fig. 11a. It can be seen that the axial potential is associated with a broad distribution of instantaneous N–H orientations about the equilibrium N–H orientation whereas the rhombic potential is associated with a narrow distribution of instantaneous N–H orientations about $C_{i-1}^{\alpha} - C_i^{\alpha}$, which is approximately perpendicular to the equilibrium N–H orientation. The solid angle $\sin\beta_{CM}\,\Delta\beta_{CM}$ is small for β_{CM} values close to zero. This creates the void in the middle of the P_{rel} function shown in Fig. 11a. Obviously, the rhombic scenario (Figs. 10c and 11c) is very different from the axial scenario (Figs. 10a and 11a). Detailed information on data fitting based on rhombic potentials appears in Ref. [50].

If the labels of the M frame axes are permuted twice counterclockwise (upon each permutation the potential coefficients change according to the relations $\widehat{c}_0^2 = -1/2\, c_0^2 - (3/2)^{1/2}\, c_2^2$ and $\widehat{c}_2^2 = -1/2\ [(3/2)^{1/2}\, c_0^2 - c_2^2]$ (see Ref. [243]) to render X_M the main ordering axis, one obtains a potential with an axial coefficient of $\widehat{c}_0^2=22$, and a rhombic coefficient of $\widehat{c}_2^2 = -5$, shown in Fig. 10d. The associated P_{rel} function is shown in Fig. 11d; the latter illustrates relatively narrow slightly rhombic distribution of instantaneous N–H orientations about $C_{i-1}^{\alpha} - C_i^{\alpha}$. Obviously, the physical scenario underlying Figs. 10d and 11d is the same as the physical scenario underlying Figs. 10c and 11c, only the geometric perspective is different.

The average S^2 MF value obtained in Ref. [240] for AKeco at 20 °C is 0.88 (Fig. 3a of Ref. [240]). This corresponds to $c_0^2=16.1$ and $c_2^2=0$, yielding the potential shown in Fig. 10b. This is a strong axial potential along N–H. The associated P_{rel} function is shown in Fig. 11b. Limited excursion from Z_C, as shown by the small amplitudes along X_C and Y_C, are illustrated. This N–H distribution is inconsistent with the dashed curve in Fig. 5.

5.2. Ribonuclease H: loop dynamics

Ribonuclease H (RNase H) is a single-domain enzyme comprising 155 residues. It features the flexible loop α_D/β_5. ^{15}N spin relaxation data have been analyzed previously with MF [96, 244,245] and by us with SRLS [20,48]. Similar to AKeco, it was necessary to allow for rhombic symmetry of the local potentials to obtain physically meaningful results. The main difference between the flexible loop of RNase H and the mobile domains of AKeco is the magnitude of the time scale separation. We obtained $\tau/\tau_m = 0.23$ for residue H124 pertaining to the loop α_D/β_5 of RNase H as compared to $\tau/\tau_m \sim 0.5$ for N–H bonds within the mobile domains of AKeco. Further details appear in Ref. [20].

5.3. Xenopus Ca^{2+}-calmodulin: SRLS versus MF analyses

Ca^{2+}–ligated calmodulin (Ca^{2+}–CaM) is made of an N-terminal domain and a C–terminal domain connected by a helical linker, which is flexible in the middle. In the crystal Ca^{2+}–CaM adopts an elongated dumb-bell structure with the N–, and C–terminal regions of the helical linker parallel to one another (Fig. 12). Since the middle linker region is flexible, the N–, and C–terminal domains may adopt various relative orientations in solution. The helical target peptide, essential for Ca^{2+}–CaM recognition and regulation, binds in-between the domains. Hence molecular shape, linker flexibility, and domain mobility are related to function, and deriving a reliable dynamic picture is important.

^{15}N spin relaxation analyzed with MF was used to study backbone dynamics of Ca^{2+}–CaM. The first study of Ca^{2+}–saturated *Drosophila* CaM used data acquired at 11.7 T, 35 °C [246]. These data have been analyzed with the MF spectral density of Ref. [11], which considers the global diffusion tensor to be isotropic. This assumption is consistent with a nearly uniform ^{15}N T_1/T_2 profile, corroborated by comparing N–H orientations in the solution and crystal structures. Isotropic correlation times on the order of 6 – 8 ns were assigned to the N–, and C–terminal domains. Except for the flexible residues D78 –S81 of the central linker and two loops, the Ca^{2+}–CaM backbone was found to be "rigid", with $S^2 \sim 0.85$ and $\tau_e < 100$ ps.

At low magnetic fields, the local motion makes a relatively small contribution to the MF formula; hence, some features might have been missed in view of low sensitivity. If the MF spectral density is appropriate, the addition of higher field data will increase accuracy and precision. If it is oversimplified, then inconsistencies will arise. The Ca^{2+}–free *Xenopus* calmodulin study of Tjandra et al. [247] identified such inconsistencies when 11.7T and 14.1T data were analyzed in concert. They were reconciled by using the reduced EMF formula [13]. With S_f^2 fixed at 0.85, τ_f set equal to zero, and uniform parameters within the N–, and C–terminal domains, the fitting yielded $\tau_m = 12$ ns, $S_s^2 \sim 0.7$ and $\tau_s \sim 3$ ns. Unlike previously reported [246], the local motions appear to be slow in Ca^{2+}–CaM. The parameters S_s^2 and τ_s were interpreted to represent wobble-in-a-cone in the presence of a square-well potential. The half-cone angle was determined to be approximately 30° (this angle can be calculated from S_s^2, τ_s and an estimated value of the wobbling rate, D_w [11]).

^{15}N spin relaxation data of Ca^{2+}-saturated *Xenopus* CaM were acquired by Baber et al. [248] at 8.5, 14.1 and 18.8T, 308K. The model used was similar to the model of Tjandra et al. [247]. New aspects included removal of the restrictions that $\tau_f = 0$ and $S_f^2 = 0.85$, and the determination of an axial global diffusion tensor, $\boldsymbol{R}^{\mathbf{C}}$. The analysis of the local motion has been enhanced in this study; this may be ascribed to the contribution of the 18.8T data. However, the global diffusion tensor is field-independent. Therefore, adding data acquired at additional magnetic fields is not expected to change significantly the analysis of the $\boldsymbol{R}^{\mathbf{C}}$ tensor. However, as shown in the next section, a substantially axial $\boldsymbol{R}^{\mathbf{C}}$ tensor was determined using the combined data set.

Chang et al. [249] acquired additional experimental data. The ultimate data set included ^{15}N T_1, T_2 and {^{15}N–^1H) *NOE*s at 8.5, 14.1 and 18.8T, at 294, 300, 308 and 316K. These data were combined and analyzed using the EMF formula, assuming that (1) S_f^2, τ_f and $N = R_{\|}^C / R_{\perp}^C$ are the same for all the residues within a given domain and are independent of temperature, and (2) the temperature dependence of $1/(6\tau_m(\text{app})) \equiv 1/3(2R_{\perp}^C + R_{\|}^C)$ is given by the Stokes-Einstein formula. With this analysis a sudden decrease (increase) in S_s^2 (τ_s) was observed upon increasing the temperature from 308 to 316K. This was interpreted as 'melting' of residues R74 – K77 of the central linker (which are actually not present in the experimental data), which is considered important from a biological point of view. We focus below on the process that led to these conclusions.

5.3.1. Global diffusion—The global diffusion tensor, $\boldsymbol{R}^{\mathbf{C}}$, was determined from a combined multi-field multi-temperature ^{15}N T_1/T_2 data set, which is supposed to be free of local motional effects. Since the analysis of the local motion was based on using the EMF formula that detected slow local motions throughout the protein, this assumption cannot be valid.

Based on the coordinates of the crystal structure [250], the analysis has yielded $R_{\|}^{C}/R_{\perp}^{C}=1.6$ and a tilt angle of $\Theta = 67°$ (69°) between Z_C (the principal axis of $\boldsymbol{R}^{\mathbf{C}}$) and Z_I (the principal value of the inertia tensor of the crystal structure), for the C-terminal (N-terminal) domain (Fig. 12). The extent of axiality, $R_{\|}^{C}/R_{\perp}^{C}$, is the same in the crystal and in solution. The effective correlation time, $1/(6\tau_m(\text{app}))$, was found to be 10.1 ns at 308K.

Since the ^{15}N T_1/T_2 data contain local motional effects, one may suspect force-fitting. This is supported by the experimental ^{15}N T_1/T_2 data (filtered according to traditional criteria [202, 203]) shown in Fig. 13. The width of the distribution in ^{15}N T_1/T_2 divided by the average error is an empirical estimate of the extent to which the global diffusion tensor is axially symmetric. The value of this parameter is 6.0, 8.5 and 13.0 for 8.5, 14.1 and 18.8T, respectively, at 294K, and 4.0, 9.0 and 14.0 for 8.5, 14.1 and 18.8T, respectively, at 316K. It can be seen that the shape of this distribution is temperature-dependent although $\boldsymbol{R}^{\mathbf{C}}$ was assumed to be temperature-independent (the temperature-dependent τ_m values do not affect the shape of the ^{15}N T_1/T_2 profile). It is also strongly field-dependent, although it definitely should not change with the external field.

If the combined multi-field multi-temperature analysis described above is appropriate, it should agree with single-field single-temperature analyses. Using the filtered ^{15}N T_1/T_2 data shown in Fig. 13 we determined (using the program QUADRIC [204]) the axial global diffusion tensor, $\boldsymbol{R}^{\mathbf{C}}$, for each magnetic field and temperature separately, using a simplified method appropriate for $R_{\|}^{C}/R_{\perp}^{C} \leq 2$ developed in Ref. [166]. This method provides local diffusion constants, $\gamma_{CM} R_C(\theta_i)$ (θ_i is the angle between the bond vector $(N–H)_i$ and Z_C). If $\boldsymbol{R}^{\mathbf{C}}$ is axially symmetric $R^C(\theta_i)$ will depend linearly on $P_2(\cos\theta_i)$ [204,208,209].

We show in Fig. 14 $R^C(\theta_i)$ as a function of $P_2(\cos\theta_i)$ for 8.5, 14.1 and 18.8T, 294 and 316K. The expected linear dependence is not borne out. The largest distribution of points is obtained for 8.5T, 316K, although in this case χ^2 assumes the smallest value ($\chi^2 = 2$). This is not expected for models matching the data to which they are applied, but can occur when force-fitting is in effect. All four parameters defining the global diffusion tensor are field-dependent. In all the cases except for 8.5T, 316K, the angle Θ of the individual analyses is much closer to 0° than to 67° or 69°, obtained with the combined multi-field multi-temperature analysis.

It can be concluded that the axiality of $\boldsymbol{R}^{\mathbf{C}}$ absorbed unaccounted for factors. Based on experience acquired with AKeco, which also comprises internally mobile domains, these factors are mode-coupling and the anisotropy of the local potential, which are not accounted for in the EMF formula. The EMF spectral density is based on $C(t) = C^C(t)\times C^L(t)$. In this section we examined $C^C(t)$; in the next section we focus on $C^L(t)$.

5.3.2. Local motion: MF analysis—Figure 15 shows the S_s^2 and τ_s temperature-dependent profiles obtained by Chang et al. [249]. The squared generalized order parameter S_s^2 exhibits very limited temperature dependence between 294 and 308K and decreases abruptly upon increasing the temperature from 308K to 316K. The slow local motional correlation time, τ_s, is temperature-independent between 294 and 308K and *increases* abruptly upon increasing the temperature from 308K to 316K. Within the scope of the cone model τ_s depends analytically on S_s^2 and D_w. The respective expression is used to show that the abrupt increase in τ_s is due to the abrupt decrease in S_s^2, while D_w increases with temperature, as expected. However,

inspection of the absolute values of D_w shows that $1/(6D_w)$ is equal at 316K to 8.3 (6.8) ns for the N-terminal (C-terminal) domain, while the apparent global motional correlation time is 6.88 ns. Within the scope of spin relaxation, local motions may not be slower than the global motion.

The discontinuities in S_s^2 and τ_s between 308 and 316K in Fig. 15 are likely to result from the ^{15}N T_2 values changing significantly between 308K and 316K at 8.5T (Fig. 16), while all the other experimental parameters change monotonically [20]. This implies a different parameterizing scenario at 316K, evidenced by τ_m being outstandingly small and the angle Θ outstandingly large for 8.5T, 316K (Fig. 14).

The local motional parameters obtained with MF are likely to be also force-fitted. To test this assumption we analyzed the ^{15}N spin relaxation data from Ca^{2+}–CaM with the SRLS model.

5.3.3. Local motion: SRLS analysis—Separate analyses were carried out for each temperature and magnetic field using our fitting scheme for SRLS based on axial potentials [19]. In view of the large-amplitude motions executed by the N-terminal and C-terminal domains we assumed that $\boldsymbol{R}^{\mathbf{C}}$ is (similar to the global diffusion tensor of AKeco) on average isotropic. This is consistent with the ^{15}N relaxation analyses of Ca^{2+}–CaM in Ref. [246], AKeco in Ref. [46], and the ribonuclease binase in Ref. [251].

The ^{15}N relaxation data from Ref. [249] were analyzed in SRLS with the parameter combination including c_0^2, β_{MD} and $\tau_\perp/\tau_m$. This corresponds formally to "model 5" MF [96, 97]. The SRLS parameter $(S_0^2)^2$ (obtained from c_0^2) and $\tau_\perp$ are shown in Fig. 17 as a function of temperature for magnetic fields of 8.5, 14.1 and 18.8T. The correlation time $\tau_\perp$ decreases monotonically from approximately 6 ns at 294K to roughly 3 ns at 316K. The value of $\tau_\perp$ is on average twice larger than τ_s, and $(S_0^2)^2$ SRLS is approximately half of S_s^2 MF; unlike S_s^2, it decreases monotonically with increasing temperature. No sudden change is observed between 308 and 316K in either $(S_0^2)^2$ or $\tau_\perp$. The fact that $(S_0^2)^2$ and $\tau_\perp$ are field-dependent, and the unduly small value of $(S_0^2)^2$, are ascribed to the utilization of axial potentials. These inappropriate features are expected to be eliminated in future work, where rhombic potentials will be used.

5.3.4. The MF picture—In the crystal Ca^{2+}–CaM prevails as an elongated dumb-bell shaped molecule comprising an N-terminal domain and a C-terminal domain. Its shape is preserved in solution but the molecular symmetry axes are tilted with respect to one another by 67° – 69°.

In solution, the Ca^{2+}–CaM domains experience *ns* wobbling motions in the temperature range of 294 – 308 K. These motions occur within cones with constant half-cone angles of 22.5° for the N-terminal domain and 27° for the C-terminal (calculated from S_s^2, τ_s and D_w [11]). The wobbling rates, D_w, are very close to, and in some cases slower than, the rate for global diffusion. Nevertheless, the motions are assumed to be decoupled.

Between 308 and 316K the half-cone angles change abruptly from 22.5° to 27° for the N-terminal domain and from 27° to 37° for the C-terminal domain. This reflects 'melting' of the residues R74 – K77. The process detected has biological implications for target peptide binding by prolonging the flexible part of the central linker by 50%.

5.3.5. The SRLS picture—Ca^{2+}–CaM comprised two domains connected through a central linker flexible in the middle. In the crystal, the central linker is extended rendering the overall

shape cylindrical. In solution, the domains move with respect to one another, rendering the molecular shape on average spherical. This agrees with a nearly constant experimental ^{15}N T_1/T_2 profile at 11.7T. AKeco and ribonuclease binase, which experience extensive internal mobility as well, exhibit similar scenarios.

The perpendicular component for local N–H motion, $\tau_\perp$. is 6.2 – 2.2 times faster than the correlation time for global tumbling and decreases monotonically with increasing temperature. Based on its geometric context the correlation time, $\tau_\perp$, may be associated with domain motion. Based on its absolute value of $6 \geq \tau_\perp \geq 3$ ns in the temperature range of 294 – 316K, while $11.6 \geq \tau_m \geq 6.9$ ns in this temperature range, $\tau_\perp$ must be coupled dynamically to τ_m; SRLS accounts for this factor.

The squared axial order parameter, $(S_0^2)^2$, is 0.2 – 0.35 in the 294 – 316 K temperature range, and $(S_0^2)^2$ decreases monotonically with increasing temperature. The form of the local potential (hence of the local ordering tensor) is oversimplified because axial symmetry was imposed. An improved analysis allowing for rhombic local potentials is expected to yield the realistic picture of high local ordering about the $C_{i-1}^\alpha - C_i^\alpha$ axis with different extent of rhombicity at the various N–H sites [20,50]. Despite the simplified potentials used, the SRLS analysis of ^{15}N spin relaxation from Ca^{2+}–CaM is significantly better than the MF analysis.

6. Domain motion

6.1. Mode coupling

We presented above SRLS analysis of domain motion in AKeco and in Ca^{2+}–CaM. Let us consider in general slow internal motions in proteins that occur on the same (*ns*) time scale as the global motion. The body engaged in global motion exerts spatial restrictions on the body engaged in the somewhat faster internal motion. Consequently, their rotational degrees or freedom become statistically inter-dependent. We call this “mode- coupling”.

In SRLS “mode-coupling” is brought into effect by a local potential [16]. In its absence, the protein and the probe would be freely reorienting rotators. Each (axial) rotator is associated with three degrees of freedom or modes, with decay constants given by $(\tau_{m,K})^{-1}$ for the protein and $(\tau_K)^{-1}$ for the probe, where $K = 0,1,2$ $(\tau_K^{-1} = 6R_\perp^C + K^2(R_\parallel^C - R_\perp^C))$. The solution of the two-body SRLS Smoluchowski equation leads to an eigenvalue spectrum, $(\tau_i)^{-1}$, $i = 1,\ldots\infty$. Each eigenvalue is associated with a weighting factor or “eigenmode”, which represents the relative contribution of the corresponding eigenfunction to the time correlation function. The eigenmodes are determined by the parameter set considered, e.g., $R^C/R^L = \tau/\tau_m$ (in full notation $\tau_0/\tau_{m,0}$) and the coefficients of the coupling potential, c_0^2 and c_2^2.

Each degree of freedom is represented by a set of basis vectors that span the (infinite dimensional) vector space. The complete set of degrees of freedom is represented in the product space of these basis vectors. The eigenmodes are linear combinations of the vectors in the product space representation. The basic degrees of freedom, or modes, are thereby “mixed’ by the potential giving rise to coupled modes, i.e., “eigenmodes” [16]. The tensors $\boldsymbol{R}^{\mathbf{C}}$ and $\boldsymbol{R}^{\mathbf{L}}$ obtained by data fitting may represent more complex global and local rotators, and not just simple rotators [45].

A Smoluchowski equation of the form of Eq. (49), where the SRLS diffusion operator $\hat{\Gamma}$ is written in two equivalent forms given by Eq. (50) or Eq. (51), is solved. In Eq. (50) the orientation of each body is referred to the lab (inertial) frame, in the presence of a potential coupling them, which depends on their relative orientation. Simple products of basis functions

of the two rotators are utilized to provide a matrix representation of the operator $\hat{\Gamma}$. This is a convenient basis set when the potential is relatively small, i.e., the coupling is weak. In Eq. (51) only the global motion of the protein is referred to the lab frame, whereas the local motion of the probe is referred to the local director frame fixed in the protein. The product basis functions for the overall motion and the relative internal motion are used to provide the matrix representation of the operator $\hat{\Gamma}$. This is a more natural choice when the coupling potential is large. Since these two approaches are mathematically equivalent, one may use either choice. In our past work we have utilized Eq. (50) [19,40,46–50] whereas in recent work we utilized Eq. (51) [20,34,35,90].

According to the Eq. (50) perspective on mixed modes, as a coupling potential is added, the eigenmodes of $\hat{\Gamma}$ become linear combinations of the product functions of the two free rotors. This is a point of view where there are two types of "mixed-modes". The first type results from the coupling between the two rotors so that the motion of the internal rotor becomes more that of its motion relative to the protein. This is a feature that exists even when there is time-scale separation, i.e., $R^C/R^L \ll 1$. The second type of "mixed modes" arises when there is no longer a significant time-scale separation. In that case the diffusive reorientation of the internal rotor becomes a mixture of the global and local motions.

When Eq. (51) and its convenient basis set are used, the intuitive picture changes somewhat, but the final analyses are equivalent. In simple mathematical terms this means that the eigenvalues of $\hat{\Gamma}$ are unchanged, but the eigenmodes are represented in (or referred to) different basis sets. For very high axial ordering and $R^C/R^L \ll 1$ there are, within a good approximation, two eigenmodes that represent the overall motion and the relative internal motion. The eigenvalues are $1/\tau_m$ and $c_0^2/2\tau$, respectively, and the eigenfunctions are given in Refs. [14, 31]. As the coupling potential is reduced (but $R^C/R^L \ll 1$), the time correlation functions for the relative motion (i.e., for the $D^2_{MK}(\Omega_{CM})$) become more complex, involving several eigenmodes of this motion. As R^C/R^L increases, there will be "mixed modes" of the two coupled dynamic processes.

The notion of "mode-coupling" has its origin in theoretical approaches for treating deviations from Brownian motion of Debye particles in solution. A summary of early theories addressing this problem appears in the Introduction of Ref. [16]. Thus, coupling between the degrees of freedom of a particle engaged in restricted motion, and the degrees of freedom of the entity that imposes the restrictions, is a general concept.

The "diffusive mode-coupling" theories [121,122] do not belong to the category discussed in the previous paragraph. These are single-body theories that treat the effect of fast local bond-vector fluctuations on the eigenfunctions of the global diffusion tensor, in the context of a numerical solution of the diffusion equation. Here "mode-coupling" is conceived as a change in the global diffusion tensor by fast local motions.

It was pointed out in an earlier MD study that macromolecular tumbling and side-chain motions are "coupled" when the internal motions change significantly the dimensions or size of the protein [252]. A similar comment appears in Ref. [26] in the context of NMR spin relaxation in proteins. This perception of "mode-coupling" is in the spirit of "diffusive mode-coupling"; it differs in essence from the conceptualization of "mode-coupling" in liquid dynamics theories, including SRLS, which was outlined above. In practice, it implies a change in τ_m on the part of τ_e. In this case $\tau_m \gg \tau_e$ is no longer valid; neither are $C(t) = C^C(t) \times C^L(t)$ and $1/\tau_e^{|} = 1/\tau_m + 1/\tau_e \sim 1/\tau_e$. This is not always realized – for example, see Ref. [120]. Similarly the parameters τ_{c2} and τ_{c3} in the relations $1/\tau_{c2} = 1/\tau_{c1} + 1/\tau_c$ and $1/\tau_{c3} = 1/\tau_{c1} + 4/\tau_c$ in Woessner's model have been considered in some cases to represent a change in the shape of the protein,

τ_{c1}, by the local motion, τ_c. This is inconsistent with $\tau_{c1} \gg \tau_c$, which underlies Woessner's model.

We found with SRLS calculations that as long as $\tau \leq \tau_m/2$ the value of τ_m does not change as compared to its input value, i.e., the "diffusive-mode-coupling" effect is small.

"Non-separability" between the global and local motions is invoked in Refs. [25,26]. This geometric parameter does not represent correlation between the rotatational degrees of freedom of the protein and the probe.

6.2. SRLS analysis: activation energies

We consider the rate for domain motion in AKeco, R^L, obtained with rhombic local potentials for the N–H bonds located within AMPbd and LID and examine its temperature-dependence [50]. For completeness, we also examine the temperature-dependence of the potential coefficients and related order parameters obtained with the calculations that yielded R^L. Average values of these quantities, obtained at 288, 296.5 and 302K for the AMPbd and LID domains, are shown Table 7.

Except for c_0^2 the general trend is a decrease in parameter magnitude with increasing temperature. The non-monotonic change in c_0^2 is assigned to its value being very sensitive to changes in the local ordering in the high ordering regime – see Fig. 3. Since various potential forms can lead to the same order parameter components, we consider S_{xx}, S_{yy} and S_{zz} as the principal descriptors of the local spatial restrictions. It can be seen that the order parameters are very similar within AMPbd and LID, and their temperature-dependence is small.

The local motional correlation times within AMPbd and LID, $\tau = 1/(6\, R^{L)}$, are shown in Fig. 18d-f. As expected, τ decreases with increasing temperature. This parameter discriminates among secondary structure elements and loops. The correlation time for local motion is, on average, larger for the helices α_2 and α_3 of the AMPbd domain than for the loops α_2/α_3 and α_3/α_4 of this domain. Based on comparable τ values the "block" comprising β_7, loop β_7/β_8, β_8 and loop β_8/α_7 appears to be engaged in collective motion not necessarily identical to the motion of the entire LID domain. Fig. 18a-c show the analogous results obtained with axial potentials. The absolute values are not the same, and the discrimination among secondary structure elements is reduced significantly.

Activation energies, E_a, were calculated with the Arrhenius equation, $R^L = A \exp(-E_a/RT)$ (Table 8). They are nearly twice as large as their counterparts obtained with axial potentials. This indicates that rhombic potentials are required to obtain accurate activation energies. Allowing for potential asymmetry led to activation energies for domain motion of 63.8 ± 7.0 and 53.0 ± 9.1 kJ/mol for AMPbd and LID, respectively (Table 8). These values are approximately 1.5 times smaller than typical activation energies of reactions catalyzed by multidomain enzymes, which are on the order of 80 – 90 kJ/mol [253,254]. The activation energies obtained for several elements of secondary structure within AMPbd (helix α_3) and LID (strands β_5, β_6 and the β_7/β_8 block) are close to 80 – 90 kJ/mol.

Note that deriving activation energies for internal motion in proteins from ^{15}N spin relaxation is not trivial. To our knowledge, there are very few, if any, reports in the literature on this important physical quantity because in many cases the temperature-dependence of the MF parameter τ_e is qualitatively inconsistent with Arhhenius's equation [200,255].

6.3. MF analysis

The MF treatment of domain motion in Ca^{2+}–CaM has been outlined in Appendix E.

In Refs. [256] and [257] monomer motion in di-ubiquitin is modeled as two-site exchange which is decoupled from the global motion. A mode-decoupling-type time correlation function is used. Data fitting yielded exchange rates that are comparable to $1/(6\tau_m)$ at pH 6.8 and on average 3.5 *slower* than $1/(6\tau_m)$ at pH 4.5. Within the scope of spin relaxation, local motions may not be slower than the global motion.

In reference [258] a model that involves jumps between discrete conformers with different overall diffusion tensors, and a master (rate) equation to describe the transitions between these conformers, is presented. For two conformers the time correlation function is formally analogous to Eq. (2), with the parameters k_{eff}, D_{eff} and S^2 formally analogous to τ_e, $1/(6\tau_m)$ and S^2, respectively. The quantities k_{eff} and D_{eff} are given by algebraic expressions of the physical exchange rates, k_1 and k_2, from site 1 to site 2 and vice-versa, and the overall diffusion constants of the two sites, D_1 and D_2. The quantity S^2 depends in addition on $P_2(\boldsymbol{n_1}\cdot\boldsymbol{n_2})$, where $\boldsymbol{n_1}$ and $\boldsymbol{n_2}$ denote the orientations of the exchanging vectors with respect to similarly oriented global diffusion axes.

This represents a more intricate change in protein shape on the part of internal motions. The time correlation function is of the $C(t) = C^C(t)\times C^L(t)$ type, i.e., the global and internal motions are statistically independent. It is pointed out that the model developed in Refs. [256,257] is a limiting case of this model.

In Ref. [259] stochastic simulations were performed on a dual vector system “to drive hydrodynamics and domain coupling”. Two vectors, A and B, with common origin, reorient with respect to the vector A–B. The motions of A and B are correlated via a potential, u, which is either a squared-well potential, $k\cos\theta$, $-k\cos\theta^2$ or $k\cos\theta^3$, where θ is the inter-vector angle. The equilibrium orientation of θ is 180°, and its minimum allowed value is 90°; this results in wobbling motions of A and B within opposite cones with common tip.

A Langevin equation is solved for this system. An order parameter S is defined in terms of the potential u. The correlation time for the correlated motions of A and B (the motion of A–B) is denoted τ_s (τ_m). When $S = 1$ then the vectors A and B reorient with correlation time $\tau_0 = 10$ ns, and the vector A–B reorients with correlation time $2\tau_0$. The time scale separation, τ_s/τ_m, is restrained to lie within the range of 0.25 to 1.

The Langevin trajectory is reproduced by one exponent when $S \rightarrow 1$ and by two exponents otherwise within the scope of the reduced EMF formula. The order parameter is given by $S \equiv \langle P_2\cos(\pi/2 - \theta/2)\rangle$. This model has $C^L(t)$ given by wobble-in-a-cone in the presence of the potential u; $C(t)$ is given by $\exp(-t/\tau_m)\times C^L(t)$. The vector A–B is the local director, C′, fixed in the protein with respect to which the local ordering frame M ≡ A and M ≡ B (by cone duplication) are moving. The rotational degrees of freedom of the probe, $\Omega_{C'M}$, defining $C^L(t)$, are independent of the rotational degrees of freedom of the protein, Ω_{LC}, defining $C^C(t) = \exp(-t/\tau_m)$.

6.4. RNA elongation

When the local and global motions occur at comparable rates, one can no longer distinguish between them. Al-Hashimi and co-workers [260,261] developed a strategy whereby the global motion of an internally mobile RNA molecule is slowed down selectively by elongating it with an NMR invisible segment. The implied increase in time scale separation renders detectable previously undetected slow internal motions.

This method has been applied to a particular RNA fragment [260]. NMR peak intensities and ^{13}C R_2/R_1 ratios measured for this molecule were uniform. Upon elongation they became non-uniform, singling out segments expected to experience slow internal motions.

The qualitative evidence is unambiguous. However, the quantitative analysis, which is based on ^{15}N imino [260] and ^{13}C base and sugar [261] relaxation data analyzed with the EMF formula, can be improved significantly. The deficiencies of the EMF formula have been pointed out above. Furthermore, merely increasing the time scale separation between the global and local motions does not render MF-type treatments valid. One must also account for the effect of the local potential on the eigenfunctions of the uncoupled diffusion operators, the rhombicity of the local potential, and realistic local geometry.

An effort was made in Ref. [261] to account for the asymmetry of the nucleobase ^{13}C CSA interaction, and the non-collinearity between the ^{13}C CSA tensor frame and the frames of the ^{13}C–^{13}C and ^{13}C–^{1}H dipolar tensors. To account for these aspects one has to calculate $J^{CC}(\omega)$ and $J^{DC}(\omega)$. This requires the spectral density components $j_{00}(\omega)$, $j_{11}(\omega)$ and $j_{22}(\omega)$ for axial ^{13}C CSA tensors and also cross terms, $j_{KK'}(\omega)$, for rhombic ^{13}C CSA tensors (see paragraphs after Eqs. (57) and (58)). MF provides only $j_{00}(\omega)$. Hence, it is not possible to account adequately for these aspects of the analysis within the scope of MF.

Appendix F: Methyl dynamics by SRLS

1. The SRLS model

The probe considered in this article is $^{13}CDH_2$, with the 2H nucleus being observed. Typical experimental data sets comprise ^{2}H T_1 and T_2 acquired at two magnetic fields. The only anisotropic interaction causing spin relaxation is the quadrupolar interaction. The linewidths are large, with $1/T_2$ being often quite similar at different magnetic fields. Only $j_{KK'}(0)$, $j_{KK'}(\omega_D)$ and $j_{KK'}(2\omega_D)$ (ω_D is the ^{2}H Larmor frequency) enter the expressions for T_1 and T_2. The experimentally accessible region of the $j_{KK'}(\omega)$ functions is limited even when data acquired at several magnetic fields are combined, and/or rank 2 coherences are included in the experimental data set used [35]. For N–H bonds the spectral density functions are better defined due to the presence of the dipolar interaction with the proton which render accessible experimentally high-frequency values of the $j_{KK'}(\omega)$ functions.

Methyl dynamics are intrinsically more complex than N–H bond dynamics because of the flexibility of the side chain to which all the methyl groups except for alanine are attached. Therefore one has to conceive of a model that is simple enough not to overfit the experimental data, but elaborate enough to capture the dominant factors that determine methyl dynamics.

We found that the parameter combination that is necessary but still compatible with the sensitivity of typical data sets consists of c_0^2, c_2^2, and $R^C = \tau/\tau_m$. A rhombic mean-field potential, which is given by c_0^2 and c_2^2, accounts simply and economically for the effect of the dynamic local structure on the manner in which the methyl group occupies the conformational space while moving locally. In this scenario, one has only one additional free variable (c_2^2) as compared to Eq. (43), with the benefit of analyzing the experimental data with a physical model.

The local geometry, i.e., the relative orientation of the local ordering/local diffusion frame (M) and the magnetic frame (Q), is treated as follows. We assume that Z_M lies along the C–CH_3 axis; this implies $\beta_{MQ} = 110.5°$. Setting $\alpha_{MQ} = 90°$ [90] leads to a physical picture in which Z_D is tilled at 110.5° from Z_M, at 90o from X_M and at 159.5° from Y_M. This is as close as one can get without invoking additional parameters to the M frame being consistent with the tetrahedral carbon geometry. In most cases we fixed Ω_{MQ} at (90°, 110.5°, 0°); in some cases we allowed β_{MQ} to vary in the vicinity of 110.5° to account empirically for the complexity of methyl dynamics.

We present below SRLS analyses of methyl dynamics in the complex of Ca^{2+}-calmodulin (CaM) with a peptide smMLCKp corresponding to the calmodulin-binding domain of the smooth muscle myosin light chain kinase (Ca^{2+}–CaM*smMLCKp) [262], and in the B1 immunoglobulin binding domain of *Peptostreptococcal* protein L (in short, protein L) [24]. Sections 6.2 – 6.4 illustrate general features; Section 6.5 presents SRLS analysis of all the experimentally accessible methyl groups of protein L.

The following comment is in order. The statistical measure used in our calculation is the percentile value for a χ^2 distribution. For two degrees of freedom χ^2 has to be below 5.99, and for one degree of freedom χ^2 has to be below 3.84, for a commonly used 5% threshold [150]. In most cases our results have complied with this requirement. We also require physical viability of the best-fit parameters. In the present case, we required the temperature dependence of R_L to be given by the Arrhenius equation. To ascertain that over-fitting is not occurring we typically check the effect of lowering the symmetry of the various physical quantities involved. For methyl dynamics we found that allowing the tensor $\boldsymbol{R}^{\mathbf{L}}$ to be axially symmetric led in many cases to overfitting; therefore we used isotropic local diffusion. This is justified in the large time scale separation limit.

2. Typical spectral densities

SRLS spectral densities calculated for typical rhombic potentials at methyl sites in proteins are illustrated in Figs. 19–21[35]. Fig. 19 shows the $j_{KK'}(\omega)$ functions calculated using the best-fit parameters obtained for methyl 23T of protein L using combined ^{2}H T_1, T_2 and rank 2 coherence experimental data acquired at 11.7 and 14.1T, 25 °C [24], and setting $\beta_{MQ} = 110.5°$ and $\gamma_{MQ} = 90°$[3]. These parameters are $c_0^2=1.82, c_2^2=-0.67$ and $R^C = 0.017$.

The insert shows a compressed ω-range extending from zero to 4000 MHz. It can be seen that the portion of the $j_{KK'}(\omega)$ functions sampled consists of a relatively narrow region outside of which these functions are not defined experimentally. Note that the magnetic field range scanned is almost as large as feasible with currently available technology. Fig. 20 shows the $j_{KK'}(\omega)$ functions calculated for $c_0^2=1.5, c_2^2=-0.5$ and $R^C = 0.05$, and Fig. 21 shows the $j_{KK'}(\omega)$ functions of Fig. 20 assembled into the measurable spectral density $J^{QQ}(\omega)$ for $\beta_{MQ} = 110.5°$ and $\gamma_{MQ} = 90°$.

The following important point is illustrated in Figs. 20 and 21. Let us assume that the six $j_{KK'}(\omega)$ simulated functions shown in Fig. 20 represent an actual scenario. Using SRLS one can reproduce them with $c_0^2=1.5, c_2^2=-0.5$ and $R^C = 0.05$. The $J^{QQ}(\omega)$ function comprising the $j_{KK'}(\omega)$ functions will also be reproduced if β_{MQ} and γ_{MQ} are supplied. ^{2}H T_1 and T_2 will also be reproduced if the magnetic interactions are supplied.

Let us now consider analyzing this scenario with MF. The functions $j_{KK'}(\omega)$ cannot be reproduced because such functions do not exist in MF. However, Eq. (43) might reproduce the function $J^{QQ}(\omega)$ with good statistics, obviously with different best-fit parameters, which are perforce physically vague. Quite a few variants of Eq. (43) might also parameterize $J^{QQ}(\omega)$ – see, for example, Refs. [24,192]. Similarly quite a few simple functions can parameterize MD time correlation functions (e.g., see Ref. [132,157,159]). This situation generates ambiguity and leads to inaccurate parameters.

3. Conformational entropy

The squared order parameter, S_{axis}^2, has been used extensively to calculate conformational entropy [55–57]. This calculation requires an equilibrium probability density function (Boltzmann factor), which is obtained in MF as follows. It is assumed that S_{axis}^2 (obtained with

data fitting) is an axial physical order parameter defined in terms of a local potential, $u(c)$. The form of this potential is guessed, and it is assumed that it depends exclusively on the rotational degrees of freedom of the probe [55,57]. The coefficient of the potential, c, is derived based on the axial form of Eq. (59), determining thereby the Boltzmann factor.

In SRLS the local potential, $u(c_0^2, c_2^2)$, hence the Boltzmann factor, are available at the completion of the fitting process which determines c_0^2 and c_2^2. The form of $u(c_0^2, c_2^2)$ is intrinsic to the theory (Eq. (50)). By definition this potential depends only on the rotational coordinates of the probe relative to the protein, $\Omega_{C'M}$.

We calculated the conformational entropy for 45 methyl groups of Ca^{2+}–CaM*smMLCKp. The expression $S_p/k_B = -\int_\nu p(q)\ln[p(q)]d\nu$, as defined in Ref. [57], was used. The parameter q denotes coordinates of the probe, k_B is the Boltzmann constant, and $p(q)$ is the equilibrium probability density function.

The coefficients c_0^2 and c_2^2 (and local motional rates, $R^{L)}$ were obtained by fitting with SRLS ^{2}H T_1 and T_2 data acquired at 14.1 and 17.6T, 295K. We obtained $0 \le c_0^2 \le 2.5$ and c_2^2 in the range of −0.26 to −0.94 for the 45 methyl groups studied (with β_{MQ} and γ_{MQ} set equal to 110.5° and 90°, respectively). These data were used to calculate S_p/k_B.

In Figs. 22c-e we show S_p/k_B as a function of $0 \le c_0^2 \le 2.5$, S_0^2 and S_2^2 for c_2^2 equal to −0.26, −0.51, −0.87 and −0.94. For comparison, we show in Fig. 22a S_p/k_B as a function of c_0^2 with $c_2^2 \equiv 0$, as in MF. In Fig. 22b we show S_p/k_B as a function of the S_0^2 values that correspond to the c_0^2 values shown in Fig. 22a. Since MF analyses feature $0 < S_{axis} < 1$ [6], we show in Figs. 22d S_p/k_B as a function of $0 \le S_0^2 < 1$, for the c_2^2 values given above. In Figs. 22c we show S_p/k_B as a function of the c_0^2 values corresponding to the S_0^2 values shown in Figs. 22d, for the c_2^2 values given above.

In Fig. 22e we show S_p/k_B as a function of S_2^2 for the c_2^2 values given above. With this presentation (used to facilitate comparison between the axial and rhombic potential scenarios), the variations in S_p/k_B as a function of c_2^2 are suppressed in Figs. 22c,d. However, they are conspicuous in Fig. 22e, which does not have an axial counterpart.

The following picture emerges. (1) The diversity of the experimental data is interpreted in SRLS as variations in the shape of the local potential. In MF it is interpreted as variations in the amplitude of axial fluctuations presumably executed by the C–CH_3 bond. (2) The conformational entropy S_p/k_B does not vary much throughout the protein according to SRLS; it varies a great deal according to MF [6]. This result has significant implications for the characterization of methyl sites in proteins in terms of conformational entropy [6]. (3) S_p/k_B from SRLS has a well defined physical meaning. No assumptions are made beyond the basic tenets of the SRLS model. Once the coefficients c_0^2 and c_2^2 have been determined with fitting of the experimental data, one can readily calculate S_p/k_B, S_0^2 and S_2^2. Several assumptions are made in the MF scenario and S_{axis}^2 is also problematic in nature.

Yang and Kay considered rhombic potentials in the context of MF [57]. A new method for calculating conformational entropy has been developed recently; it was associated with the generalized MF order parameter [263].

4. Local potentials and relative probability

To gain further insight into the local ordering at methyl sites in proteins we present below local potentials, $u(c_0^2, c_2^2)$, and associated relative probability, P_{rel}, for typical potential shapes obtained with SRLS analysis. The methyl groups of residues 10A and 85Iγ of Ca^{2+}–CaM*smMLCKp have been selected as examples. The experimental ^2H T_1 and T_2 data acquired at 11.6 and 17.7T, 295K [262], have been subjected to data fitting. The best-fit parameters obtained in these calculations are c_0^2=1.76, c_2^2= − 0.59, β_{MQ} = 109° and τ/τ_m = 0.0054 for A10, and c_0^2=0.74, c_2^2= − 0.48, β_{MQ} = 112° and τ/τ_m = 0.01 for 85Iγ. The errors in the various best-fit parameters are estimated to be on the order of 10%.

The rhombic potential prevailing at the site of methyl A10, given by c_0^2=1.76 and c_2^2= − 0.59, is shown in Fig. 23a; the corresponding P_{rel} function in shown in Fig. 23b. The Cartesian tensor components given in Table 9 indicate that Z-ordering prevails at this methyl site. The shape of P_{rel} in Fig. 23b corresponds to $|S_{xx}| > |S_{yy}|$; the depression in the center is due to small solid angles close to $(\beta_{C'M},\gamma_{C'M}) = (0,0)$. The rhombicity of the potential may be estimated by $|c_2^2/c_0^2|$ that is equal to 0.36; this represents substantial asymmetry.

The rhombic potential prevailing at the site of methyl Iγ85, given by c_0^2=0.74 and c_2^2= − 0.48, is shown in Fig. 23c; the corresponding P_{rel} function is shown in Fig. 23d. The Cartesian tensor components given in Table 9 show that X-ordering prevails at this methyl site. The $|c_2^2/c_0^2|$ ratio is 0.65. This represents very high rhombicity.

The MF analysis gives values of S_{axis}^2 of the A10 methyl as 0.84 and the S_{axis}^2 value of the Iγ85 methyl as 0.303 at 295K [262]. Thus, according to MF the C–CH_3 bond of A10 is highly ordered; this is expected. On the other hand, the C–CH_3 bond of Iγ85 is involved in large-amplitude axial fluctuations. As pointed out above, this is incompatible with the local stereochemistry and the packing properties of protein cores.

According to SRLS the A10 and Iγ85 methyl groups, and in general all the methyl groups in proteins, reorient in the presence of rhombic local potentials. Different methyl groups experience different potential forms in agreement with the structural differences in their immediate surroundings. Correlations between the SRLS potentials and the local structure will be established in future work.

5. Protein L: application

Kay and co-workers studied ^2H spin relaxation of $^{13}CDH_2$ groups in protein L with MF [24]. Auto-correlated relaxation rates and relaxation rates associated with rank 2 coherences were acquired at 9.4, 11.7, 14.1 and 18.8T, in the temperature range of 288 – 318K. We analyzed these data, kindly provided by Prof. Lewis E. Kay, with SRLS, and compared results with the MF analysis of Ref. [24]. Detailed information appears in Ref. [35]. Selected results are presented below.

Table 10 shows methyl groups ordered approximately according to the S_{axis}^2 values obtained using Eq. (43) [24]. Data obtained at 298K were used in these calculations; τ_e from Ref. [24] was also used. The c_0^2 values were calculated assuming that S_{axis} represents S_0^2. The SRLS results shown in Table 10 were obtained from the same experimental data by fixing β_{MQ} at 110.5° and γ_{MQ} = 90°, and allowing c_0^2, c_2^2 and R^C to vary in the data fitting process [35].

The penultimate and ultimate columns on the right show $R(c_0^2)=c_0^2(\mathrm{SRLS})/c_0^2(\mathrm{MF})$ and $R(\tau) = \tau(\mathrm{SRLS})/\tau_e(\mathrm{MF})$, respectively. It can be seen that these ratios are larger than unity and in many cases vary considerably within a given group of similar $S_{\mathrm{axis}}{}^2$ values.

For relatively small values of $S_{\mathrm{axis}}{}^2$, which are the most useful ones in MF analyses, $S_{\mathrm{axis}}{}^2$ taken as $(S_0^2)^2$ is approximately linear in c_0^2 (Fig. 3). Therefore the qualitative disagreement between the trends exhibited by $c_0^2(\mathrm{SRLS})$ and $c_0^2(\mathrm{MF})$ implies qualitative disagreement between the trends exhibited by $c_0^2(\mathrm{SRLS})$ and $S_{\mathrm{axis}}{}^2$.

Since $c_0^2(\mathrm{SRLS})$ is a physical parameter whereas $S_{\mathrm{axis}}{}^2$ is a composite parameter with a vague physical meaning, caution is to be exerted in MF analyses in interpreting variations in $S_{\mathrm{axis}}{}^2$ in terms of biological phenomena. A new term called, “polar dynamics”, based on relative $S_{\mathrm{axis}}{}^2$ values, was set forth recently [264]. Small differences in $S_{\mathrm{axis}}{}^2$ and τ_e have been used to elucidate communication pathways in proteins and detect manifestations of allostery [265–267]. Such inferences should be based on physical parameters.

The parameter τ_e is problematic not only because of its mathematical definition and the associated unspecified validity ranges, but also because of its multiple inconsistent roles in Eq. (43). Such a parameter typically does not obey physical laws, e.g., Arrhenius-type temperature-dependence. In quite a few temperature-dependent studies, τ_e values are not even reported (e.g., Ref. [262]). Occasionally τ_e might exhibit Arrhenius-type temperature-dependence over narrow temperature-ranges. Nevertheless, one should be cautious in interpreting such trends in terms of physical activation energies. This has been attempted in Ref. [268] for selected methyl groups of the SH3 domain of α-spectrin for a temperature range of 17K.

Appendix G: SRLS eigenmodes: methyl dynamics

The SRLS time correlation functions comprise sums of weighted exponents with decay constants given by the eigenvalues of the SRLS solution, and weighting factors, or “eigenmodes”, determined by the eigenvectors of the SRLS solution. We depict below the eigenmode composition of a hierarchy of SRLS time correlation functions associated with methyl dynamics. Gradual enhancement of relevant tensorial properties is carried out. Within the scope of this scheme, we search for a physical scenario that Eq. (43) might represent.

The ^{2}H T_1 and T_2 relaxation times of the $^{13}CDH_2$ methyl group of alanine A10 of Ca^{2+}–CaM*smMLCKp, acquired at 14.1 and 17.6T, and 295K (Ref. [262]), have been selected as a representative example. They were subjected to SRLS-based data fitting for several different parameter combinations. The best-fit parameters determined thereby, and those kept fixed in these calculations, were used as input to calculate SRLS time correlation functions, $C_{KK'}(t)$. The eigenmodes contributing to these functions are delineated below, and the emerging picture is discussed.

The results of the MF analysis of methyl group A10 are illustrated in Fig. 24a. $S_{\mathrm{axis}}{}^2$ is equal to 0.84; hence the weighting factor of the global motional mode is $S^2 = 0.084$ (circled point in Fig. 24a). The decay constant associated with the effective local motion is not available since τ_e values are not reported in Ref. [262]. For example, a value of 12 ps would yield $R^{\mathrm{C}} = 0.006$ (in units of R^{L}), using $\tau_m = 11.81$ ns (taken from Ref. [262]). The eigenmode associated with the effective local motion is $(1 - S^2) = 0.916$; the corresponding eigenvalue is 6 (in units of R^{L}).

The generic MF spectral density used for methyl dynamics analysis is Eq. (2), where S^2 and τ_e are varied; $S_{\mathrm{axis}}{}^2$ is obtained as $S^2/0.1$. The formally analogous SRLS parameters are c_0^2 and

R^C. The best-fit values obtained for methyl A10 with a SRLS calculation where these parameters were varied are c_0^2=0.87 (corresponding to $(S_0^2)^2$=0.036) and R^C = 0.0015. These values were used as input to the calculation of the functions C_{KK} (*t*), *KK* = 00, 11, 22. The eigenmodes comprising these functions are shown in Table 11. We compare below Figs. 24a and 24b.

The angle β_{MQ} is implicitly zero in MF and set equal to zero in the SRLS calculation. Therefore only C_{00} (*t*) (j_{00} (ω) in the frequency domain) is relevant in the present context. The function C_{00} (*t*) comprises three dominant local motional eigenmodes given by 0.350, 0.509 and 0.094, corresponding to eigenvalues of 5.96, 5.63 and 6.93, respectively. The global motional eigenmode is 0.0376 and the corresponding eigenvalue is 0.0355. A large number of small eigenmodes (not shown) makes the remaining fractional contribution of 0.0094. The eigenmodes contributing to C_{00} (*t*) are shown in Fig. 24b.

The eigenmode compositions shown in Figs. 24a and 24b differ significantly. The spectral density underlying Fig. 24a is a simple limit of the spectral density underlying Fig. 24b. The physical scenario examined in these calculations is diffusive local motion in the presence of a small axial potential in the large time scale separation limit. Clearly, the spectral density given by Eq. (2) does not represent this physical scenario properly; if it did, the results shown in Figs. 24a,b would have been similar.

The calculation illustrated in Fig. 24b does not account for the 110.5° tilt between the magnetic and local ordering/local diffusion axes, which is an important geometric feature in methyl dynamics; hence, it must be enhanced to do this. We repeated the SRLS-based fitting of the data of methyl group A10 with β_{MQ} fixed at 110.5° instead of 0°. The best-fit parameters obtained are c_0^2=2.97 (corresponding to $(S_0^2)^2$=0.36) and R^C = 0.0009. Using these parameters as input (with β_{MQ} = 110.5°) we calculated the time correlation functions C_{00} (t), C_{11} (t) and C_{22} (t). Since β_{MQ} = 110.5° all of these functions contribute to *C*(*t*) with coefficients of 0.1, 0.323 and 0.577, respectively. The properly scaled (according to the local geometry) eigenmodes contributing to the various C_{KK}(*t*) functions are shown in Fig. 24c; the unscaled eigenmodes are shown in Table 12.

The (scaled) global motional eigenmode is 0.0329 and c_0^2 is 2.97 when β_{MQ} = 110.5° (Fig. 24c). The (scaled) global motional eigenmode is 0.0376 and c_0^2 is 0.87 when β_{MQ} = 0° (Fig. 24b). Instead of three dominant (unscaled) eigenmodes of 0.350, 0.509 and 0.094 in C_{00} (t) (j_{00} (ω)), corresponding to eigenvalues of 5.96, 5.63 and 6.93, respectively, for β_{MQ} = 0 (Table 11), one has two (unscaled) local motional eigenmodes of 0.378 and 0.130, corresponding to eigenvalues of 7.65 and 6.93, respectively, for β_{MQ} = 110.5° (Table 12). Eigenmodes of C_{11} (t) (j_{11} (ω)) and C_{22} (t) (j_{22} (ω)) dominate J^{QQ} (ω) for β_{MQ} = 110.5°; they do not contribute to J^{QQ} (ω) for β_{MQ} = 0°. The very large differences in eigenmode composition, implied by different local geometries, are associated with very different best-fit parameters. Clearly the β_{MQ} = 110.5 ° geometry is correct.

We compare these parameters with their counterparts in Eq. (47), which is the physical representation of Eq. (43). Equation (47) features $(S_0^2)^2$=0.84. The *K* = 0 term of this equation (Eq. 46a) comprises a global motional eigenmode of $0.1 \times (S_0^2)^2$ with eigenvalue of 6 R^C, and a local motional eigenmode of $0.1 \times [1 - (S_0^2)^2]$ with eigenvalue of 6. The C_{11} (*t*) and C_{22} (*t*) functions contribute eigenmodes of 0.323 and 0.577, respectively, both with eigenvalue of 6.

The actual case features $(S_0^2)^2$=0.329. Table 12 shows that the dominant eigenmodes are 0.419 with eigenvalue of 1.21 contributed by C_{11} (t), and 0.735 with eigenvalue of 4.47 contributed by C_{22} (t). Additional eigenmodes with eigenvalues in the range of 6 – 10 are contributed by all the C_{KK} (t) functions. The difference between the eigenmode composition of Fig. 24c (Table 12) and the eigenmode composition of Eq. (47) is large.

The physical scenario examined in the latter comparison is diffusive local motion in the presence of an axial potential with a "diffusion tilt" of 110.5° in the large time scale separation limit. Clearly, the spectral density given by Eq. (47) does not represent this physical scenario either.

We showed in previous work that SRLS analysis of methyl dynamics based on axial potentials yields results which have several problematic aspects [34,35]. Many of these problems could be resolved by allowing for rhombic potentials. We therefore proceeded by subjecting the experimental data of A10 to SRLS analysis where rhombic potentials were allowed for.

The parameter combination including c_0^2, c_2^2, β_{MQ} and R_C was used in this calculation. The best-fit parameters obtained are c_0^2=1.76, c_2^2= − 0.59, R^C = 0.0054 and β_{MQ} = 109° (similar results were obtained by fixing β_{MQ} at 110.5°). Note that for rhombic potentials the functions j_{00} (ω), j_{11} (ω), j_{22} (ω), j_{20} (ω), j_{1-1} (ω) and j_{2-2} (ω) contribute to J^{QQ} (ω) with coefficients of 0.14, 0.354, 0.474, −0.095, 0.045 and 0.082, respectively. For simplicity we only display in Figure 24d the dominant eigenmodes of C_{00} (t), C_{11} (t) and C_{22} (t) (which correspond to j_{00} (ω), j_{11} (ω) and j_{22} (ω), respectively).

Let us compare the rhombic and axial potential scenarios. C_{00} (t) of Table 13 (Table 12) comprises a global motional eigenmode of 0.079 (0.329) corresponding to an eigenvalue of 0.042 (0.006). The local motional eigenmodes contributing to C_{00} (t) of Table 13 correspond to eigenvalues spanning the range of 5.20 – 8.93. This should be compared to the eigenvalues of 7.65 and 6.93 shown in Table 12. C_{11} (t) of Table 13 (Table 12) comprises "faster" local motional eigenmodes corresponding to eigenvalues in the range of 5.23 – 8.00 (7.65 – 8.93) and two "slower" local motional eigenmodes (one "slower" eigenmode) corresponding to eigenvalues (an eigenvalue) of 1.82 and 1.37 (1.21). C_{22} (t) of Table 13 comprises quite a few local motional eigenmodes corresponding to eigenvalues in the range of 2.93 – 8.93. C_{22} (t) of Table 12 comprises only three local motional eigenmodes corresponding to eigenvalues of 4.47, 8.94 and 10.1.

The eigenmode/eigenvalue patterns for the axial and rhombic potential cases are very different. The time scale separation is 6-fold smaller in the rhombic potential case due primarily to a larger number of "slower" eigenmodes (corresponding to smaller eigenvalues). Such eigenmodes are also missing in MF calculations yielding inaccurate τ_e values. There are reports in the literature that τ_e MF is often too small [269].

All the calculations illustrated in Fig. 24 are associated with sufficiently low χ^2 values [150]. Only the calculation illustrated in Fig. 24d, featuring a rhombic potential, is appropriate from a physical point-of-view. Ample evidence that rhombic potentials underlie methyl dynamics in proteins appear in Refs. [34,35,38,71,76,193]. Figure 24d indicates that the mixed modes implied by rhombic potentials make comparable contributions to $C(t)$. Axial potentials generate a dominant eigenmode contributed by the C_{22} (t) function – cf. Fig. 24c. A uniform eigenmode distribution agrees better with a potential representing non-specifically the complexity of methyl dynamics.

Note that mode-coupling has a small effect on methyl dynamics because the local motion of the methyl group is much faster than the global tumbling of the protein. The analysis presented

above illustrates the importance of allowing for rhombic symmetry and arbitrary orientation of the local ordering tensor. It also illustrates that Eq. (43) does not represent a physical scenario. S_{axis}^2 is physically vague, as pointed out in Section 3.2.3. As already shown, trends in S_{axis}^2 may be misleading. As an additional example we note that for methyl group A10 $(S_2^0)^2$=0.36 whereas S_{axis}^2 = 0.84; for methyl group M76 $(S_2^0)^2$=0.14 where S_{axis}^2 = 0.11. Based on extensive calculations we found that the parameterizing values, S_{axis}^2, span a significantly larger range than the physical values, $(S_0^2)^2$. The relation between $(S_0^2)^2$ and S_{axis}^2 is not linear.

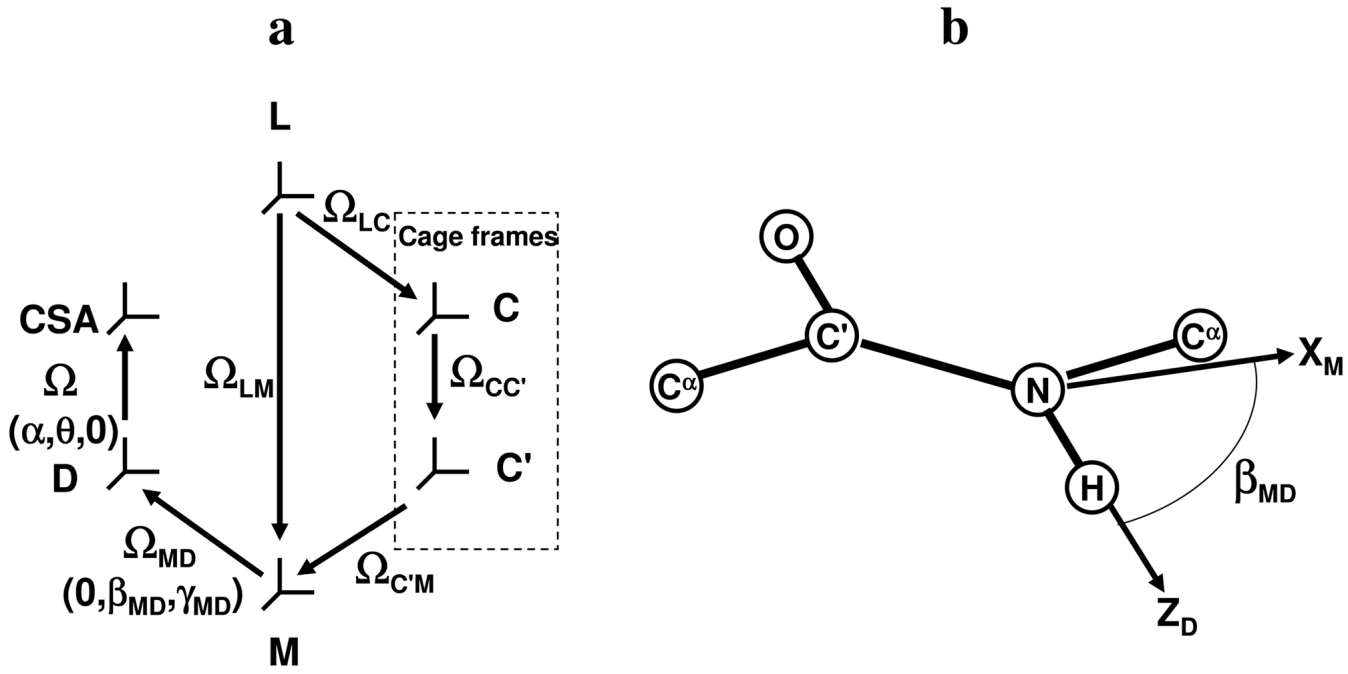

Fig. 1.

(a) Various reference frames that define the SRLS model. L is the laboratory frame; C is the global diffusion frame associated with protein shape; C′ is the (uniaxial) local director frame (with $Z_{C'}$ along the equilibrium orientation of the N–H bond) and $X_{C'} = Y_{C'}$; M denotes the local ordering/local diffusion frame fixed in the N–H bond; D is the magnetic ^{15}N–^{1}H dipolar frame and CSA the magnetic ^{15}N chemical shift anisotropy frame, both fixed in the N–H bond. Ω_{LC} are $\Omega_{C'M}$ are time-dependent angles associated with the global motion and the relative local motion, respectively. (b) Schematic drawing showing the peptide plane and the Z_D axis of the ^{15}N–^{1}H dipolar (D) frame. The Y_D axis (not shown) is perpendicular to the peptide plane, and the axes X_{CSA}, Y_{CSA} and Z_{CSA} (not shown) are defined to be aligned with the most shielded (σ_{11}), intermediate (σ_{22}) and least shielded (σ_{33}) components of the ^{15}N shielding tensor, respectively [19]. The orientation of the M frame with respect to the D frame is given by the best-fit value of β_{MD}, and $\gamma_{MD} = 90°$ (γ_{MD} was fixed at 90° based on stereo-chemical considerations [20]). The orientation preferences of the M frame axes in the local director frame, C′, are determined by the relative magnitudes and signs of c_0^2 and c_2^2 [14].

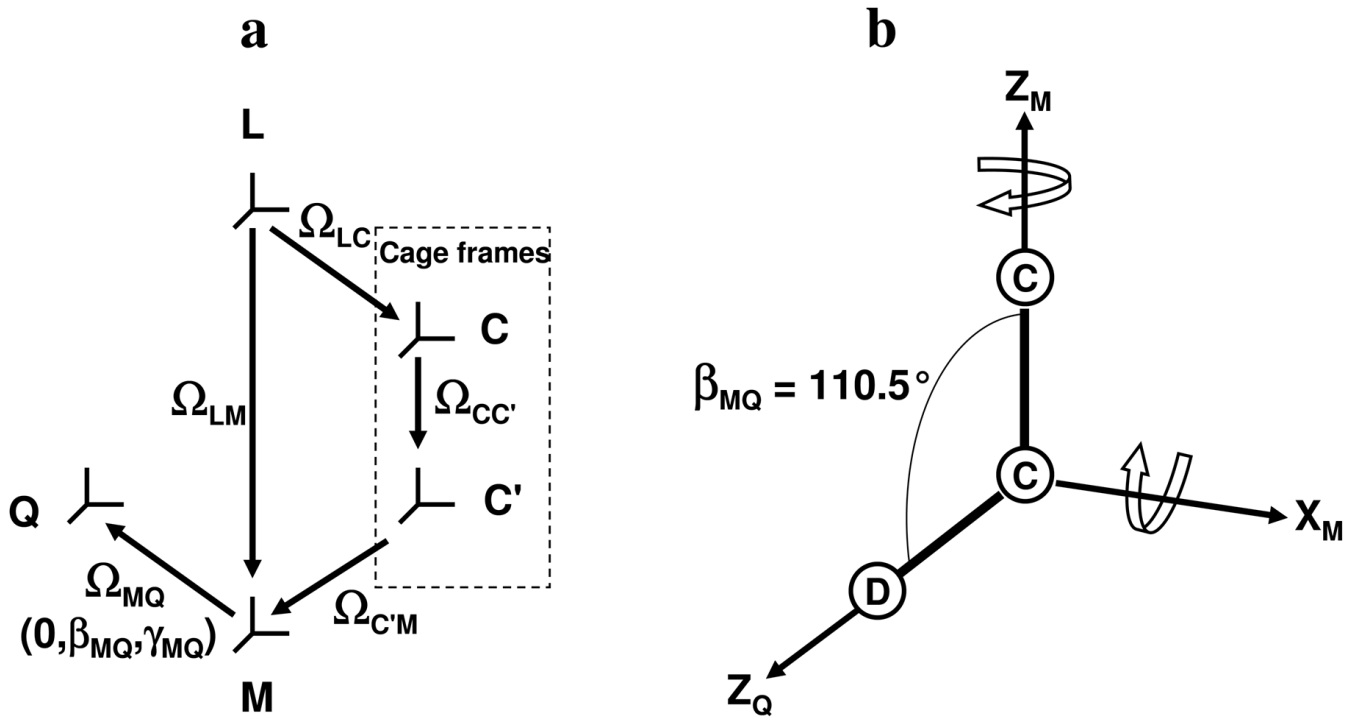

Fig. 2.

(a) Same as the captions of Fig. 1a, except for the magnetic frames; Q denotes the axial quadrupolar tensor. (b) Methyl group schematic corresponding to a rhombic local ordering scenario. Z_Q denotes the principal axis of the quadrupolar tensor. X_M denotes the main ordering axis lying along the C–CDH_2 bond.

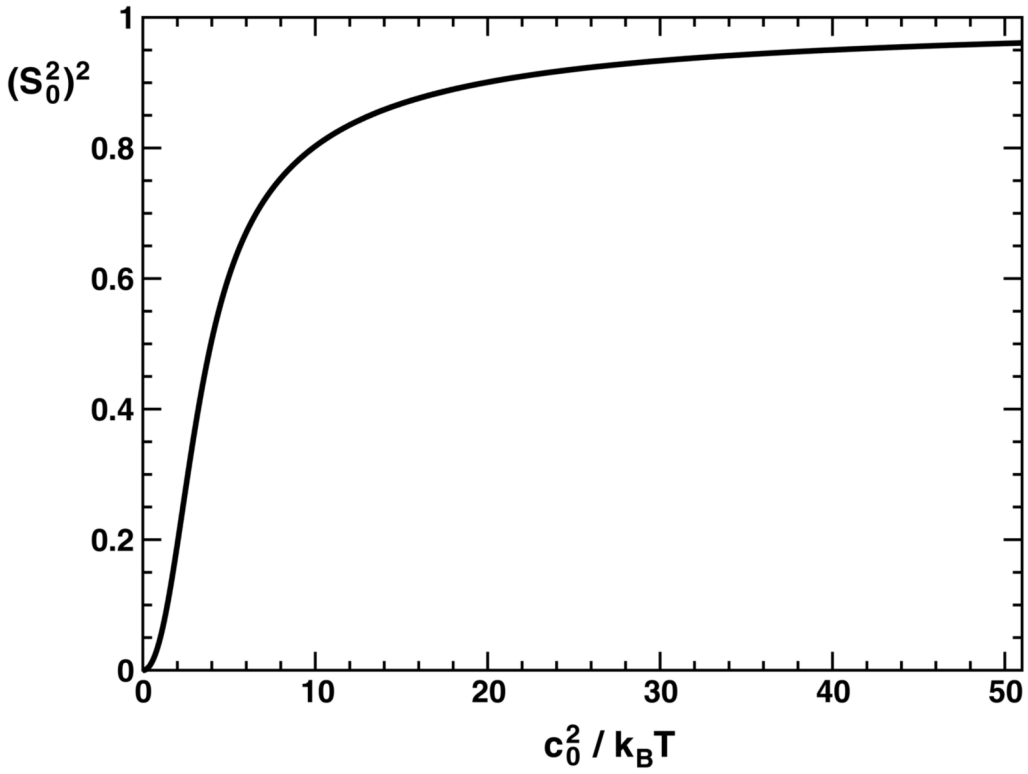

Fig. 3.

Squared order parameter, $(S_0^2)^2$, as a function of the potential coefficient, c_0^2 (see Eqs. (52) and (59)).

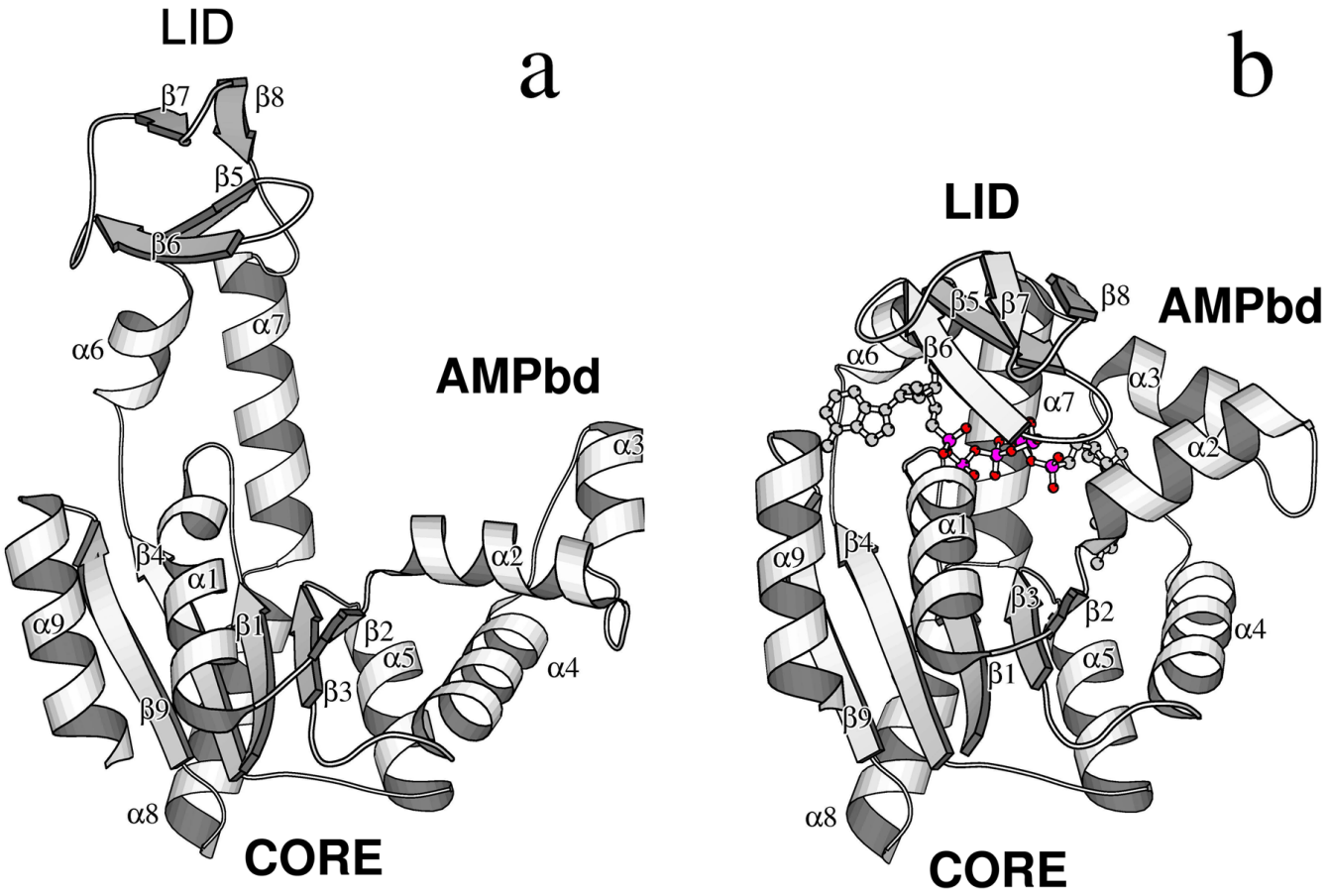

Fig. 4.

Ribbon diagrams of the molecular structures from X-ray crystallography of (a) AKeco [212] and (b) AKeco in complex with the two-substrate-mimic inhibitor AP_5A [215]. The diagrams were drawn with the program Molscript [217] using the PDB coordinate files 4ake for AKeco and 1ake (complex II) for AKeco*AP_5A.

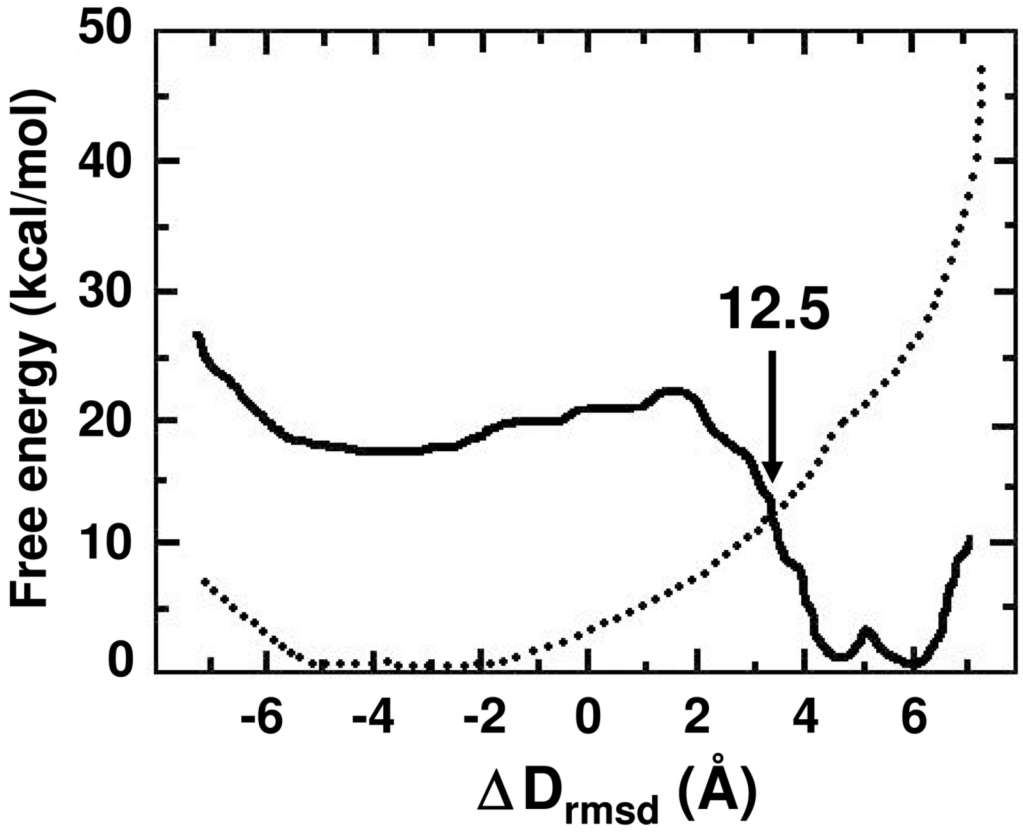

Fig. 5.

(a) The one-dimensional free energy profile along the ΔD_{rmsd} reaction coordinate in the ligand-free (dotted line) and AP_5A-bound (solid line) adenylate kinase pathways. The intersection region of the two profiles locates the transition state of the conformational transition, which is associated with a free-energy barrier of 12.5 (kcal/mol). The stabilities of the open unbound and closed bound states are assumed to be the same (Fig. 6 of Ref. [233], reproduced with permission).

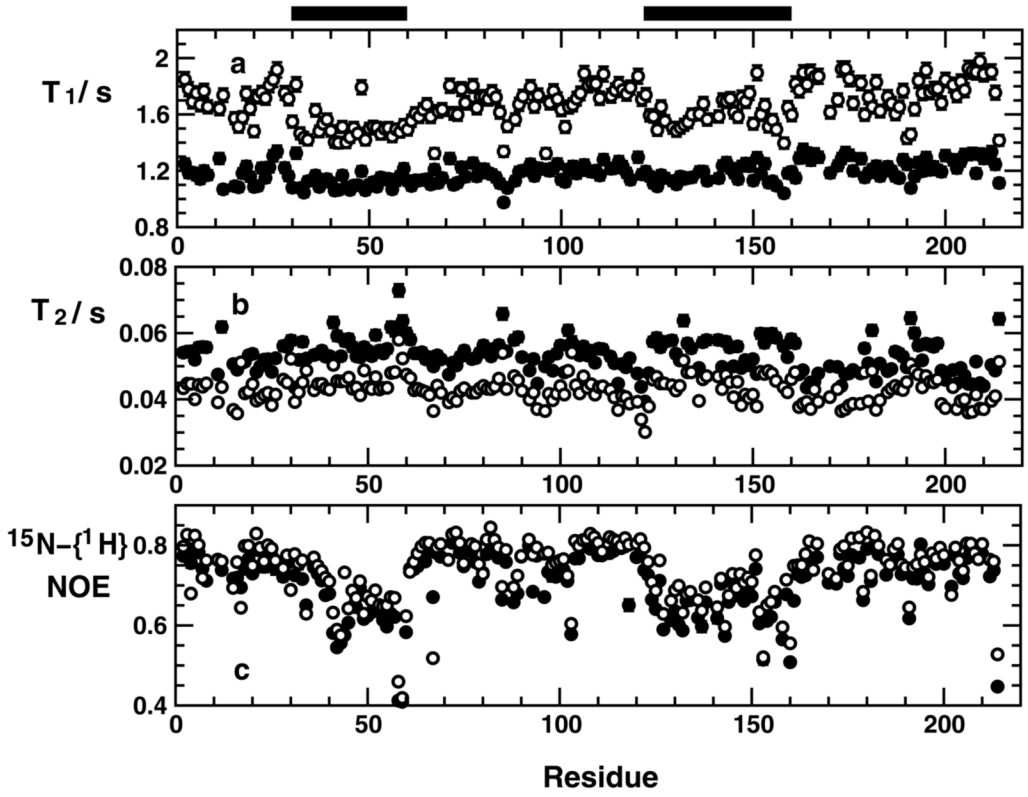

Fig. 6.

Experimental relaxation parameters (a) ^{15}N T_1 (ms), (b) ^{15}N T_2 (ms), and (c) ^{15}N–{^{1}H} *NOE* of AKeco acquired at 14.1T (filled circles) and 18.79T (empty circles) and 303K, as a function of residue number. The black bars denote the mobile domains AMPbd and LID [46].

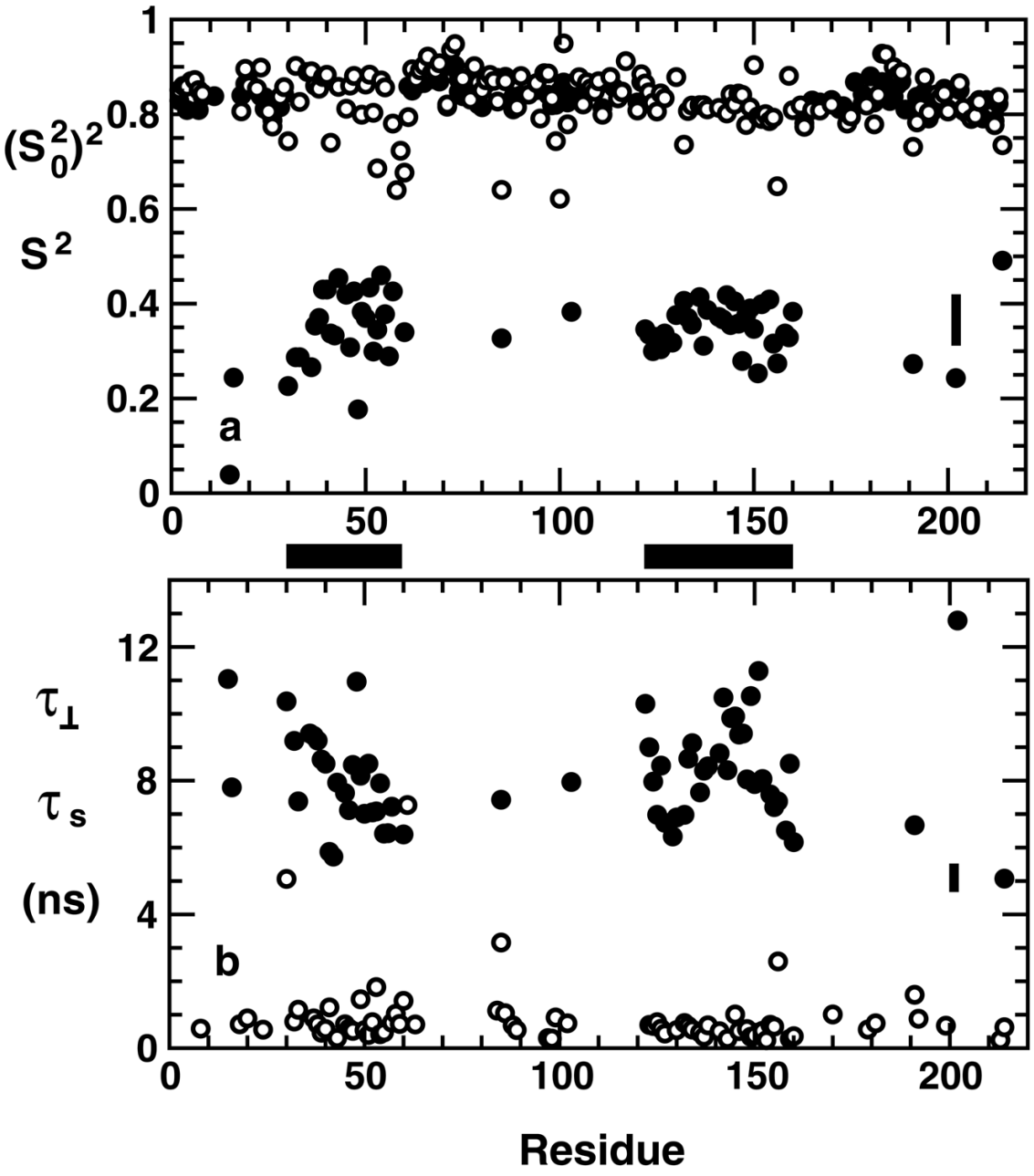

Fig. 7.

Best-fit parameters obtained with SRLS-based fitting (filled circles) and MF-based fitting (empty circles) of the experimental data of AKeco shown in Fig. 6 [46]. The SRLS analysis used the fitting scheme described in Ref. [19], and the MF analysis used the program DYNAMICS [97]. The parameters on the ordinate of Fig. 7a represent the SRLS squared axial order parameter, $(S_0^2)^2$ (filled circles), and the MF squared generalized order parameter, S^2 (empty circles). In Fig. 7b the SRLS parameter, $\tau_\perp$ (filled circles), represents the perpendicular correlation time for local motion, and the MF parameter, τ_s (empty circles), represents the effective correlation time for slow local motion. Further details are given in Ref. [46].

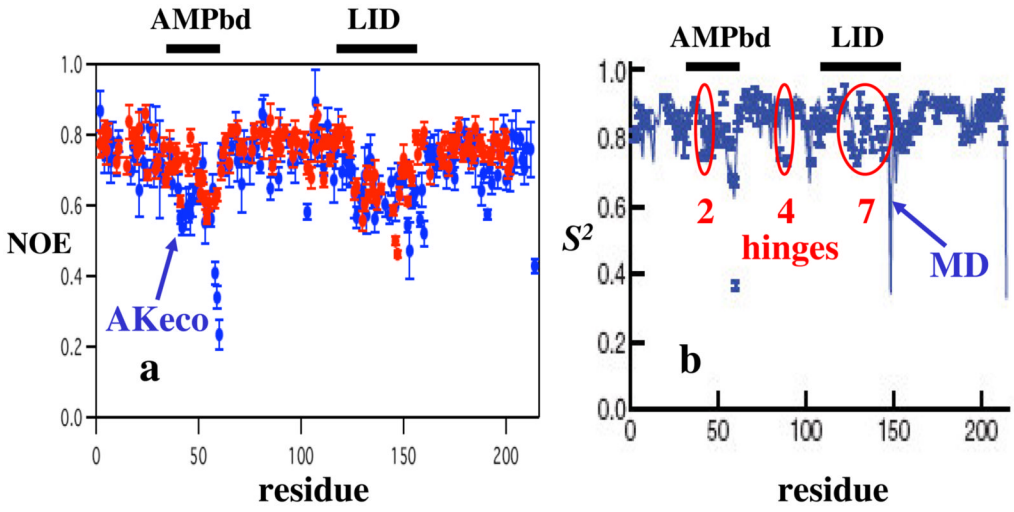

Fig. 8.

(a) Fig. S1C of the supplementary information of Ref. [240] (reproduced with permission). The blue circles represent experimental $^{15}N–\{^1H\}$ *NOE*s obtained from AKeco at 11.7 T, 293 K. (b) Fig. 3a of the supplementary information of Ref. [240] (reproduced with permission). The blue circles represent S^2 values obtained by analyzing with MF the experimental data shown in Fig. 8a. The error bars represent standard deviations. The solid blue curve represents the profile of the squared order parameter obtained with straightforward MD [240].

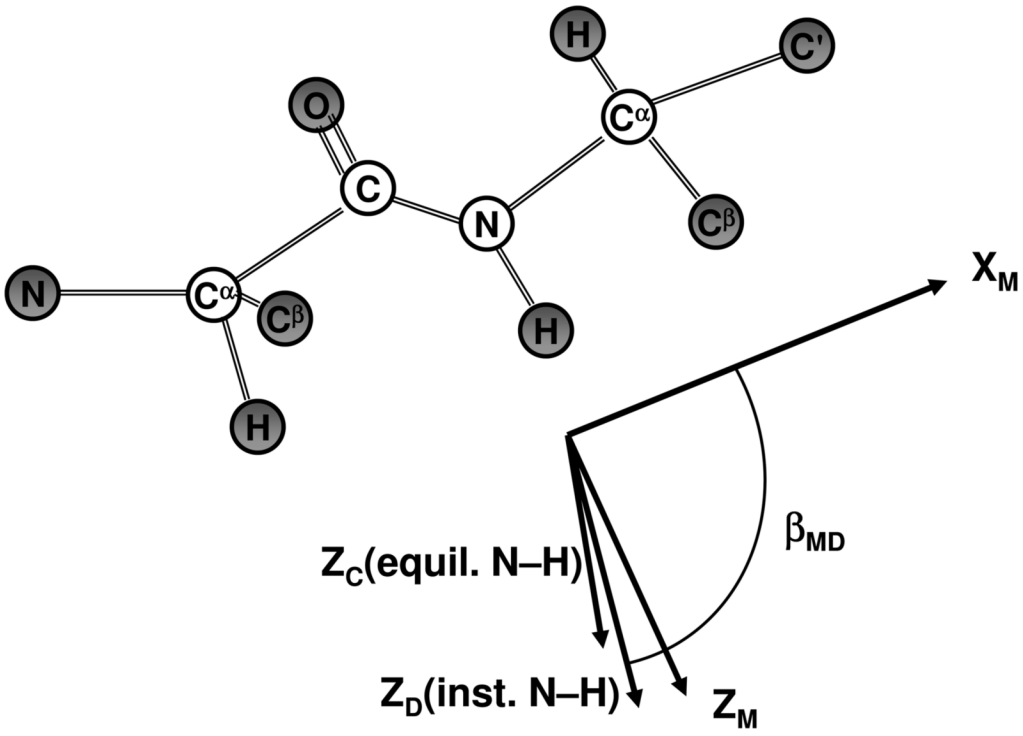

Fig. 9.

Equilibrium orientation of the backbone fragment comprising a given peptide bond and the adjacent C^{α} atoms, in the context of the SRLS frames of reference. Z_C(equil. N–H orient.) is the uniaxial local director fixed in the protein, which lies along the equilibrium orientation of the N–H bond. Z_D(inst. N–H orient.) is the principal axis of the dipolar tensor, which lies along the instantaneous orientation of the N–H bond. X_M is the main ordering axis that lies along the $C^{\alpha}_{i-1} - C^{\alpha}_{i}$ axis, as implied by $\beta_{MD} \sim 100°$. The D and M frames are fixed in the N–H bond.

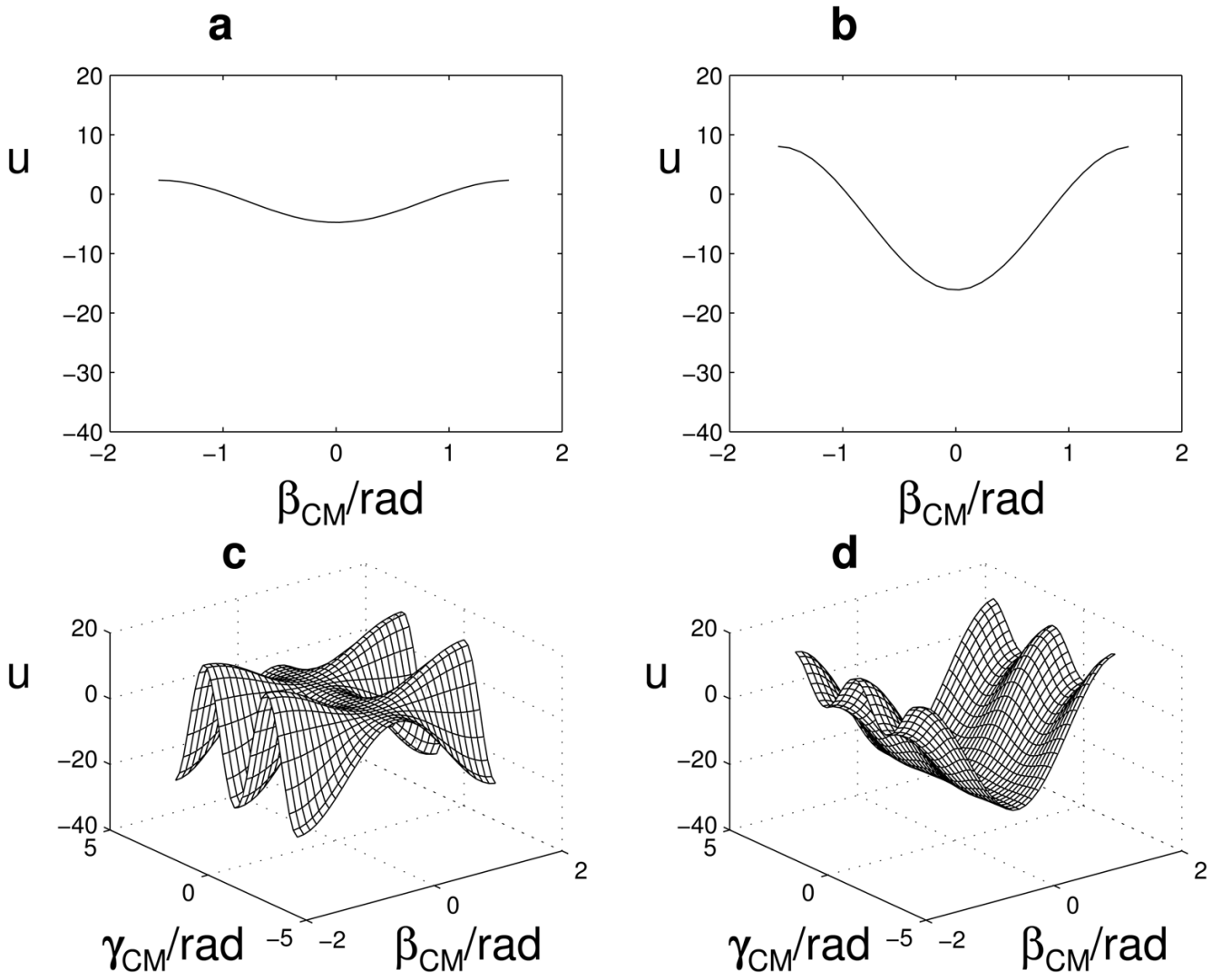

Fig. 10.

(a) The potential $u = -4.74\times(3/2\cos^2\beta_{CM} - 1/2)$ as a function of β_{CM} given in radians. (b) The potential $u = -16.1\times(3/2\cos^2\beta_{CM} - 1/2)$ as a function of β_{CM} given in radians. (c) The potential $u = 4.57\times(3/2\cos^2\beta_{CM} - 1/2) - 16.11\times(3/2)^{1/2}\sin^2\beta_{CM}\cos2\gamma_{CM}$ as a function of β_{CM} and γ_{CM} given in radians. (d) The potential shown in Fig. 10c recast by permuting twice the labels of the M frame so that X_M becomes the main ordering axis [243]; $u = -22.0\times(3/2\cos^2\beta_{CM} - 1/2) + 5.21\times(3/2)^{1/2}\sin^2\beta_{CM}\cos2\gamma_{CM}$ as a function of β_{CM} and γ_{CM} given in radians. The X axis is shown in the front and the Y axis is shown on the left.

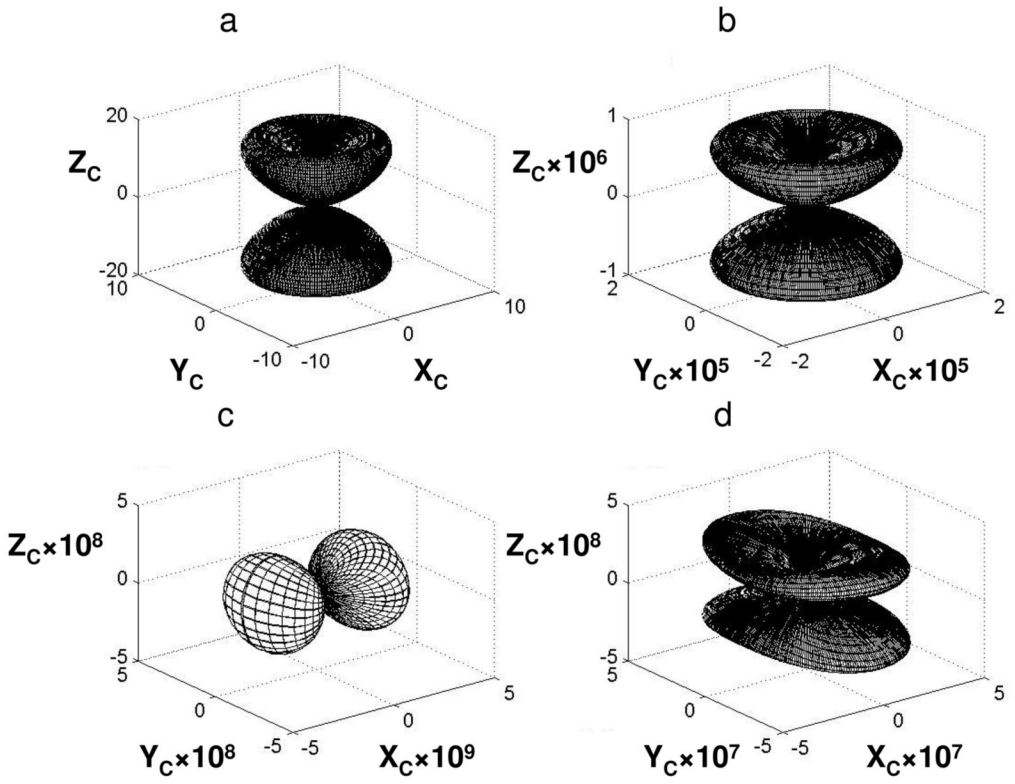

Fig. 11.

(a) The relative probability P_{rel} of the N-H bond having an orientation in the infinitesimal range $\beta_{CM} \pm \Delta\beta_{CM}$, for any α and γ, given by $\exp[4.74\times(3/2\cos^2\beta_{CM} - 1/2)]\sin\beta_{CM}\Delta\beta_{CM}$, as a function of the spherical coordinates (β_{CM},γ_{CM}). (b) The relative probability of the N-H bond having an orientation in the infinitesimal range $\beta_{CM} \pm \Delta\beta_{CM}$, for any α and γ, given by $\exp[16.1\times(3/2\cos^2\beta_{CM} - 1/2)]\sin\beta_{CM}\Delta\beta_{CM}$ as a function of the spherical coordinates ($\beta_{CM,}\gamma_{CM}$). (c) The relative probability of the $C^{\alpha}_{i-1} - C^{\alpha}_{i}$ axis having an orientation in the infinitesimal range $\beta_{CM} \pm \Delta\beta_{CM}$ and $\gamma_{CM} \pm \Delta\gamma_{CM}$, for any α, given by $\exp[-4.57\times(3/2\cos^2\beta_{CM} - 1/2)] + 16.11\times(3/2)^{1/2}\sin^2\beta_{CM}\cos2\gamma_{CM}]\sin\beta_{CM}\Delta\beta_{CM}\Delta\gamma_{CM}$ as a function of the spherical coordinates (β_{CM}, γ_{CM}). (d) The relative probability of the $C^{\alpha}_{i-1} - C^{\alpha}_{i}$ axis having an orientation in the infinitesimal range $\beta_{CM} \pm \Delta\beta_{CM}$ and $\gamma_{CM} \pm \Delta\gamma_{CM}$, for any α, given by $\exp\{[22.0\times(3/2\cos^2\beta_{CM} - 1/2)] - 5.21\times(3/2)^{1/2}\sin^2\beta_{CM}\cos2\gamma_{CM}\}\sin\beta_{CM}\Delta\beta_{CM}\Delta\gamma_{CM}$ as a function of the spherical coordinates ($\beta_{CM,}\gamma_{CM}$). The principal axes of the uniaxial local director frame are X_C, Y_C and Z_C, with Z_C parallel to the equilibrium N–H orientation, and $X_C = Y_C$. The axes have been scaled consistently to make possible comparison among drawings, and the illustration of highly peaked P_{rel} functions.

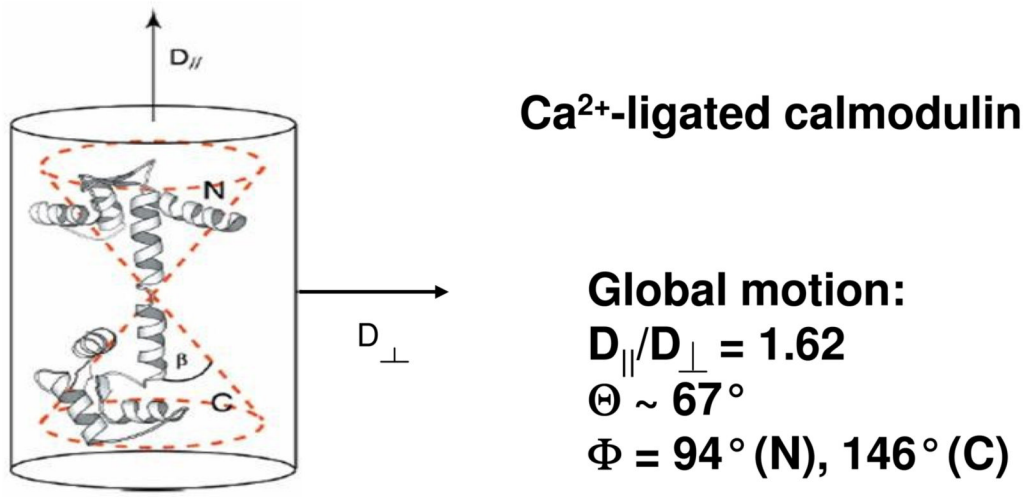

Fig. 12.

Ribbon diagram of Ca^{2+}–CaM reproduced from Ref. [248]. The data depicted describe the global diffusion tensor as determined in Ref. [248]. 'N' and 'C' denote the N–, and C–terminal domains of Ca^{2+}–CaM.

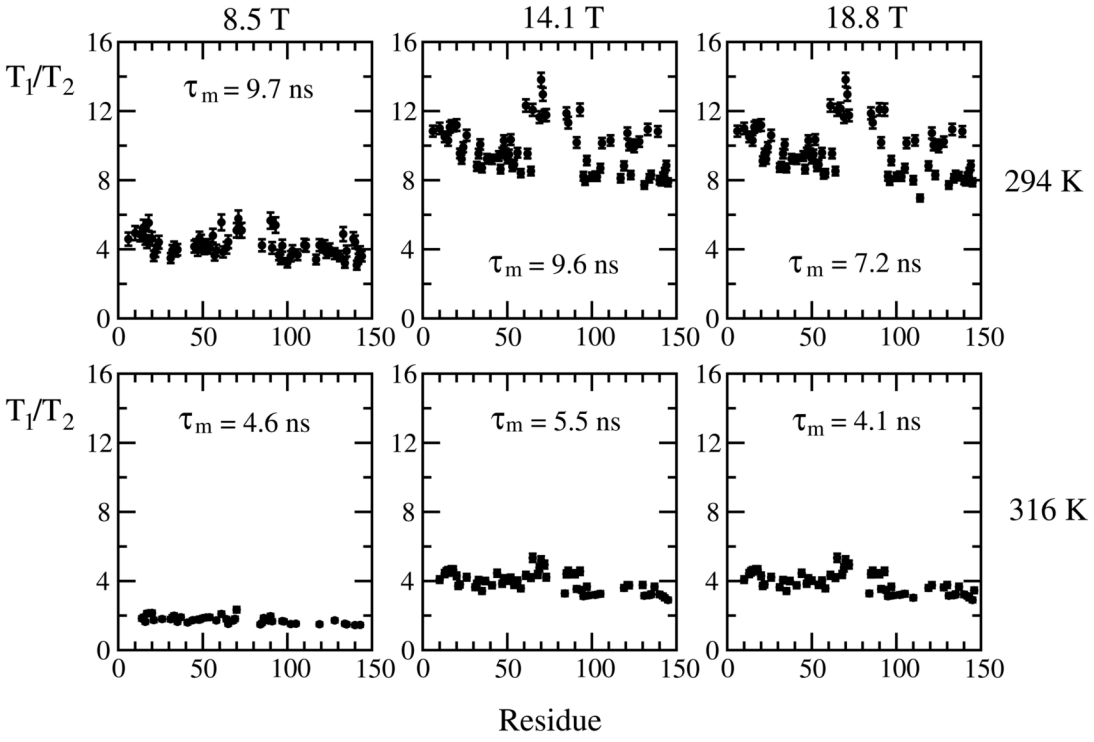

Fig. 13.

Experimental ^{15}N T_1/T_2 ratios based on ^{15}N T_1 and T_2 from Ca^{2+}–CaM acquired at 8.5, 14.1 and 18.8T, 294 and 316K, taken from Ref. [249]. The program QUADRIC [204] was used to obtain the global diffusion correlation time, τ_m, at the various temperatures studied.

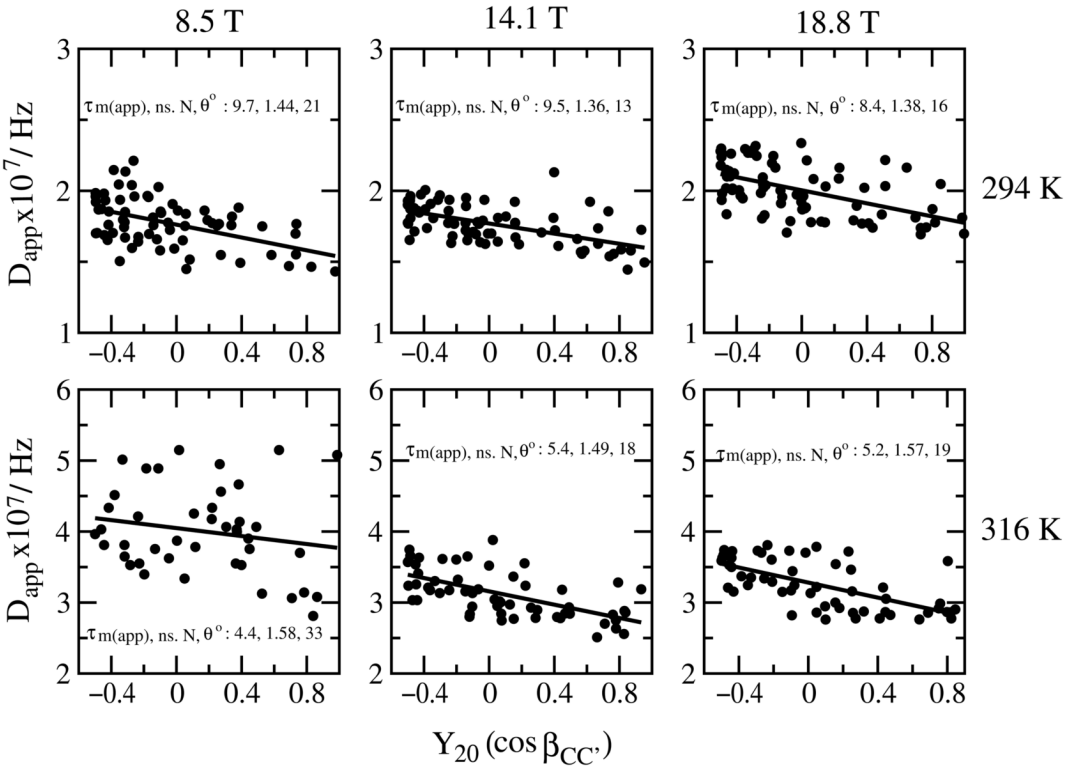

Fig. 14.

The results of analyzing the experimental data from Ca^{2+}–CaM depicted in Fig. 13 in terms of an axial global diffusion tensor, $\boldsymbol{R}^{\mathbf{C}}$, with the program QUADRIC [204]. The straight lines were obtained with linear regression.

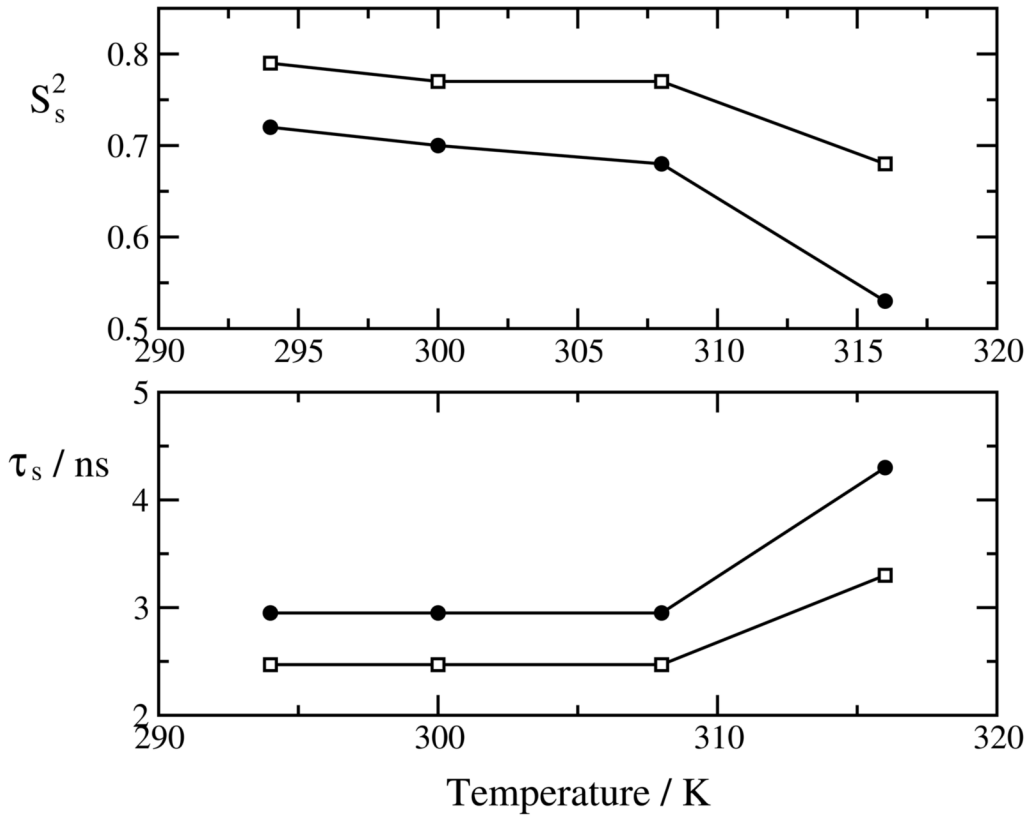

Fig. 15.

Best-fit S_s^2 and τ_s values obtained with EMF-based fitting of the experimental ^{15}N relaxation parameters from Ca^{2+}–CaM [249]. The empty squares correspond to the N–terminal domain and the filled circles correspond to the C–terminal domain. Additional best-fit parameters are $\langle S_f^2 \rangle = 0.86$, $\langle \tau_f \rangle = 15$ ps. The global diffusion tensor was determined as $R_{\parallel}^C / R_{\perp}^C = 1.62$, $\Theta = 67°$ (69°), $\Phi = 146°$ (94°) for the C–terminal domain (N–terminal domain), and τ_m values of 11.55, 9.87, 8.12 and 6.88 ns at 294, 300, 308 and 316K, respectively [249].

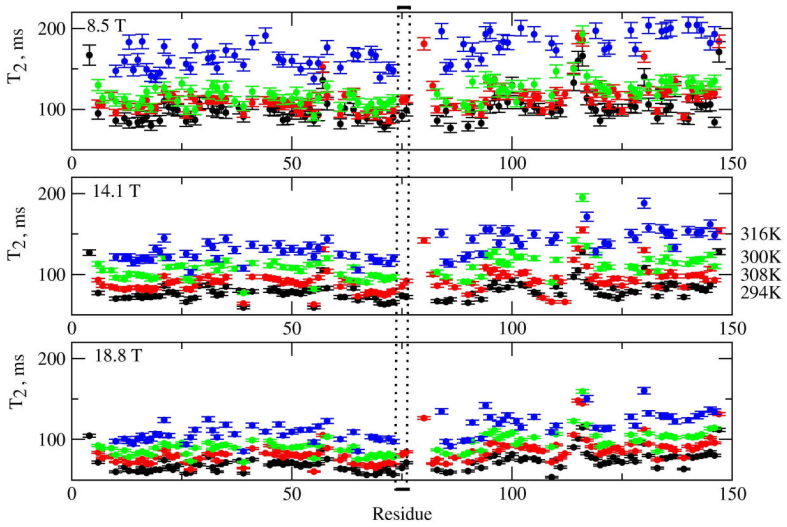

Fig. 16.

Experimental ^{15}N T_2 relaxation times of Ca^{2+}–CaM acquired at 294K (black), 300K (red), 308K (green) and 316K (blue), and 8.5, 14.1 and 18.8T [249]. The region between the vertical dashed lines represents the central linker (residues 74 – 78).

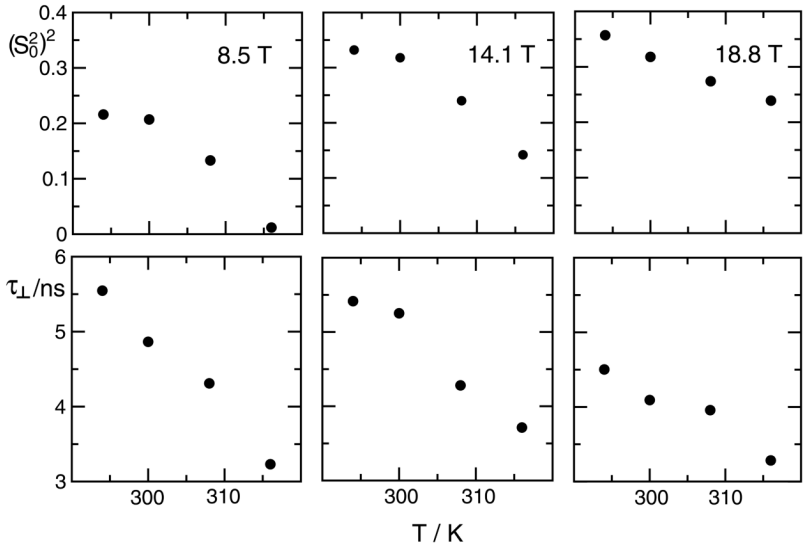

Fig. 17.

Average best-fit $(S_0^2)^2$ and $\tau_\perp$ values obtained with SRLS-based fitting of the same data used to obtain the results shown in Fig. 15 [20]. S_0^2 was calculated from the best-fit values of c_0^2. The best-fit angle β_{MD} is on average 15°. The τ_m values of 11.55, 9.87, 8.12 and 6.88 ns at 294, 300, 308 and 316K, respectively, were taken from Ref. [249].

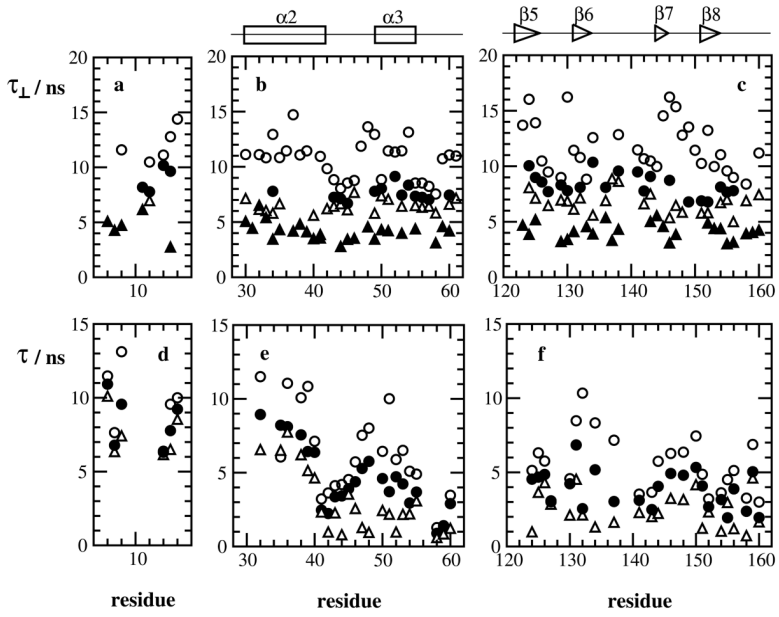

Fig. 18.

Best-fit correlation times for domain motion, $\tau_{\perp}$, obtained with axial-potential-based fitting for (a) the P-loop (residues G7 – A13), (b) the AMPbd domain and (c) the LID domain of AKeco [49]. Best-fit correlation times for domain motion, τ, obtained with rhombic-potential-based fitting for (d) the P-loop, (e) the AMPbd domain and (f) the LID domain [50]. Empty circles, filled circles, empty triangles and filled triangles denote results obtained at 288, 296.5, 302 and 310K, respectively. Elements of secondary structure are shown on the top.

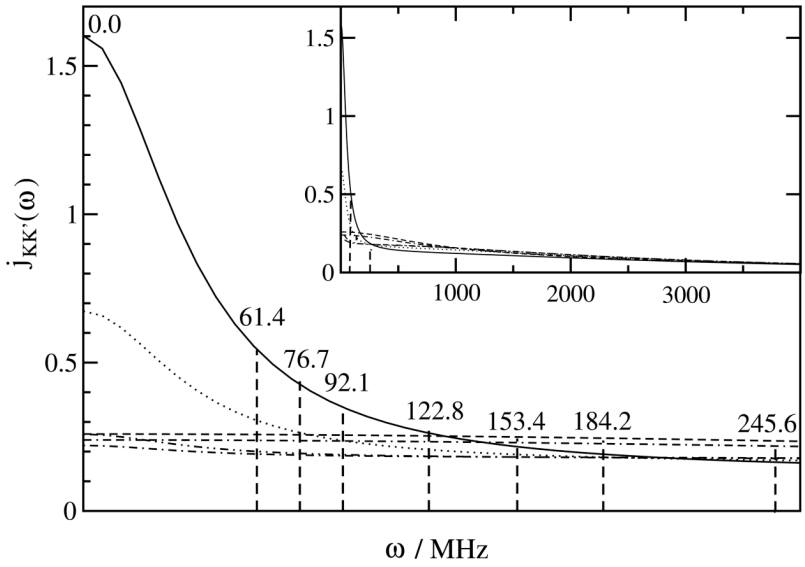

Fig. 19.

$j_{KK'}$ (ω) functions for KK' = (0,0) − solid line, (1,1) − dashed line, (2,2) − dotted/dashed line, (2,0) − dotted line, (2,−2) − double-dotted/dashed line, and (1,−1) − dotted/double-dashed line, calculated using Eq. (55a). These calculations used c_0^2=1.82, c_2^2= − 0.67 and R^C = 0.017, obtained as best-fit parameters with SRLS-based fitting of the experimental ^{2}H T_1 and T_2 data from methyl T23 of protein L acquired at 11.8 and 14.1T, 298K [24]. The inset shows a compressed ω range extending from 0 to 4000 MHz. $j_{KK'}$ (ω) is given in units of $1/R^L$ and ω is given in units of R^L. The first four values above the dashed vertical lines are the ^{2}H Larmor frequencies (ω values) at 9.36, 11.7, 14.1 and 18.8T, i.e., ω = 400, 500, 600, 800 MHz. The last four values are 2ω values at 9.36, 11.7, 14.1 and 18.8T, i.e., 800, 1000, 1200 and 1600 MHz.

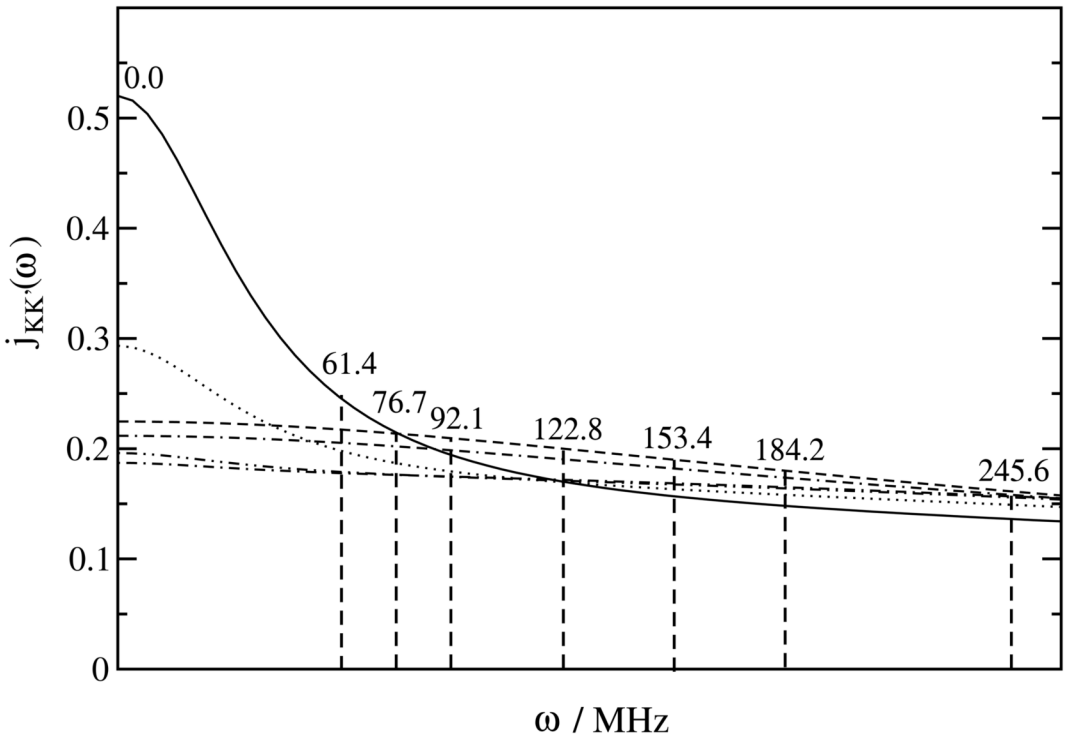

Fig. 20.

$j_{KK'}$ (ω) functions for KK' = (0,0) − solid line, (1,1) − dashed line, (2,2) − dotted/dashed line, (2,0) − dotted line, (2,−2) − double-dotted/dashed line, and (1,−1) − dotted/double-dashed line, calculated using Eq. (55a). The parameter combination including c_0^2=1.5, c_2^2= − 0.5 and R^C = 0.05 was used as input to these calculations. The first four values above the dashed vertical lines are the ^{2}H Larmor frequencies at 9.36, 11.7, 14.1 and 18.8T, i.e., ω = 400, 500, 600, 800 MHz. The last four values are 2ω at 9.36, 11.7, 14.1 and 18.8T, i.e., 800, 1000, 1200 and 1600 MHz. The values above the dashed vertical lines are the same as in Fig. 19.

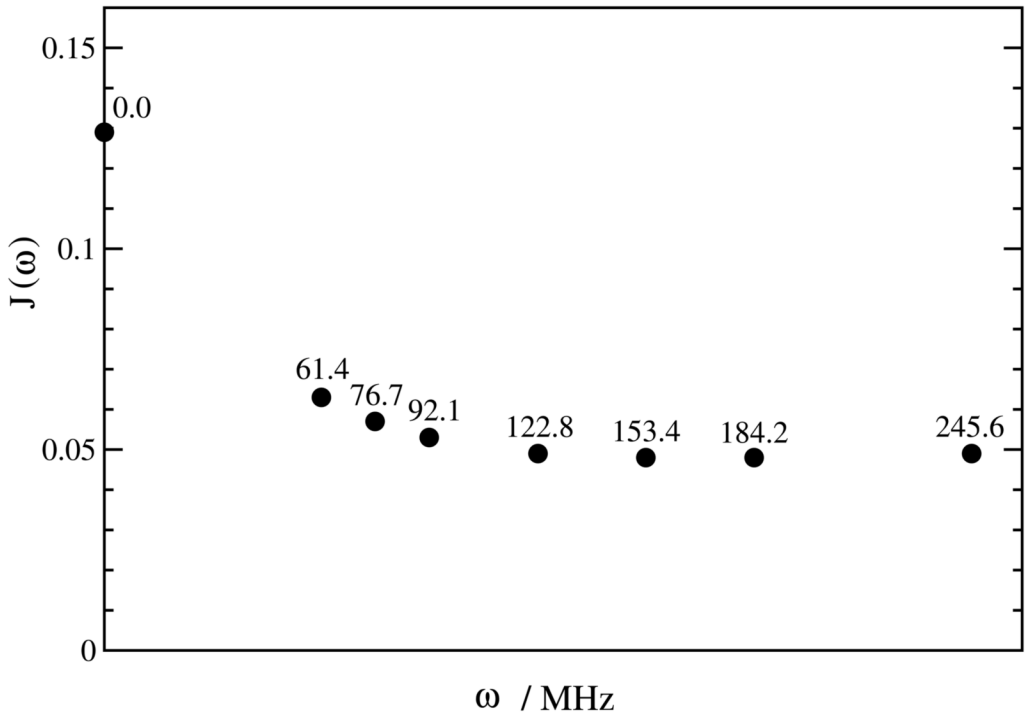

Fig. 21.
The $J^{QQ}(\omega)$ function assembled from the $j_{KK'}(\omega)$ functions shown in Fig. 20, using β_{MQ} = 69.5° (Eq. (62)).

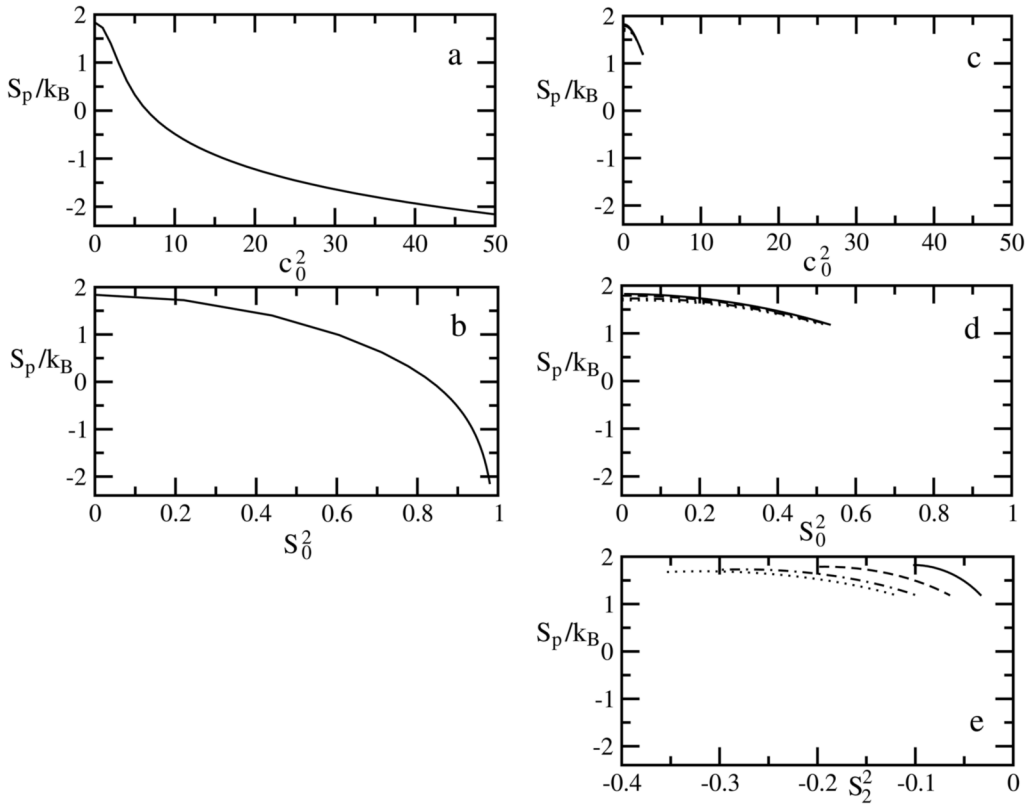

Fig. 22.

Conformational entropy $S_p/k_B = -\int_v p(q)\ln[p(q)]dv$ [57]. The probability density function, $p(q)$, is defined in terms of $u(c_0^2, c_2^2)$, with c_0^2 and c_2^2 obtained with SRLS-based fitting of the experimental data of CaM*smMLCKp from Ref. [262]. Figs. (a) and (b) illustrate the functional dependence of S_p/k_B on c_0^2 and S_0^2, for $u = -c_0^2 P_2(\cos\theta)$. Figs. (c), (d) and (e) show S_p/k_B as a function of c_0^2, S_0^2 and S_2^2, respectively, for $c_2^2 = -0.26$ (solid line), −0.51 (dashed line), −0.78 (dotted/dashed line) and −0.94 (dotted line).

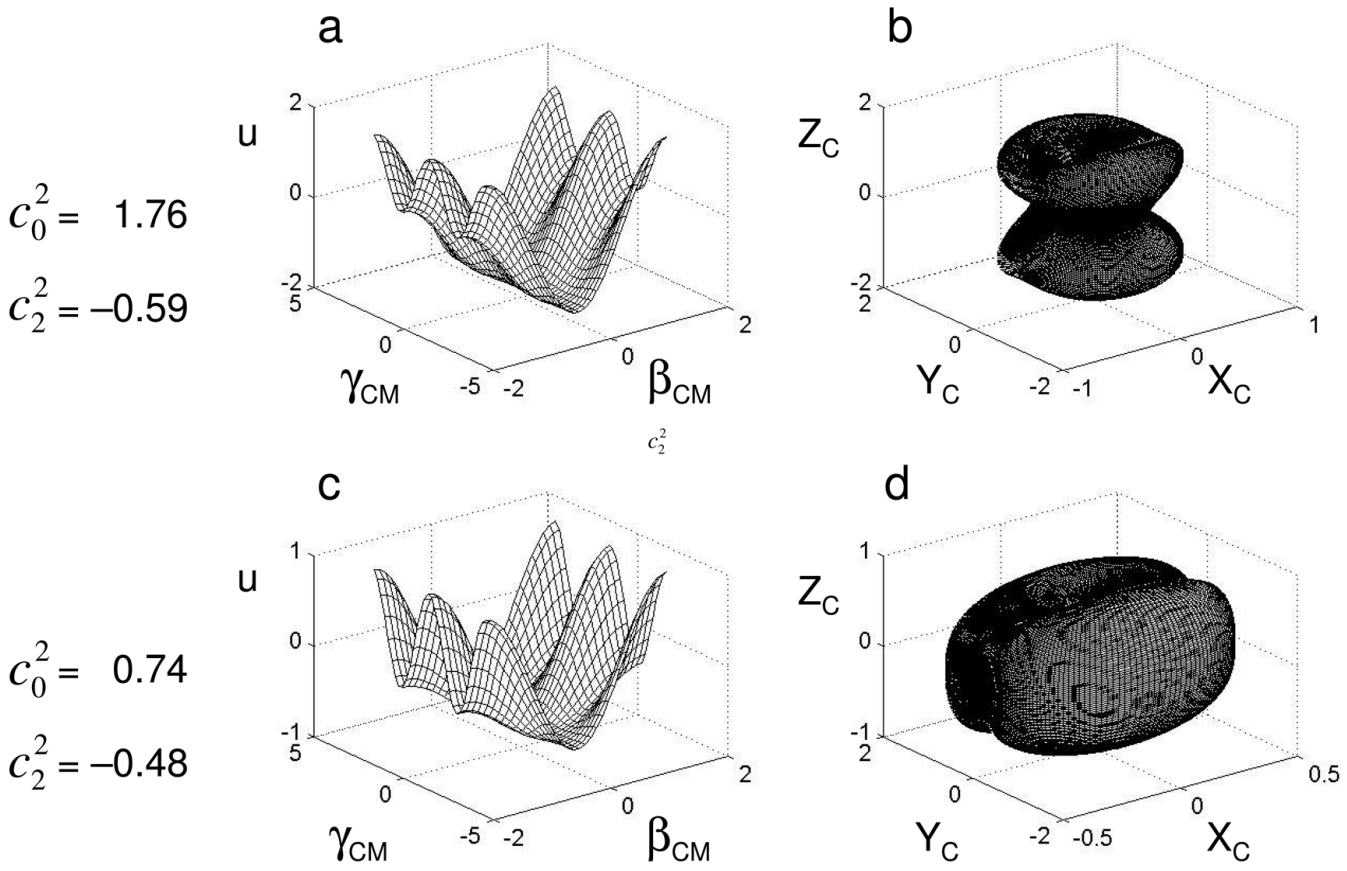

Fig. 23.

(a) The potential $u = -1.76\times(1.5\cos^2\beta_{CM} - 1/2) + 0.59\times(3/2)^{1/2}\sin^2\beta_{CM}\cos 2\gamma_{CM}$ as a function of β_{CM} and γ_{CM} given in radians. The potential coefficients are best-fit values obtained by fitting with SRLS the experimental data of methyl group A10 of Ca^{2+}–CaM*smMLCKp (see text for details). (b) The relative probability P_{rel} of the $C–^{13}CDH2$ axis having an orientation in the infinitesimal range $\beta_{CM} \pm \Delta\beta_{CM}$ and $\gamma_{CM} \pm \Delta\gamma_{CM,}$ for any α, given by $\exp[1.76\times(3/2\cos^2\beta_{CM} - 1/2) - 0.59\times(3/2)^{1/2}\sin^2\beta_{CM}\cos 2\gamma_{CM}]\sin\beta_{CM}\Delta\beta_{CM}\Delta\gamma_{CM}$, as a function of the spherical coordinates (β_{CM},γ_{CM}). The principal axes of the uniaxial local director frame are X_C, Y_C and Z_C, with Z_C parallel to the equilibrium $C–^{13}CDH_2$ orientation, and $X_C = Y_C$. (c) The potential $u = -0.73\times(3/2\cos^2\beta_{CM} - 1/2) + 0.48\times(3/2)^{1/2}\sin^2\beta_{CM}\cos 2\gamma_{CM}$ as a function of β_{CM} and γ_{CM} given in radians. The potential coefficients are best-fit values obtained by fitting with SRLS the experimental data of methyl group 85Iγ of Ca^{2+}–CaM*smMLCKp (see text for details). (d) The relative probability of the $C–^{13}CDH_2$ axis having an orientation in the infinitesimal range $\beta_{CM} \pm \Delta\beta_{CM}$ and $\gamma_{CM} \pm \Delta\gamma_{CM,}$ for any α, given by $\exp[0.73\times(3/2\cos^2\beta_{CM} - 1/2) - 0.48\times(3/2)^{1/2}\sin^2\beta_{CM}\cos 2\gamma_{CM}]\sin\beta_{CM}\Delta\beta_{CM}\Delta\gamma_{CM}$, as a function of the spherical coordinates (β_{CM},γ_{CM})

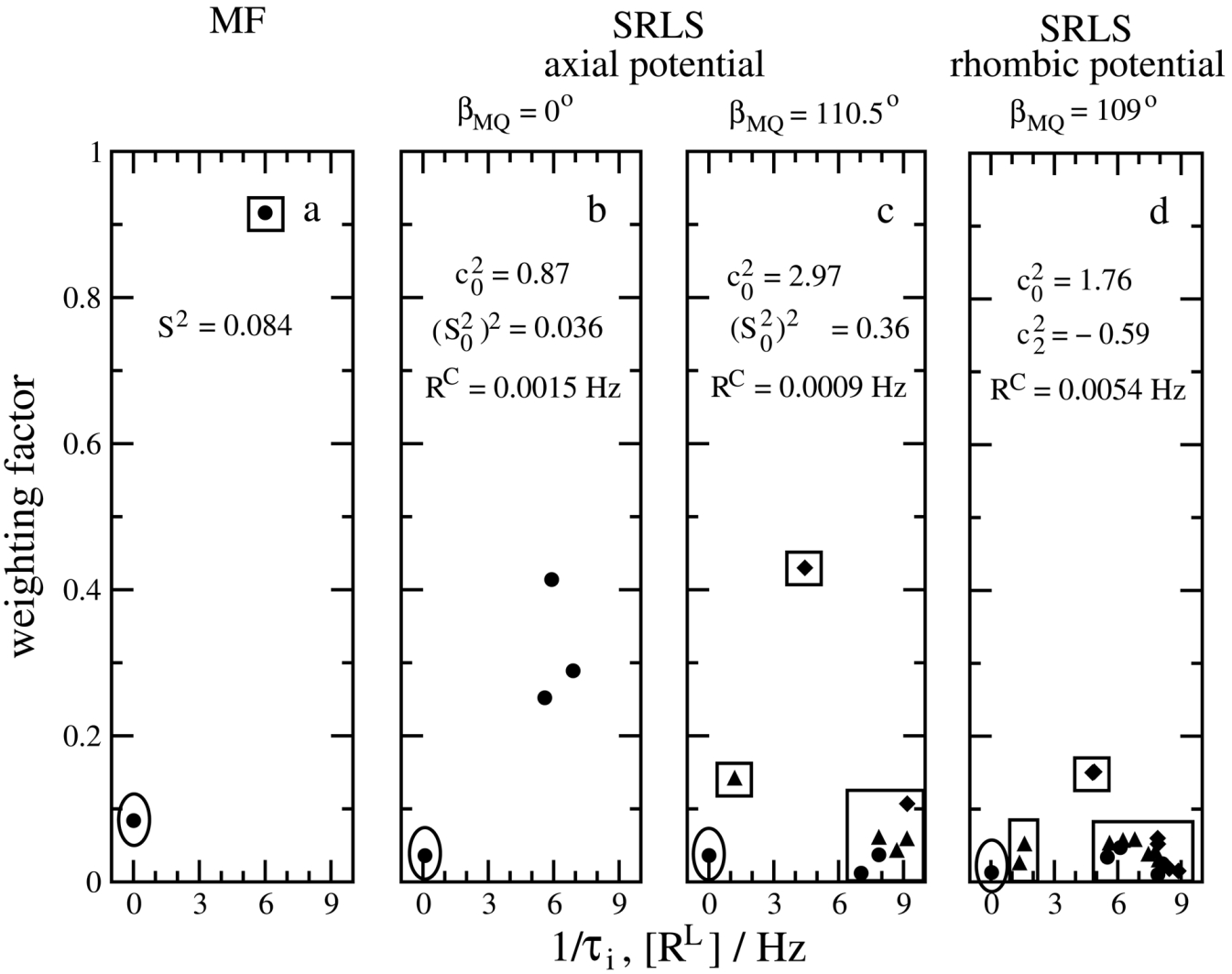

Fig. 24.

SRLS eigenmodes (ordinate) and corresponding eigenvalues (abscissa) of C_{00} (t) (circles), C_{11} (t) (triangles) and C_{22} (t) (diamonds). The parameters within the panels (except for the S_0^2 values which were calculated from corresponding c_0^2 values) are best-fit values obtained by analyzing with SRLS-based fitting (Figs. 24b–d) or MF-based fitting (Fig. 24a) the experimental ^{2}H R_1 and R_2 data of methyl group A10 of Ca^{2+}–CaM*smMLCKp, acquired at 14.1 and 17.6T, and 295K (Ref. [262]). The parameters on the top were fixed in the respective data fitting calculation. The various panels correspond to different parameter combinations used. The boxes mark clusters of eigenvalues comparable in magnitude.

Table 1

Results of the SRLS-based fitting to the ^{15}N relaxation parameters of selected residues of AKeco acquired at 14.1 and 18.8 T, and 302 K. A correlation time for global diffusion of 14.9 ns was used [50]. The underlined $\tau_\perp$ value in row 5 was fixed at 14.9 ns in the calculation. The parameter values of $r_{NH(eff)}$ = 1.015 Å (Ref. [147]), $\Delta\sigma = -169$ ppm (Ref. [148]) and $\beta_{D-CSA} = 17°$ (Ref. [149]) were used. The local ordering and local diffusion frame were taken to be the same. A value of $L_{max} = 18 - 24$ was used. The angles α_{MD} and β_{MD} were fixed at 90° and 101.3°, respectively. The program DYNAMICS [97] was used to perform the MF calculations. Further details are given in the text.

Residue	Method	$c_0^2\left(\left(S_0^2\right)^2\right)$**	$\tau_\perp$/ns	$\tau_\parallel$/ns	β_D/deg	R_{ex}/s^{-1}	χ^2
197	MF	12.4 (0.84)	0.078***	0.078***			2.0
197	SRLS ax	11.6 (0.83)	0.069	0.069			0.6
209	MF	9.0 (0.78)	0.042***	0.042***		4.4	8.8
209	SRLS ax	10.1 (0.81)	0.031	0.006		3.6	5.8
209	SRLS rh	−15.9*	<u>14.9</u>	0.013			2.4
46	MF	8.9 (0.778)	0.91	0.0	12.2****	1.8	5.1
46	SRLS ax	3.6 (0.448)	7.12	0.004	21.4	4.0	0.9
46	SRLS rh	−6.8*	4.0	0.021			2

* In the calculation of residue 209, carried out with the method designated SRLSrh, the local potential used was given by $c_0^2 = -15.9$ and $c_2^2 = -3.4$. In the calculation of residue 46, carried out with the method designated SRLSrh, the local potential used was given by $c_0^2 = -6.8$ and $c_2^2 = -4.4$).

** In the SRLS calculations the parameter that is varied is the axial coefficient, c_0^2, of the potential, u; the latter is defined by Eq. (52) where $c_2^2 = 0$. The order parameter, S_0^2, is calculated using this form of u and the axial versions of Eq. (59). In the MF calculations the parameter that is varied is S^2. We calculated a corresponding potential coefficient, c_0^2, using the axial versions of Eqs. (52) and (59).

*** The MF calculation yielded τ_e (formally analogous to $\tau = \tau_\parallel = \tau_\perp$), which in the limit of high axial local potentials agrees with the "renormalized" correlation time, $\tau_{ren} \sim 2\tau/c_0^2$ (Ref. [14]). The data that appear in the Table are τ values obtained from τ_e using this formula. These values should be compared with τ from SRLS.

**** The angle β_{MD} is derived from the MF parameters S_f^2 according to $S_f^2 = (1.5\cos^2\beta_{MD} - 0.5)^2$ (Ref. [19]).

Table 2

Squared order parameters, S^2, and local motional correlation times, τ, obtained from the total MD time correlation function as outlined in Ref. [163], and from MF applied to the corresponding experimental ^{15}N relaxation data [164,167]; “ubi” is a shorthand notation for ubiquitin.

	MD		MF	
residue	S^2	**τ/ns**	S^2	τ_e/ns
63 of ubi	0.90	0.07	0.82	0.037
11 of ubi	0.56	0.64	0.71	0.058
73 of ubi	0.46	2.00	0.57	0.071
49 of GB3	0.82	0.01	0.82	NA
13 of GB3	0.60	1.30	0.67	NA
41 of GB3	0.34	2.10	0.50	NA

Table 3

Average best-fit values, c_0^2, and corresponding values, $(S_0^2)^2$, obtained with SRLS-based fitting [20] of the ^{15}N spin relaxation data of relatively rigid residues of VHHS [199]. Average best-fit values, S^2, and corresponding values, c_0^2, obtained with MF analysis of the same experimental data [96]. %diff represents 100×[(MF parameter) − (SRLS parameter)]/(SRLS parameter) [20]. "Model 1" refers to calculations where S^2 is allowed to vary in MF; in analogy, c_0^2 is allowed to vary in SRLS. "Model 2" refers to calculations where S^2 and τ_e are allowed to vary in MF; in analogy, c_0^2 and τ/τ_m are allowed to vary in SRLS (τ_m taken from Ref. [199]).

	Model 1			Model 2		
	SRLS	**MF**	**%diff**	**SRLS**	**MF**	**%diff**
$(S_0^2)^2$	0.87	0.83	−4.5	0.73	0.78	+6.8
c_0^2	15.4	11.7	−23	7.5	9.0	+20

Table 4

Percent difference [var(axial) − var(rhombic)]/var(axial)×100, where "var" denotes "variable", between ^{15}N T_1, T_2 (ms) and ^{15}N–{^{1}H} *NOE* values calculated with τ_m = 15 ns, R^C = 0.01, and an axial potential with c_0^2=8 and c_2^2=0 or a rhombic potential with c_0^2=8 and c_2^2=4. Calculations are shown for magnetic fields of 11.7, 14.1 and 18.8T [20].

	11.7T	**14.1T**	**18.8T**
T_1	−2.4	−1.0	+1.5
T_2	−7.6	−7.5	−7.6
NOE	+31.6	+39.3	+46.3

Table 5

Percent difference [var($\beta_{CC'} = 0°$) − var($\beta_{CC'} = 90°$)]/[var($\beta_{CC'} = 0°$)]×100 between ^{15}N T_1, T_2 (ms) and $^{15}N-\{^1H\}$ *NOE* values calculated with $\tau_m = 15$ ns, an axial potential given by $c_0^2=8$, and an axial global diffusion tensor. The latter was given by R^C (eff) = 0.01, $R_\parallel^C/R_\perp^C=1.2$, and $\beta_{CC'}$ (the angle between the equilibrium orientation of the N–H bond and the principal axis of the $\boldsymbol{R}^{\mathbf{C}}$ tensor) set equal to 0° or 90°. Calculations are shown for magnetic fields of 11.7, 14.1 and 18.8T [20].

	11.7T	**14.1T**	**18.8T**
T_1	+7.4	+7.1	+6.1
T_2	−9.0	−9.0	−9.2
NOE	−2.7	−3.5	−4.0

Table 6

Best-fit parameters obtained with SRLS-based fitting of the ^{15}N spin relaxation data from AKeco acquired at 14.1 and 18.8 T, and 303 K. For residues G46 and K47 the parameters varied include c_0^2, c_2^2, $\tau_\perp/\tau_m$, $\tau_\parallel$ and β_{MD}, with τ_m = 15.1 ns [20]. For residue L35 the parameters varied include c_0^2, c_2^2, τ and β_{MD}, with τ_m = 14.9 ns [50]. S_{xx}, S_{yy} and S_{zz} are the components of the Cartesian ordering tensor corresponding to the best-fit values of c_0^2 and c_2^2. The axiality of the local diffusion tensor is given by $N = \tau_\parallel/\tau_\perp$

Residue	c_0^2	c_2^2	R^C	$\tau_\perp$ or τ ns*	S_{xx}	S_{yy}	S_{zz}	β_{MD}°	N
G46	5.7	10.5	0.82	12.4	0.827	−0.465	−0.361	101.4	9.6
K47	4.3	10.3	0.73	11.0	0.761	−0.470	−0.291	100.7	6.3
L35	7.8	22.3	0.43	6.5	0.940	−0.490	−0.450	99.0	1.0

*$\tau_\perp$ corresponds to G46 and K47 [20]; τ corresponds to L35 [50].

Table 7

Average best-fit potential coefficients c_0^2 and c_2^2 obtained with SRLS-based fitting of the ^{15}N relaxation data from the AMPbd and LID domains of AKeco acquired at 14.1 and 18.8T at the temperatures depicted in the Table. The parameters varied include c_0^2, c_2^2, β_{MD} and τ/τ_m. The average best-fit value of β_{MD} is on the order of 100°; the average best-fit value of τ/τ_m is on the order of 0.25. The errors in the order parameters are estimated at 10%, and the errors in the potential coefficients, at 20% [50].

Temperature, K	c_0^2	c_2^2	S_{xx}	S_{yy}	S_{zz}	S_0^2	S_2^2
AMPbd							
288	−4.45	19.10	0.954	−0.484	−0.471	−0.471	1.174
296.5	−0.52	18.90	0.947	−0.483	−0.463	−0.464	1.168
302	−4.80	15.79	0.941	−0.480	−0.461	−0.461	1.160
LID							
288	−4.05	18.54	0.955	−0.483	−0.472	−0.472	1.174
296.5	−1.50	18.20	0.949	−0.483	−0.467	−0.467	1.169
302	−4.35	16.43	0.948	−0.481	−0.467	−0.467	1.166

Table 8

Average activation energies and pre-exponential factors for domain motion obtained from the rate constant $R^L = 1/(6\tau)$ using the Arrhenius equation. Data for the domains AMPbd and LID, and the P-loop (residues G7 – A13) of AKeco, are shown. R^L was obtained with SRLS-based fitting of the ^{15}N relaxation parameters from these domains. The parameters varied in these calculations include c_0^2, c_2^2, β_{MD} and τ/τ_m; the correlation time τ_m was determined independently [50]. Results obtained using axial potentials, where the parameters varied in the data fitting process include c_0^2, β_{MD}, $\tau_\perp/\tau_m$ and $\tau_\parallel$, are also shown [49].

Domain	E_a (kJ/mol)	ln A	Correlation coefficient
Axial local potential [49]**:**			
P-loop	30.4 ± 4.3	29.1 ± 1.7	− 0.981
AMPbd	29.7 ± 3.3	29.0 ± 1.3	− 0.989
LID	32.1 ± 4.3	29.9 ± 1.7	− 0.984
Rhombic local potential [50]**:**			
P-loop	16.5 ± 6.4	23.5 ± 2.6	− 0.930
AMPbd	63.8 ± 7.0	43.8 ± 2.9	− 0.987
LID	53.0 ± 9.1	39.3 ± 3.7	− 0.966

Table 9

Potential coefficients, c_0^2 and c_2^2, obtained with SRLS-based fitting of the experimental ^{2}H T_1 and T_2 relaxation parameters from the methyl groups A10 and Iγ85 of Ca^{2+}–CaM*smMLCKp. Details are given in the text. The order parameters S_{xx}, S_{yy} and S_{zz} were calculated from c_0^2 and c_2^2.

Methyl group	c_0^2	c_2^2	S_{xx}	S_{yy}	S_{zz}	$(S_{xx} - S_{yy})/S_{zz}$
A10	+1.76	−0.59	−0.256	−0.116	+0.372	−0.38
85Iγ	+0.74	−0.48	−0.164	+0.019	+0.144	−1.27

Table 10

Best-fit c_0^2, c_2^2 and τ values obtained with SRLS-based fitting of ^{2}H T_1, T_2, and the three relaxation rates associated with rank 2 coherences from the $^{13}CDH_2$ methyl groups of protein L (Ref. [35]) acquired at 11.7 and 14.1T, 298K [24]. The best-fit value of the angle β_{MD} is (69 ± 1.5)°. The data under the heading "MF" were taken from Ref. [24]; c_0^2 was calculated from S^2 using Eqs. (52) and (59). The penultimate and ultimate columns on the right show $R(c_0^2)=c_0^2(\text{SRLS})/c_0^2(\text{MF})$ and $R(\tau) = \tau(\text{SRLS})/\tau_e(\text{MF})$, respectively. The residues marked in boldface letters required the utilization of the MF formula where τ_m was also allowed to vary [24].

Methyl	MF				SRLS					
	S_{axis}^2	c_0^2	τ_e/ps	R^C	c_0^2	c_2^2	τ/ps	R^C	$R(c_0^2)$	$R(\tau)$
V2γ_1	0.73	1.22	54	0.013	1.77	−0.82	101	0.025	1.5	1.9
T37	0.74	1.23	50	0.012	1.89	−0.92	97	0.024	1.5	1.9
T55	0.98	1.41	51	0.012	1.83	−0.95	113	0.028	1.3	2.2
T17	0.97	1.42	45	0.011	1.56	−0.82	117	0.029		
I9δ	0.38	0.89	24	0.006	1.57	−0.50	28	0.007	1.8	1.2
L8δ_1	0.30	0.79	35	0.009	−0.29	−0.50	53	0.013		
L8δ_2	0.30	0.79	41	0.010	−0.35	−0.50	57	0.014		
T15	0.57	1.09	69	0.017	1.79	−0.95	105	0.026	1.6	1.5
L38δ_1	0.56	1.08	34	0.008	1.68	−0.74	61	0.015	1.6	1.8
V47γ_1	0.57	1.09	55	0.014	1.51	−0.58	93	0.023	1.4	1.7
I58δ	0.58	1.10	17	0.004	1.86	−0.56	32	0.008	1.7	1.9
V49γ_2	0.62	1.13	40	0.010	1.68	−0.82	61	0.015	1.5	1.5
L56δ_1	0.61	1.12	70	0.017	1.89	−1.09	117	0.029	1.7	1.7
L56δ_2	0.61	1.12	38	0.009	1.60	−0.68	65	0.016	1.4	1.7
A61	0.60	1.11	46	0.011	1.68	−0.73	77	0.019	1.5	1.7
T3	0.88	1.33	39	0.010	1.78	−0.89	85	0.021	1.3	2.2
T28	0.88	1.33	41	0.010	1.82	−1.02	85	0.021	1.4	2.1
I4γ	0.87	1.32	24	0.006	1.84	−0.78	73	0.018	1.4	3.1
A33	0.89	1.34	37	0.009	1.87	−0.91	101	0.025	1.4	2.7
A11	0.82	1.29	49	0.012	1.98	−1.02	134	0.033	1.5	2.7
A18	0.81	1.28	57	0.014	1.90	−1.00	109	0.027	1.5	1.9
I58γ	0.82	1.29	27	0.007	1.79	−0.96	53	0.013	1.4	2.0

Methyl	MF				SRLS					
	S_{axis}^2	c_0^2	τ_e/ps	R^c	c_0^2	c_2^2	τ/ps	R^c	$R(c_0^2)$	$R(\tau)$
T46	0.69	1.20	63	0.016	1.89	−1.00	105	0.026	1.6	1.7
V49γ_1	0.68	1.18	34	0.008	1.72	−0.68	69	0.017	1.5	2.0
T23	0.84	1.31	39	0.010	1.84	−0.94	81	0.020	1.4	2.1
A50	0.84	1.31	24	0.006	1.81	−0.93	53	0.013	1.4	2.2
A31	0.83	1.30	77	0.019	1.94	−1.15	134	0.033	1.5	1.7

Table 11

Dominant eigenmodes, $c_{KK',i}$ and corresponding eigenvalues, $1/\tau_i$, comprising C_{00} (t), C_{11} (t) and C_{22} (t), calculated with c_0^2=0.87, c_2^2=0, β_{MQ} = 0° and R^C = 0.0015. The values of c_0^2 and R^C are best-fit parameters obtained with SRLS-based fitting of the ^{2}H T_1 and T_2 data from the A10 methyl of Ca^{2+}–CaM*smMLCKp acquired at 14.1 and 17.6T, and 295K. The experimental data and τ_m = 11.81 ns were taken from Ref. [262]. The fractional contributions of the j_{KK} (ω) functions to J^{QQ} (ω), and the MF data from Ref. [262] obtained with Eq. (2), are also shown. The eigenvalues, $1/\tau_i$, are given in units of R^L.

C_{00} (t)		C_{11} (t)		C_{22} (t)	
$1/\tau_i$	$c_{00,i}$	$1/\tau_i$	$c_{11,i}$	$1/\tau_i$	$c_{22,i}$
5.96	0.350	5.96	0.330	5.34	0.527
5.63	0.328	6.22	0.302	6.57	0.374
5.63	0.181	6.54	0.292	6.98	0.096
6.93	0.094	1.73	0.069		
0.0355	0.0376				
1.0		0.0		0.0	
MF [261]:					
6	0.916				
N.A.	0.084				

Table 12

Dominant eigenmodes, $c_{KK',i}$, and corresponding eigenvalues, $1/\tau_i$, comprising the time correlation functions C_{00} (t), C_{11} (t) and C_{22} (t), calculated with c_0^2=2.97, c_2^2=0, β_{MQ} = 110.5° and R^C = 0.0009. The values of c_0^2 and R^C are the best-fit parameters obtained with SRLS-based fitting of the same experimental data as outlined in the title of Table 11. The fractional contributions of the corresponding j_{KK} (ω) functions to J^{QQ} (ω) are also shown. The eigenvalues, $1/\tau_i$, are given in units of R^L.

C_{00} (t)		C_{11} (t)		C_{22} (t)	
$1/\tau_i$	$c_{00,i}$	$1/\tau_i$	$c_{11,i}$	$1/\tau_i$	$c_{22,i}$
7.65	0.378	1.21	0.419	4.47	0.735
0.006	0.329	7.65	0.193	8.94	0.193
6.93	0.130	8.93	0.190	10.1	0.045
		8.46	0.145		
10%		32.3%		57.7%	

Table 13

Dominant eigenmodes, $c_{KK',i}$, and corresponding eigenvalues, $1/\tau_i$, comprising the time correlation functions C_{00} (t), C_{11} (t) and C_{22} (t) calculated with c_0^2=1.76, c_2^2= − 0.59, β_{MQ} = 109.5° and R^C = 0.054. The values of c_0^2, c_2^2, β_{MQ} and R^C are the best-fit parameters obtained with SRLS-based fitting of the same experimental data as outlined in the title of Table 11. The fractional contributions of the corresponding j_{KK} (ω) functions to J^{QQ} (ω) are also shown. The eigenvalues, $1/\tau_i$, are given in units of R^L.

C_{00} (t)		**C_{11} (t)**		**C_{22} (t)**	
$1/\tau_i$	**$c_{00,i}$**	**$1/\tau_i$**	**$c_{11,i}$**	**$1/\tau_i$**	**$c_{22,i}$**
5.81	0.317	6.24	0.187	5.12	0.280
5.20	0.265	5.85	0.182	4.90	0.274
7.74	0.201	5.23	0.164	7.92	0.134
0.042	0.079	1.82	0.122	7.90	0.109
7.90	0.064	7.61	0.118	2.93	0.05
4.90	0.041	7.65	0.109	5.81	0.04
8.93	0.013	8.00	0.07	8.22	0.03
		1.37	0.03	8.93	0.03
				5.20	0.03
C_{02} (t)		C_{1-1} (t)		C_{2-2} (t)	
$1/\tau_i$	$c_{02,i}$	$1/\tau_i$	$c_{1-1,i}$	$1/\tau_i$	$c_{2-2,i}$
5.81	0.286	5.85	0.363	4.90	0.546
5.20	0.232	5.23	0.328	7.90	0.218
7.74	0.148	7.61	0.237	5.81	0.075
5.12	0.137	1.37	0.057	8.93	0.056
7.92	0.07			5.20	0.056
4.90	0.05			7.74	0.019
2.93	0.025			0.042	0.018
0.042	0.017				
8.22	0.015				
KK′	0,0	1,1	2,2	0,2	1,−1	2,−2
%	13.95	35.43	47.42	−9.5	4.46	8.23